


50 mm



**BEARING FAULT DETECTION USING
DISCRETE WAVELET TRANSFORM**

SYAHRIL AZEEM ONG BIN HAJI MALIKI ONG

UNIVERSITI MALAYSIA PAHANG



50 mm

 30mm	<p>SYAHRIL AZEEM ONG DEGREE OF MECHANICAL ENGINEERING 2012 UMP</p> <p>(16 gold coloured font)</p>	 30mm
--	--	--

UNIVERSITI MALAYSIA PAHANG

BORANG PENGESAHAN STATUS TESIS ♦

JUDUL: BEARING FAULT DETECTION USING DISCRETE WAVELET TRANSFORM

SESI PENGAJIAN: 2011/2012

Saya,

SYAHRIL AZEEM ONG BIN HAJI MALIKI ONG (880914-07-5155)

mengaku membenarkan tesis (Sarjana Muda / ~~Sarjana / Doktor Falsafah~~)* ini disimpan di perpustakaan dengan syarat-syarat kegunaan seperti berikut:

1. Tesis ini adalah hakmilik Universiti Malaysia Pahang (UMP).
2. Perpustakaan dibenarkan membuat salinan untuk tujuan pengajian sahaja.
3. Perpustakaan dibenarkan membuat salinan tesis ini sebagai bahan pertukaran antara institusi pengajian tinggi.
4. **Sila tandakan (✓)

☐

SULIT

(Mengandungi maklumat yang berdarjah keselamatan atau kepentingan Malaysia seperti yang termaktub di dalam AKTA RAHSIA RASMI 1972)

☐

TERHAD

(Mengandungi maklumat TERHAD yang telah ditentukan oleh organisasi / badan di mana penyelidikan dijalankan)

☒

TIDAK TERHAD

Disahkan oleh:

(TANDATANGAN PENULIS)

(TANDATANGAN PENYELIA)

Alamat Tetap:
**No 243, Lorong Berlian 2/1,
Taman Berlian,
09000 Kulim,
Kedah Darul Aman**

CHE KU EDDY NIZWAN BIN CHE KU HUSIN

Tarikh: **21 JULAI 2012**

Tarikh: **21 JULAI 2012**

CATATAN: * Potong yang tidak berkenaan.

** Jika tesis ini SULIT atau TERHAD, sila lampirkan surat daripada pihak berkuasa/organisasi berkenaan dengan menyatakan sekali tempoh tesis ini perlu dikelaskan sebagai SULIT atau TERHAD.

♦ Tesis dimaksudkan sebagai tesis bagi Ijazah Doktor Falsafah dan Sarjana secara Penyelidikan, atau disertasi bagi pengajian secara kerja kursus dan penyelidikan, atau Laporan Projek Sarjana Muda (PSM).

BEARING FAULT DETECTION USING DISCRETE WAVELET TRANSFORM

SYAHRIL AZEEM ONG BIN HAJI MALIKI ONG

Report submitted in partial fulfillment of the requirements
for the award of the degree of Bachelor of Mechanical Engineering

Faculty of Mechanical Engineering
UNIVERSITI MALAYSIA PAHANG

JUNE 2012

UNIVERSITI MALAYSIA PAHANG
FACULTY OF MECHANICAL ENGINEERING

I certify that the project entitled “Bearing fault detection using discrete wavelet transform” is written by Syahril Azeem Ong bin Haji Maliki Ong. I have examined the final copy of this project and in my opinion; it is fully adequate in terms of scope and quality for the award of the degree of Bachelor of Engineering. I herewith recommend that it be accepted in partial fulfillment of the requirements for the degree of Bachelor of Mechanical Engineering.

MOHD FADHLAN BIN MOHD YUSOF

Examiner

Signature

SUPERVISOR'S DECLARATION

I hereby declare that I have checked this project and in my opinion this project is adequate in terms of scope and quality for the award of the degree of Bachelor of Mechanical Engineering.

Signature :

Name of Supervisor : CHE KU EDDY NIZWAN BIN CHE KU HUSIN

Position : FINAL YEAR PROJECT SUPERVISOR

Date : 21 JUNE 2012

STUDENT'S DECLARATION

I hereby declare that the work in this thesis entitled “Bearing Fault Detection using Discrete Wavelet Transform” is the result of my own research except as cited in the references. The thesis has not been accepted for any bachelor's degree concurrently submitted in candidature of any other degrees.

Signature :

Name : SYAHRIL AZEEM ONG BIN HAJI MALIKI ONG

ID Number : MA 09007

Date : 21 JUNE 2012

To my late father, beloved mother, siblings, and Aisyah Azmi

ACKNOWLEDGEMENT

In the name of Allah S.W.T the Most Beneficent and the Most Merciful. The deepest sense of gratitude to the Almighty for the strength and ability to complete this project. Infinite thanks I brace upon Him.

I would like to take this opportunity to express my sincere appreciation to my final year project's supervisor **Mr. Che Ku Eddy Nizwan bin Che Ku Hussin**, for the encouragement, guidance, morale support, and critics in bringing this project fruition. Also specifically to **Mr. Mohd Fadhlan bin Mohd Yusof**, and **Mr. Mohamad Zairi bin Baharom** for the theoretical explanation and guidance on data harnessing and MATLAB's coding. I am also thankful to **Advanced Structural Integrity & Vibration Research (ASiVR) Focus Group** for giving me the advice and related comments and critics on my project to the extent of its completion. Without their outstanding support and interest, this thesis would not have been at the best it would right now.

I would also like to express my deepest appreciation to my mother; Azizah binti Ishak, my sisters; Syahrul Hakimah Ong & Nadia Syahnaz Ong, and my brother; Nazif Syahmi Ong, whom had always supported me morally, financially, and their never-ending motivations to ensure that I complete this project with least difficulty.

Last but not least, I am also indebt to **Faculty of Mechanical Engineering, Universiti Malaysia Pahang** for the usage of workstation computer, equipments, administration, and references for analytical study purpose. My sincere appreciation also extends to all my colleagues, housemates, and friends whom had provided assistance at various occasions.

Finally to individuals who was involved either directly nor indirectly in succession of this thesis. Indeed I could never adequately express my indebtedness to all of them. Thank you.

ABSTRACT

Rolling element bearing has vast domestic and industrial applications. Appropriate function of these appliances depends on the smooth operation of the bearings. Result of various studies shows that bearing problems account for over 40% of all machine failures. Therefore this research is to design a test rig to harness data in terms of types of defects and rotation speed and also to develop method to detect features in vibration signals. Six set of bearings were tested with one of them remains in good condition while the other five has its own type of defects have been considered for analysis by using Discrete Wavelet Transform (DWT). The data for a good bearing were used as benchmark to compare with the defective ones. MATLAB's Discrete Wavelet Transform ToolBox was used to down-sample the vibration signals into noticeable form to detect defect features under certain frequency with respect to time. From the result generated, Fast Fourier Transform (FFT) and Root Mean Square (RMS) plays an important role in supporting results analyzed by using DWT from MATLAB[®] Toolbox. A system with low operating speed yields unsystematic results due to low excitation. As the speed increases, the excitation increases thus making DWT works effectively. For data of insufficient excitation, defect features still may be discovered by calculating and plotting graph for the percentage of RMS value of each decomposition level compared to the original input. This shows that DWT appears to be effective in pointing out the location and frequency of defect when the excitation is high enough. If the excitation is low, RMS value of each decomposition level may support the result. Nevertheless, DWT also proves to be an effective method for online condition monitoring tool. Future research should be detecting defect features by using envelope analysis or based on statistical tools.

ABSTRAK

Galas mempunyai aplikasi domestik dan industri yang luas. Fungsi yang sesuai bagi peralatan serta mesin-mesin bergantung kepada kelancaran galas. Hasil daripada pelbagai kajian menunjukkan bahawa masalah galas merangkumi lebih 40% daripada kesemua punca kegagalan mesin. Oleh itu, kajian ini adalah untuk mereka bentuk sebuah rig ujian bagi memperoleh isyarat getaran dari segi jenis kecacatan dan kelajuan putaran. Kajian ini juga bertujuan untuk membangunkan kaedah untuk mengesan ciri-ciri di dalam isyarat getaran tersebut. Enam set galas telah diuji dengan salah satu daripadanya masih dalam keadaan baik manakala lima yang lain mempunyai jenis-jenis kecacatan yang tertentu dan telah digunakan bagi analisis menggunakan kaedah Penjelmaan Anak Gelombang Diskrit (DWT). Isyarat getaran yang diperoleh daripada galas baik telah digunakan sebagai penanda aras untuk dibandingkan dengan isyarat getaran yang diperoleh dari galas yang tidak sempurna. DWT daripada *MATLAB ToolBox* telah digunakan untuk mengurai isyarat-isyarat getaran kepada bentuk yang lebih ketara bagi mengesan ciri-ciri kecacatan di bawah frekuensi tertentu dengan merujuk kepada masa. Hasil daripada analisis menunjukkan, Penjelmaan Fourier Pantas (FFT) dan Punca Min Kuasa Dua (RMS) memainkan peranan penting dalam menyokong keputusan yang dianalisis dengan menggunakan DWT dari *MATLAB ToolBox*. Sistem dengan kelajuan operasi yang rendah menunjukkan keputusan yang tidak sistematik kesan daripada pengujian yang rendah. Apabila kelajuan bertambah, peningkatan pengujian menyebabkan analisis DWT dapat dilakukan lebih berkesan. Untuk data yang mempunyai pengujian yang rendah, ciri-ciri kecacatan masih boleh ditemui melalui pengiraan dan graf peratusan nilai RMS bagi setiap tahap penguraian berbanding dengan input asal. Ini menunjukkan bahawa DWT berkesan dalam menunjukkan lokasi dan kekerapan kecacatan apabila mempunyai pengujian yang cukup tinggi. Jika pengujian rendah, nilai RMS bagi setiap tahap penguraian mampu menyokong keputusan. DWT juga telah terbukti menjadi kaedah yang berkesan sebagai alat pemantauan keadaan talian. Kajian akan datang perlu mengesan ciri-ciri kecacatan dengan menggunakan analisis sampul surat atau berdasarkan alat statistik.

TABLE OF CONTENTS

	PAGE
EXAMINER’S DECLARATION	ii
SUPERVISOR’S DECLARATION	iii
STUDENT’S DECLARATION	iv
ACKNOWLEDGEMENT	v
ABSTRACT	vi
ABSTRAK	vii
TABLE OF CONTENTS	viii
LIST OF TABLES	x
LIST OF FIGURES	xi
LIST OF SYMBOLS	xiv
LIST OF ABBREVIATIONS	xv
 CHAPTER 1 INTRODUCTION	 1
1.1 Introduction	1
1.2 Problem Statement	2
1.3 Objective	3
1.4 Hypothesis	3
1.5 Scope of Project	3
 CHAPTER 2 LITERATURE REVIEW	 4
2.1 Introduction	4
2.2 Bearing	5
2.2.1 Types of bearing defects	5
2.3 Signal Processing Analysis	7
2.3.1 Frequency domain analysis	7
2.2.2 Time frequency analysis: Short-Time Fourier Transform	10

2.2.3 Time frequency analysis: Discrete Wavelet Transform	12
2.4 Condition Monitoring Method	15
CHAPTER 3 METHODOLOGY	17
3.1 Introduction	17
3.2 Design of Experiment	19
3.3 Experimental Setup	20
3.3.1 Sensor calibration	21
3.3.2 Tested bearings	22
3.3.3 Test rig design & fabrication	25
3.4 Data Analysis	27
3.5 Data Processing Algorithm	28
3.5.1 Discrete Wavelet Transform	28
3.5.2 Analysis using Discrete Wavelet Transform Toolbox	32
CHAPTER 4 RESULTS & DISCUSSION	34
4.1 Introduction	34
4.2 Data Acquisition	35
4.3 Decomposition Result	37
4.4 Root Mean Square Percentage Analysis	47
4.4.1 RMS Data for 2664 rpm	48
4.4.2 RMS Data for 1466 rpm	50
4.4.3 RMS Data for 287 rpm	52
CHAPTER 5 CONCLUSION & RECOMMENDATIONS	56
5.1 Conclusion	56
5.2 Recommendations	57
REFERENCES	58

APPENDICES

A	RESEARCH GANTT CHART	61
B	TECHNICAL DRAWINGS	62
C	CNC MACHINE CODING	63
D	FFT GRAPH	64

LIST OF TABLES

Table No		Page
2.1	Types of bearing damage, appearance, and possible cause	6
2.2	Fault description in the ball bearings	16
3.1	Number of experiment run with various bearing defects	19
3.2	Types and location of defect	22
4.1	RMS percentage value for each level of decomposition at 2664 rpm	48
4.2	RMS percentage value for each level of decomposition at 1466 rpm	50
4.3	RMS percentage value for each level of decomposition at 287 rpm	52

LIST OF FIGURES

Figure No		Page
2.1	Cutaway view of a caged ball bearing	5
2.2	A typical spectrum obtained from a rolling element bearing with an inner race defect	9
2.3	STFT in displacement (a), velocity (b), and acceleration (c) of a good bearing. The colour associates to the higher value of the energy scale, and represents a high level of energy content	11
2.4	STFT in displacement (a), velocity (b), and acceleration (c) of a faulty bearing. The colour associates to the higher value of the energy scale, and represents a high level of energy content	12
2.5	Comparison of known transformation methods. Time-series (a), Fourier transform (b), STFT (c), and Wavelet transform (d)	14
3.1	Project's flow chart	18
3.2	Bearing fault detection test rig consist of: coupling (a), tested bearing (b), flywheel (c), healthy bearing (d), accelerometer (e), data acquisition system (f), and a PC with DASylab software (g)	20
3.3	Actual bearing test rig	21
3.4	Outer race defect	22
3.5	Inner race defect	23
3.6	Contaminated defect	23
3.7	Point defect	24
3.8	Corroded defect	24
3.9	Healthy bearing	25
3.10	Bearing housing's isometric view	26
3.11	Fly wheel's isometric view	26

3.12	Shaft's front view	27
3.13	DASYLab's layout	27
3.14	Flow chart for decomposition process by using MATLAB [®] 's command	29
3.15	Filtering process at its most basic level	30
3.16	Down-sampling process from left to right	30
3.17	Wavelet decomposition tree	31
3.18	Discrete Wavelet Transform's Toolbox main menu	32
3.19	Selecting data (a), choosing wavelet type (b), and changing display mode (c)	33
3.20	Output for MATLAB Discrete Wavelet Transform's Toolbox	33
4.1	Vibration reading when running at 287 rpm for healthy bearing (a), PD (b), OR defect (c), IR defect (d), CN defect (e), and CB defect (f)	35
4.2	Vibration reading when running at 1466 rpm for healthy bearing (a), PD (b), OR defect (c), IR defect (d), CN defect (e), and CB defect (f)	36
4.3	Vibration reading when running at 2664 rpm for healthy bearing (a), PD (b), OR defect (c), IR defect (d), CN defect (e), and CB defect (f)	37
4.4	Decomposition result for healthy bearing at 287 rpm	38
4.5	Decomposition result for healthy bearing at 1466 rpm	39
4.6	Decomposition result for healthy bearing at 2664 rpm	49
4.7	Decomposition result for outer race defect at 287 rpm	40
4.8	Decomposition result for outer race defect at 1466 rpm	40
4.9	Decomposition result for outer race defect at 2664 rpm	41
4.10	Decomposition result for inner race defect 287 rpm	41

4.11	Decomposition result for inner race defect 1466 rpm	42
4.12	Decomposition result for inner race defect 2664 rpm	42
4.13	Decomposition result for corroded defect at 287 rpm	43
4.14	Decomposition result for corroded defect at 1466 rpm	43
4.15	Decomposition result for corroded defect at 2664 rpm	44
4.16	Decomposition result for point defect at 287 rpm	44
4.17	Decomposition result for point defect at 1466 rpm	45
4.18	Decomposition result for point defect at 2664 rpm	45
4.19	Decomposition result for contaminated defect at 287 rpm	46
4.20	Decomposition result for contaminated defect at 1466 rpm	46
4.21	Decomposition result for contaminated defect at 2664 rpm	47
4.22	RMS percentage vs. decomposition level for speed of 2664 rpm	49
4.23	RMS percentage vs. decomposition level for speed of 1446 rpm	51
4.24	RMS percentage vs. decomposition level for speed of 287 rpm	53
4.25	FFT result for contaminated defect at speed 297 rpm	55

LIST OF SYMBOLS

ω_s	-	Shaft rotation frequency
α	-	Contact angle
$Han(h)$	-	Hanning function
$V(t_n)$	-	n th measured voltage sample
$\Psi(t)$	-	Mother wavelet

LIST OF ABBREVIATIONS

AE	-	Acoustic Emission
BG	-	Burnt grease
B&K	-	Brueel & Kjaer
cA	-	Approximate decomposition
CB	-	Corroded ball
cD	-	Detailed decomposition
CWT	-	Continuous Wavelet Transform
DWT	-	Discrete Wavelet Transform
FFT	-	Fast Fourier Transform
HDD	-	Hard disk drive
HFRT	-	High frequency resonance technique
IR	-	Inner race
NDT	-	Non-destructive test
NiDAQ	-	National Instrument Data Acquisition System
OR	-	Outer race
PC	-	Personal computer
PD	-	Point defect
RMS	-	Root Mean Square
RPM	-	Revolutions per minute
SPM	-	Shock Pulse Method
STFT	-	Short Time Fourier Transform
UI	-	User interface

CHAPTER 1

INTRODUCTION

1.1 INTRODUCTION

Rolling element bearings has vast domestic and industrial applications. Appropriate function of these appliances depends on the smooth operation of the bearings. In industrial applications, bearings are considered as critical mechanical components and a defect in such a bearing causes malfunction and may even lead to catastrophic failure of the machinery.

Presently, vibration monitoring method becomes the most reliable tool as a part of preventive maintenance for rotating machines (Tandon and Choudhury, 1999). The vibration data often contain fault signatures where several signal processing techniques; often adapted to a precise defect type, results to online monitoring system.

There are many condition monitoring methods used for detection and diagnosis of rolling element bearing defects such as vibration measurements, temperature measurement, shock pulse method (SPM), and acoustic emission (AE). Various researchers suggested that stator current monitoring can provide the same indications without requiring access to the motor. This technique utilizes results of spectral analysis of the stator current or supply current of any part nearest to the rolling bearing element for diagnosis purpose (Schoen *et al*, 1995). Other signal processing technique for condition monitoring method includes averaging technique (Braun and Datner, 1977), adaptive noise cancelling (Chaturvedi and Thomas, 1981), and high-frequency

resonance technique (HFRT) (Prasad *et al*, 1984) was developed to improve signal-to-noise ratio for more effective detection of bearing defect. Among all these monitoring methods, the high-frequency resonance technique is more popular for bearing fault detection. However, most of the method requires additional computations and several runs of impact tests to find the bearing resonance frequency. Therefore, extra instruments such as vibration exciters and their controller are needed for HFRT (Prabhakar *et al*, 2002).

Discrete Wavelet Transform (DWT) on the other hand, were proven to be the best condition monitoring method/effective tool for detecting single and multiple faults in the ball bearings (Djebala *et al*, 2007; Prabhakar *et al*, 2002). A clear review on using DWT as condition monitoring method and possible early detection was given by Tandon and Choudhury (1999), Kim *et al*. (2002), and Staszewski (1998).

1.2 PROBLEM STATEMENT

Rolling bearings are the major components of rotating machine. Thus they are often subjected to various excitations which can cause dangerous accidents due to certain factors. Results of various studies show that bearing problems account for over 40% of all machine failure (Schoen 1995).

This data acquisition technique is a type of non destructive test (NDT) which doesn't require the user to dismantle the bearing from the machine in order to check its condition as it may be presented through online monitoring.

Time-domain analysis lacks information in terms of frequency while frequency-domain analysis lacks information on time. Even though Short Time Fourier Transform (STFT) have both time and frequency domain analysis, but it is less accurate on both domain of analysis. But DWT on the other hand, produces vibratory signal in terms of time and frequency domain analysis which gives the most accurate readings for caged-roller bearing which is why DWT was chosen as the tool to analyze bearing defects.

1.3 OBJECTIVE

The objective of this project is:

- a) Design a test rig to harness vibration data in terms of types of defects and rotation speed
- b) Develop method to detect the defect features in the vibration signals by using time-frequency domain analysis

1.4 HYPOTHESIS

The expected result for this research is that there will be a difference in terms of vibration signals when bearing with different type of defects were tested by using wavelet transform method. DWT method is an advanced method to detect any changes in terms of vibration signal.

1.5 SCOPE OF PROJECT

In order to reach the project's objective, the following scopes are identified:

- a) Only horizontal deep groove ball bearings will be used
- b) Five types of bearing defects will be tested and they are outer race (OR) defect, inner race (IR) defect, point defect (PD), corroded ball (CB) defects, contaminated defect (CN), and a good condition bearing as the reference
- c) Three different angular speed of lowest, medium, and highest speed will be used to acquire data for each bearings
- d) Acquire vibration data from the rotating machine using a single axial accelerometer
- e) Analysis will be done by using MATLAB[®]'s Discrete Wavelet Transform ToolBox

CHAPTER 2

LITERATURE REVIEW

2.1 INTRODUCTION

This chapter discusses the literatures that are related to bearing fault detection and discrete wavelet transform. In this chapter, the types of bearings, types of bearing defects, and common causes of bearing failures will be discussed. Moreover, the signal processing analysis on different types of domain analysis, and condition monitoring methods also on different types of domain analysis will also discussed.

2.2 BEARING

Bearing; as shown in Figure 2.1, is a mechanical device that allows constrained relative motion of 2 or more parts; typically between linear and rotational movement. There are many types of bearings often used in machineries when it involves rolling element and each one of them used for different purpose. These include ball bearings, caged ball bearings, roll thrust bearings, and tapered roller thrust bearings.

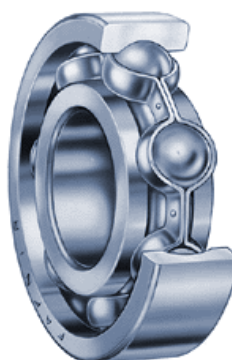


Figure 2.1: Cutaway view of a caged ball bearing

Source: The Timken Company. (2011)

2.2.1 Types of bearing defects

As well as there's continuous usage there will always be unwanted defects on the material of the bearing. Generally, a rolling bearing cannot rotate forever. Under normal operating conditions of balanced load and good alignment, fatigue failure begins with a small fissure, located between the surface of the raceway and the rolling elements, which gradually propagate to the surface, generating detectable vibrations and increasing noise levels (Eschmann *et al* 1958). Continued stress causes fragments of the material to break loose producing a localized fatigue phenomenon known as flaking or spalling (Riddle 1955). The affected area expands rapidly afterwards contaminating the lubrication and

causing localized overloading over the entire circumference of the raceway (Eschmann *et al* 1958). Eventually, the failure results in rough running of the bearing

There are several types of common defects which may be clustered into 2 main types of bearing damages; primary and secondary damage. Primary damage consists of: wear, indentations, smearing, surface distress, corrosion, and electric current damage. While secondary damage consists of flaking and cracks. Table 2.1 shows different types of bearing damage, its appearance and cause.

Table 2.1: Types of bearing damage, appearance, and possible causes

Damage Type	Appearance	Causes
Wear	<ul style="list-style-type: none"> • Small indentations around the raceways and rolling elements • Grease discoloured green • Depressions in the raceways 	<ul style="list-style-type: none"> • Lack of cleanliness during mounting • Ineffective seals • Exposed to vibration while stationary
Indentations	<ul style="list-style-type: none"> • Indentations in the raceways of both rings with spacing equal to the distance between the rolling elements • Small indentations distributed around the raceways of both rings and in the rolling elements 	<ul style="list-style-type: none"> • Mounting pressure applied to the wrong ring • Excessively hard drive-up on tapered seating • Ingress of foreign particles into the bearing
Smearing	<ul style="list-style-type: none"> • Scored and discoloured roller ends and flange faces • Scored and discoloured areas at the start of the load zone in raceways • Scored and discoloured ring bore or outside surface or faces • Diagonal smear streaks in the raceways 	<ul style="list-style-type: none"> • Sliding under heavy axial loading • Roller acceleration on entry into the loaded zone • Ring rotation relative to shaft or housing • Loading too light in relation to speed of rev
Surface Distress	<ul style="list-style-type: none"> • Small, shadow crates with crystalline fracture surface (not visible) 	<ul style="list-style-type: none"> • Inadequate or improper lubrication

Table 2.1: Continued

Damage Type	Appearance	Causes
Electric Current	<ul style="list-style-type: none"> • Dark brown/greyish black fluting in raceways and rollers • Localised burns in raceways 	<ul style="list-style-type: none"> • Passage of electric current through rotating bearing • Passage of electric current through static bearing
Flaking	<ul style="list-style-type: none"> • Heavily marked path pattern in raceways of both rings 	<ul style="list-style-type: none"> • Preloading on account of fits being too tight • Temperature differential between inner and outer rings too greatly
Cracks	<ul style="list-style-type: none"> • Bearing ring has cracked right through and lost its grip on the shaft 	<ul style="list-style-type: none"> • Excessive drive-up on a tapered seating/sleeve
Corrosion	<ul style="list-style-type: none"> • Greyish black streaks across the raceways • Raceway path pattern heavily marked at corresponding positions 	<ul style="list-style-type: none"> • Presence of water, moisture • Shaft or housing seating with errors of form

Source: SKF Handbook, 1994

2.3 SIGNAL PROCESSING ANALYSIS

2.3.1 Frequency domain analysis

Frequency-domain, also may known as spectral analysis of the vibration signal, is the most widely used method of bearing defect detection. The advent of modern Fast Fourier Transform (FFT) analysers to obtain narrowband spectra became easier and more efficient. Both low and high-frequency ranges of the vibration spectrum are of interest in assessing the condition of the bearing (Tandon and Choudhury 1999).

When an interaction of defect occurs in rolling element bearings, it produces pulses of very short duration. There will be an increase in the vibrational energy during high frequency due to the pulses excites the natural frequencies of bearing elements or the nearby structures. The resonant frequencies may be calculated theoretically as proved by (Tandon and Nakra, 1992).

Each bearing elements has their own characteristic rotational frequency. There's an increase in vibrational energy at the element's rotational frequency whenever there's a defect on a particular bearing. These characteristic defect frequencies can be calculated from kinematic considerations. For a bearing with a stationary outer race, these frequencies are given by the following expressions:

Cage frequency ω_c , proposed by Mathew and Alfredson (1984):

$$\omega_c = \frac{\omega_s}{2} \left(1 - \frac{d}{D} \cos \alpha \right) \quad (2.1)$$

Ball spinning frequency ω_b , proposed by McFadden and Smith (1984a):

$$\omega_b = \frac{D\omega_s}{2d} \left(1 - \frac{d^2}{D^2} \cos^2 \alpha \right) \quad (2.2)$$

Outer race defect frequency ω_{OD} , proposed by Kim (1984a):

$$\omega_{OD} = Z\omega_c = \frac{Z\omega_s}{2d} \left(1 + \frac{d}{D} \cos \alpha \right) \quad (2.3)$$

Inner race defect frequency ω_{ID} , also proposed by Kim (1984b):

$$\omega_{ID} = Z(\omega_s - \omega_c) = \frac{Z\omega_s}{2} \left(1 + \frac{d}{D} \cos \alpha \right) \quad (2.4)$$

and

Rolling element defect frequency ω_{rc} , proposed by Sunnersjo (1978):

$$\omega_{rc} = 2\omega_b = \omega_s \frac{D}{d} \left(1 + \frac{d^2}{D^2} \cos^2 \alpha \right) \quad (2.5)$$

where,

ω_s is the shaft rotation frequency in rad/s

d is the diameter of the rolling element

D is the pitch diameter

Z is the number of rolling elements, and

α is the contact angle.

For normal speeds, these defect frequencies are usually less than 500 Hz (Tandon and Choudhury, 1999). However, these frequencies may be slightly different from values calculated as there are other external factors that influence the results such as slipping or skidding in the rolling element bearings (Prasad, 1987). An example of typical spectrum due to an inner race defect is shown in Figure 2.2. The sidebands have been attributed to the time-related changes in defect position relative to the vibration measuring position (Igarashi and Hamada, 1982). Tandon and Choudhury in 1999 manage to derive an expression for frequencies and relative amplitudes of the various spectral lines based on the flexural vibration of races due to a localized defect on one of the bearing elements.

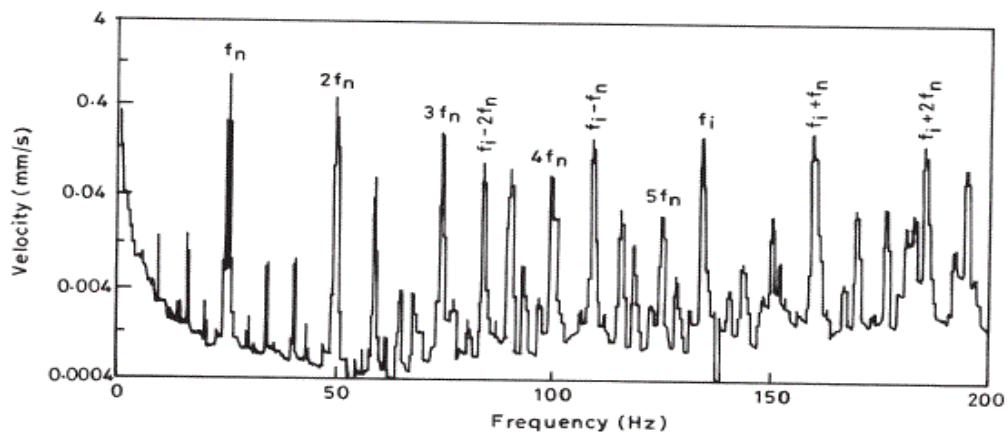


Figure 2.2: A typical spectrum obtained from a rolling element bearing with an inner race defect

Source: Tandon and Choudhury. (1999)

2.3.2 Time-frequency analysis: Short Time Fourier Transform

One of the shortcomings of the Fourier Transform is that it doesn't give information on time at which a frequency component occurs. It will be a major problem to non-stationary signals compared to stationary signals. Therefore, one approach which can give information on the time resolution of the spectrum is the Short Time Fourier Transform (STFT). The STFT as proposed by Lyon (1984) is defined as:

$$STFT(t_n, f_k) = \sum_{h=-\frac{L}{2}}^{\frac{L}{2}-1} V(t_{n-h}) Han(h) \exp(-2\pi j h f_k \Delta t) \quad (2.6)$$

where L represents the length of one block of data, t_n is the time instant of STFT and $V(t_n)$ is the n th measured voltage sample. The term $Han(h)$ represents the Hanning function chosen as the analysis window.

Figure 2.3 and Figure 2.4 represents the STFT computed for a good and a faulty bearing. The displacement measurements by laser vibrometer reveal vertical lines caused by a single dropout, which add impulse noise to the signal. The disturbances have not appeared in any of the measurements of velocity and acceleration.

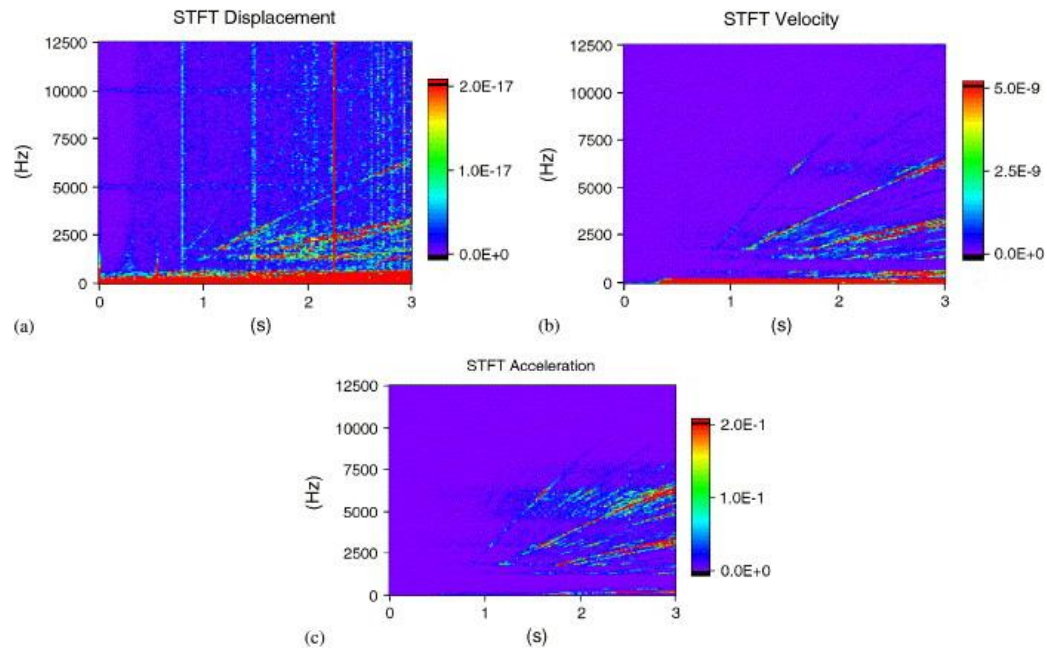


Figure 2.3: STFT in displacement (a), velocity (b), and acceleration (c) of a good bearing. The colour associates to the higher value of the energy scale, and represents a high level of energy content

Source: Cristalli *et al.* (2006)

The downside of the STFT is that it has a fixed resolution. The signal is presented with relation to the width of the windowing function. It determines whether there is good frequency resolution or good time resolution. A narrower window results to poor frequency resolution while wider window results to poor time resolution (Othman, 2009).

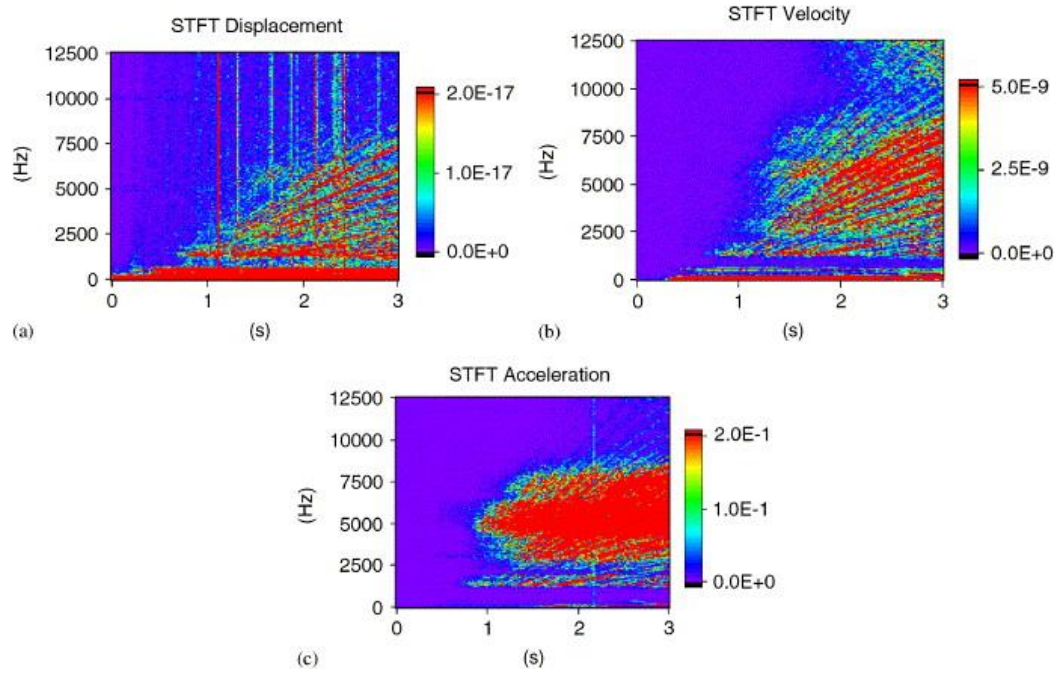


Figure 2.4: STFT in displacement (a), velocity (b), and acceleration (c) of a faulty bearing. The colour associates to the higher value of the energy scale, and represents a high level of energy content

Source: Cristalli *et al.* (2006)

2.3.3 Time-frequency analysis: Discrete Wavelet Transform

Discrete wavelet transform (DWT) provides a time-scale information of a signal, enabling the extraction of features that vary in time. This property makes wavelets an ideal tool for analyzing signal of a transient or non-stationary nature (Prabakhar, 2002). The continuous wavelet transform (CWT) of $f(t)$ is a time-scale method that may be identified as the sum over all time of the signal multiplied by scaled, shifted versions of the wavelet function $\Psi(t)$. Mathematically as proposed by McFadden and Smith (1984b),

$$CWT(a, b) = \frac{1}{\sqrt{|a|}} \int_{-\infty}^{\infty} f(t) \Psi^* \left(\frac{t-b}{a} \right) dt \quad (2.7)$$

where $\Psi(t)$ denotes the mother wavelet. The parameter a represents the scale index which is a reciprocal of frequency. The parameter b indicates the time shifting (or translation). The DWT is derived from the discretization of CWT (a, b) and the most common discretization is dyadic, given also by McFadden and Smith (1985) as,

$$DWT(j, k) = \frac{1}{\sqrt{2^j}} \int_{-\infty}^{\infty} f(t) \Psi^* \left(t - \frac{2^j k}{2^j} \right) dt \quad (2.8)$$

where a and b are replaced by 2^j and $2^j k$. An effective way to apply this method using filters was developed by Mallat in 1989. $f(t)$ passes through two complementary filters and emerges as low and high frequency signals. The decomposition may be iterated with successive approximations begin decomposed in turn, so that signals may be broken down into lower-resolution components.

Figure 2.5 shows the comparison of four transformation methods. Time-domain analysis has a better time resolution while frequency (Fourier transform) has a better frequency resolution. While STFT is equal on both where it has fixed resolution, DWT on the other hand provides a time-scale information of a signal, enabling the extraction of features that varies in time.

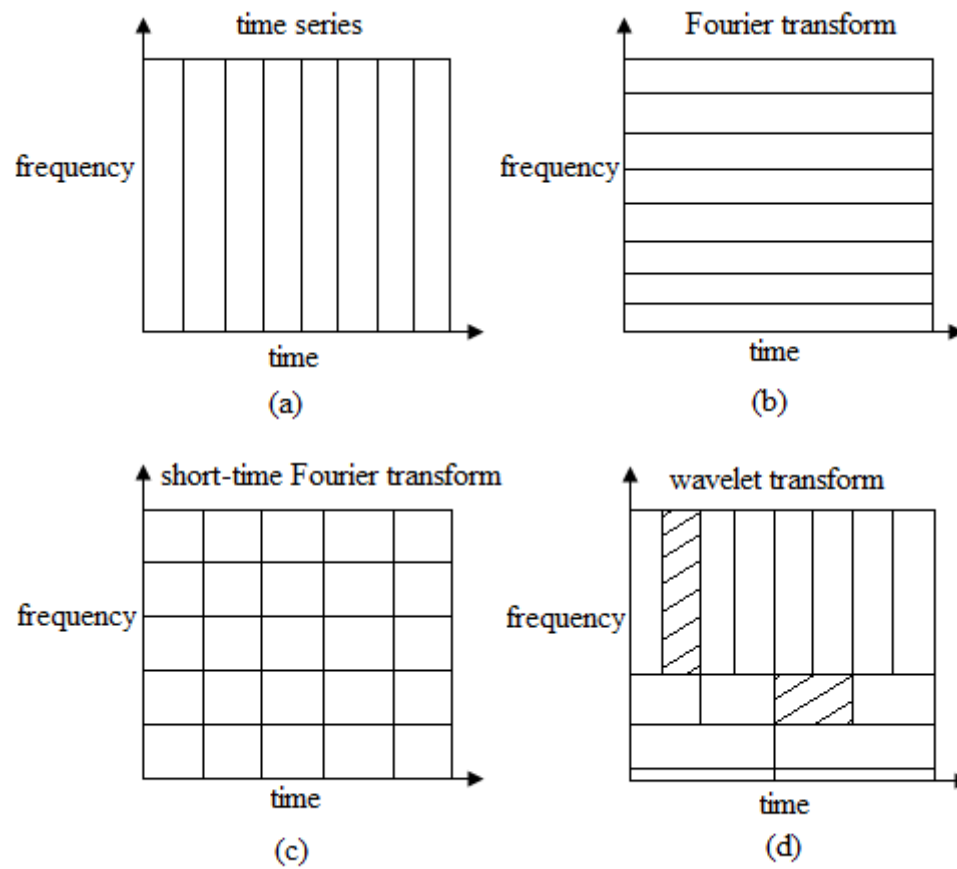


Figure 2.5: Comparison of known transformation methods. Time-series (a), Fourier transform (b), STFT (c), and Wavelet transform (d)

Source: Othman. (2009)

Various successful papers shows that DWT were proven to be an effective tool for detecting single and multiple faults, specifically for ball bearings (Purushotham *et al*, 2005; Prabhakar *et al*, 2002; Mori *et al*, 1996; Staszewski, 1998; Lou and Loparo, 2004; Kim *et al*, 2007).

2.4 CONDITION MONITORING METHOD

There are various methods used throughout the whole world for condition monitoring. Question mark arises when discussions and debates on which methods gives the best required and most precise result. The signals of rolling bearings faults are usually transient and modulated by high frequency carrier signals (Nikolaou, 2002) (Khalid, 2007).

Prabhakar *et al*, (2002) in their research in applying DWT for detection of ball bearing race faults were introduced in the inner race and outer race of the ball bearings by making a scratch mark with an electric pulse, the bearing components were then assembled as different bearings at a bearing manufacturer's plant. All scratch marks are of the same size with 2 mm length, 500 μm width, and 300 μm depth. Table 2.2 shows the type of faults introduced. In the present investigation of the bearings, the balls and cage were not scratched. The ball bearings were then tested one by one in a ball bearing noise and vibration test facility. The bearing vibration signals were acquired by mounting a Bruel & Kjaer (B&K) 4399 accelerometer directly on the outer race and an FFT analyzer with a sampling frequency of 25.6 kHz ($\Delta t = 0.039$ ms). The signals were then analyzed using DWT.

Three types of defects were simulated on a 6200 ball bearings by Djebala *et al* (2008) in their research, also to detect rolling bearing defects using DWT analysis. Defects were artificially localized in a rectangular shape by a diamante tool turning with 50,000 revolutions per minute (RPM). The defects sizes are (width \times depth) = (1 \times 0.3) mm for the small defect and (1.3 \times 0.7) mm for the great one. Measurement were taken by a B&K 4384 type accelerometer and a B&K 2035 type analyzer, the post processing is carried out on MATLAB[®]. The test rig uses two rotating discs to simulate a dynamic load.

Table 2.2: Fault description in the ball bearings

Bearing Number	Location of the defect	Type of defects
1	Good bearing	No scratch mark
2	Inner race (on the track)	One scratch mark
3	Outer race (on the track)	One scratch mark
4	Outer race (180 apart on the track)	Two scratch mark
5	Inner race (on the track) and outer race (on the track)	One scratch mark on each race

Source: Prabhakar *et al.*, 2002

CHAPTER 3

METHODOLOGY

3.1 INTRODUCTION

The project starts off with project planning by using a Gantt chart as shown in appendix A and a flow chart as shown in Figure 3.1. The flow chart acts as a guide to successfully carry out this case study step by step while the Gantt chart helps to make sure that the project is within its timeframe. It is then furthered with countless literature review throughout the whole project. Followed by designing experiment procedure and continued with experimental setup.

Data acquisition using accelerometer is the backbone of this project, therefore practicing calibration before data acquisition is imperative in order to achieve the expected result. Once this has been done, the data was further processed by using MATLAB[®]'s toolbox to develop a vibratory reading on time-frequency domain chart. Finally the analysis of the whole project may be tabulated, further discussed, and concluded in the following chapter after all of the data acquired being verified.

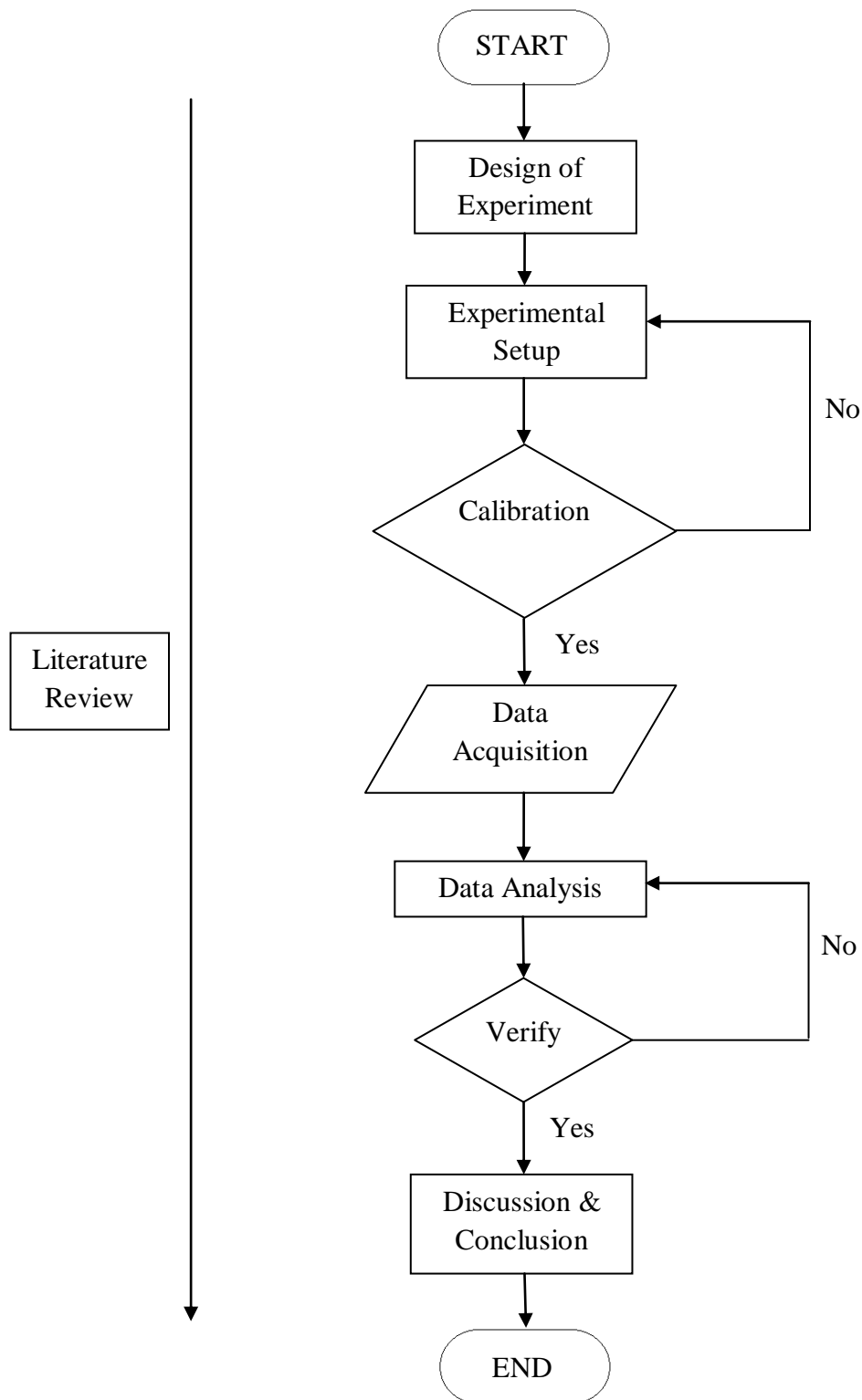


Figure 3.1: Project's flow chart

3.2 DESIGN OF EXPERIMENT

The test rig for this experiment was design to investigate failure and vibration characteristic of ball bearings. It was designed specifically to imitate the applications of ball bearings in the industry. The shaft was driven by a variable-speed 0.37kW, 50Hz electric motor with a frequency converter in order to control the speed of the motor. The motor and shaft were connected by using a spring coupling where it could minimize shaft alignment error. The front side of the shaft is fitted with tested bearing and the other will be fitted with a good bearing acting as a dummy. A set of good bearings and another five bearings with different type of defectives were used for testing. A flywheel is installed at the middle of the spindle in order to apply load to the shaft and at the same time minimizing the speed oscillations of the shaft (Nizwan *et al*, 2010). The angular speed is set to 287 rpm, 1466 rpm, and 2664 rpm and the vibration signals were acquired by using the Bruel & Kjaer (B&K) 4506B accelerometer. Sensors were placed on horizontal directions to collect the data because horizontal bearing types were tested. Accelerations signals are acquired by using a personal computer (PC) based data acquisition system. Sampling frequency of 25.6 kHz or 20 kHz ($\Delta t = 0.039$ ms) (Prabhakar *et al*, 2002). The MATLAB[®]'s coding from its Toolbox were used to process the data while DASyLab software were used to read vibration data from the data acquisition system. The summary of the experiment is shown in Table 3.1.

Table 3.1: Number of experiment run with various bearing defect types

Exp.	Speed(rpm)	Bearing Type
1	287	OR defect, IR defect, P defect, CN defect, CB defects, & Healthy
2	1,466	OR defect, IR defect, P defect, CN defect, CB defects, & Healthy
3	2,664	OR defect, IR defect, P defect, CN defect, CB defects, & Healthy

3.3 EXPERIMENTAL SETUP

The tools for this experiment are as shown in Figure 3.2.

- a) Spring coupling to minimize coupling error
- b) Tested bearing
- c) Flywheel to minimize oscillation
- d) Healthy bearing as a dummy
- e) Accelerometer B&K 4506B
 - Type: 30153 Triple Axes, AO 0526-D-050 23/06
- f) National Instrument Data Acquisition System (NiDAQ)
 - Type: N19234, 4 Input, 24-Bit, 51.2 ks/sample, S/N: 16AB336
- g) PC with DASyLab software

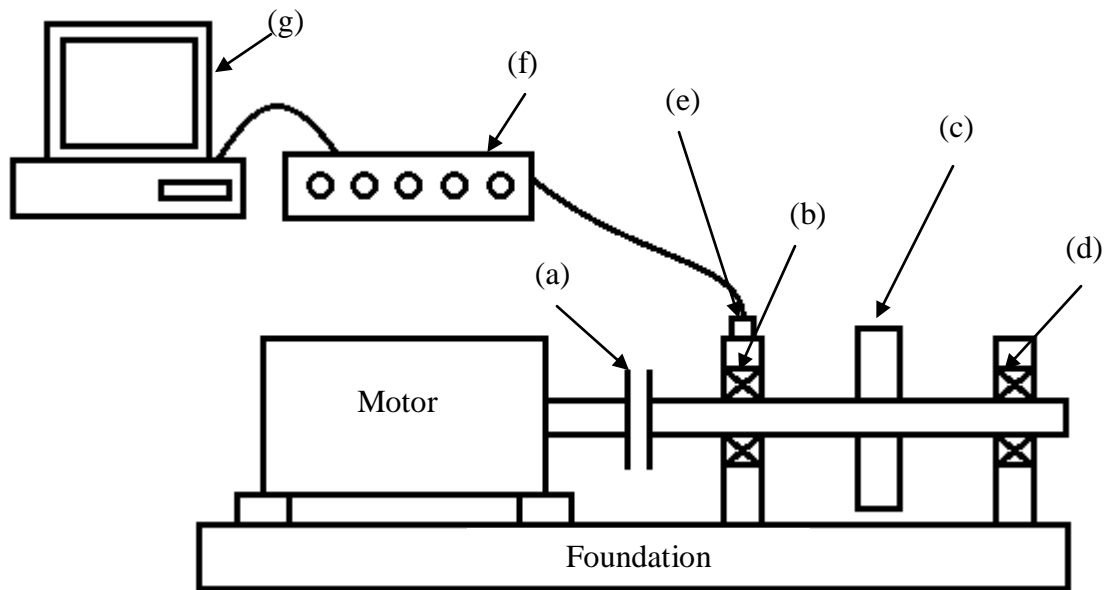


Figure 3.2: Bearing fault detection test rig consist of: coupling (a), tested bearing (b), flywheel (c), healthy bearing (d), accelerometer (e), data acquisition system (f), and a PC with DASyLab software (g).

Figure 3.3 shows the actual bearing test rig that was used during this experiment.

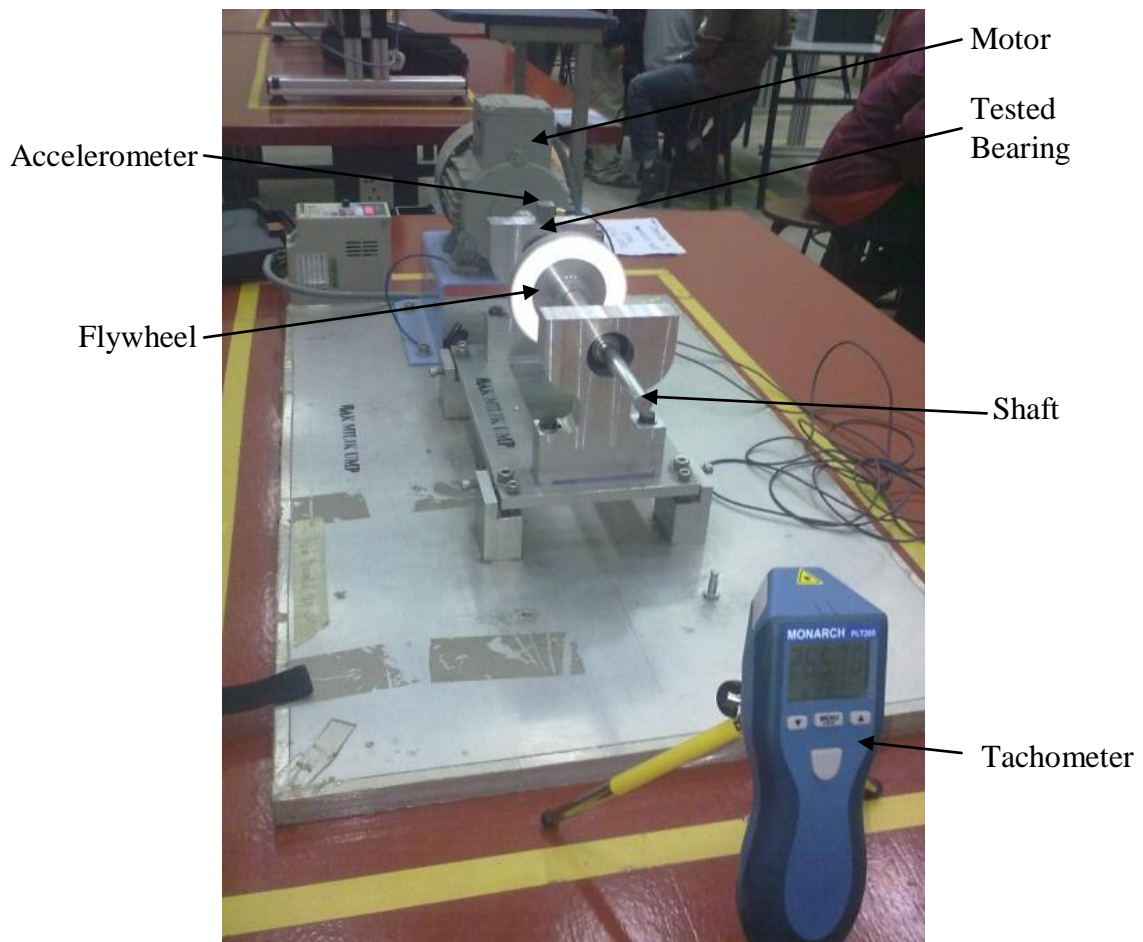


Figure 3.3: Actual bearing test rig

3.3.1 Sensor Calibration

Calibration is an important step to ensure that the instrument is performing as it is designed to. Correct and meaningful vibration transducer calibration ensures traceability to an absolute physical standard, which provides a defined degree of confidence in all of your vibration measurements. To calibrate a vibration accelerometer is to accurately determine its sensitivity (in mV/g or pC/g) where the sensitivity of the accelerometer were determined from its user manual. The sensitivity for this accelerometer is 95.21 mV/g.

3.3.2 Tested Bearings

There are six bearings that were tested for this experiment and five of them are defected. Figure 3.4 shows an outer race defect, Figure 3.5 shows an inner race defect, Figure 3.6 shows a contaminated defect, Figure 3.7 shows a point defect, Figure 3.8 shows a corroded defect, and Figure 3.9 shows a healthy bearing. Table 3.2 shows the types of defect and the location of each defect specifically.

Table 3.2: Types and location of defect

Types of Defect	Location of Defect
Outer race defect	One scratch mark on the outer race
Inner race defect	One scratch mark on the inner race
Contaminated defect	Lubrication was contaminated with tiny chips
Point defect	Single point mark on the inner race
Corroded defect	Ball bearing were left to open air and water

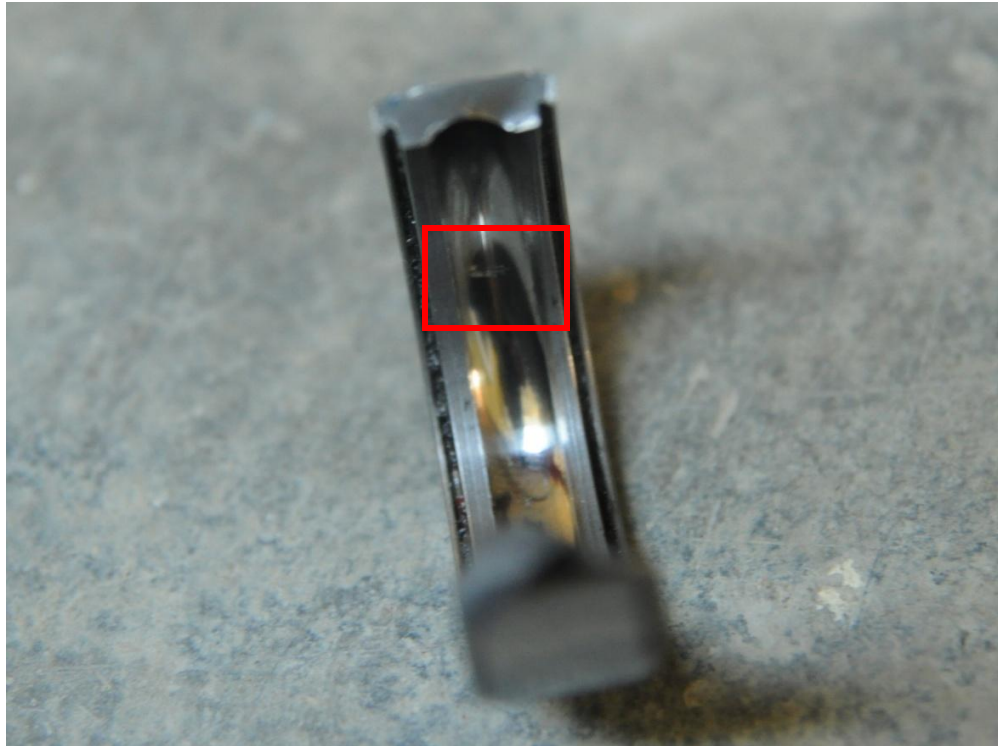


Figure 3.4: Outer race defect



Figure 3.5: Inner race defect



Figure 3.6: Contaminated defect

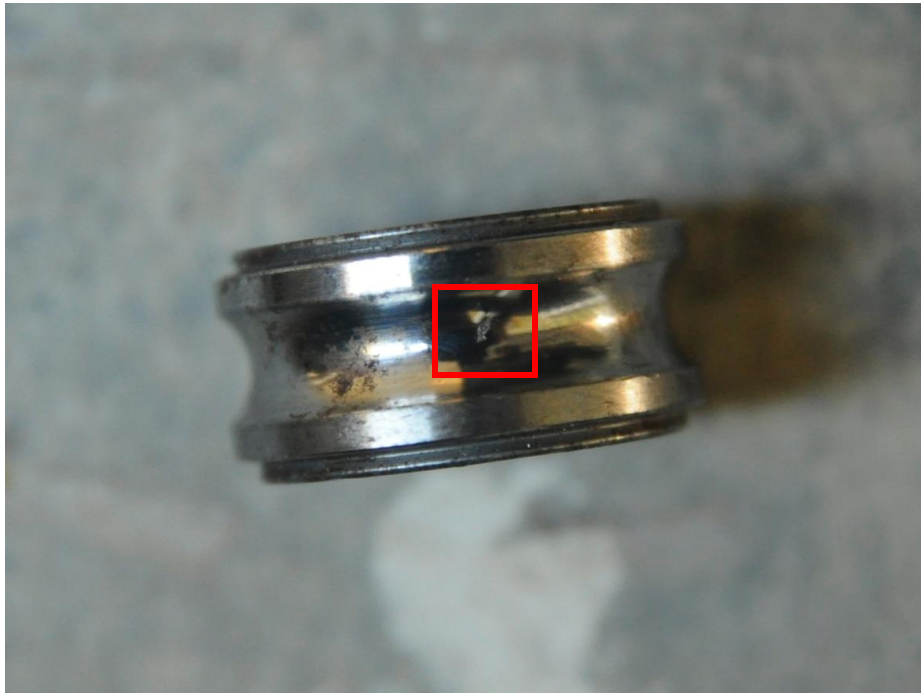


Figure 3.7: Point defect



Figure 3.8: Corroded defect



Figure 3.9: Healthy bearing

3.3.3 Test Rig Design & Fabrication

In developing the test rig to acquire sufficient vibration data, the test rig must be as practical as possible. Thus the accelerometer will be placed as nearest as possible to the bearing so that the vibration could quickly reach the accelerometer. Figure 3.10 shows the isometric view of the designed bearing housing, Figure 3.11 shows the isometric view of the flywheel, and Figure 3.12 shows the front view of the shaft. Detailed technical drawings with dimensions for all these three parts may be referred in appendix B.

The bearing housing were fabricated by using a CNC-FANUC Milling Machine because ultimate precision is needed during machining where the tolerance allowed for bearing tight-fitting is only 20 μm to avoid skidding (SKF Handbook, 1994). Coding used for the fabrication process may be referred in appendix C.

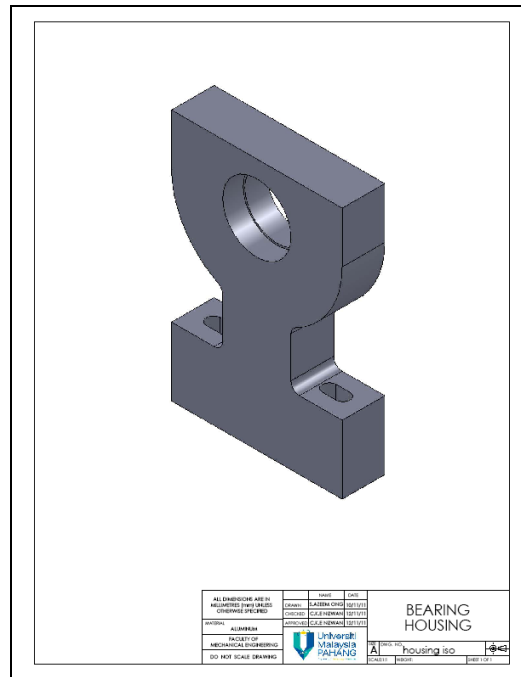


Figure 3.10: Bearing housing's isometric view

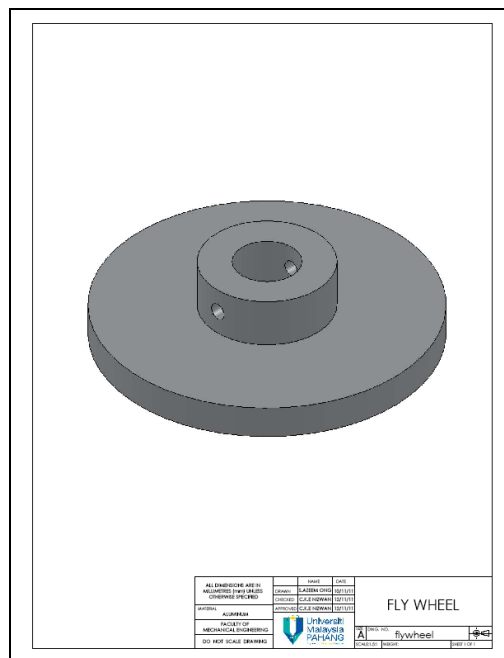


Figure 3.11: Fly wheel's isometric view

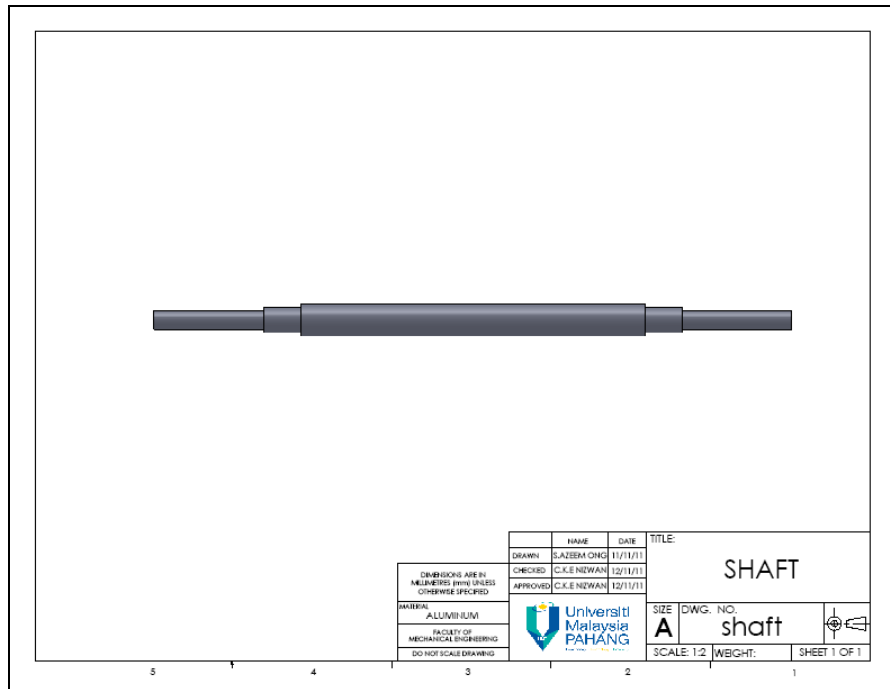


Figure 3.12: Shaft's front view

3.4 DATA ANALYSIS

DASYLab is a software used for various acoustic emission and vibration analysis. This software prepares the module for vibration analysis, acoustic analysis, transient analysis, and correlation analysis between 3 channels. Figure 3.13 shows the layout of DASYLab used during data retrieval process.

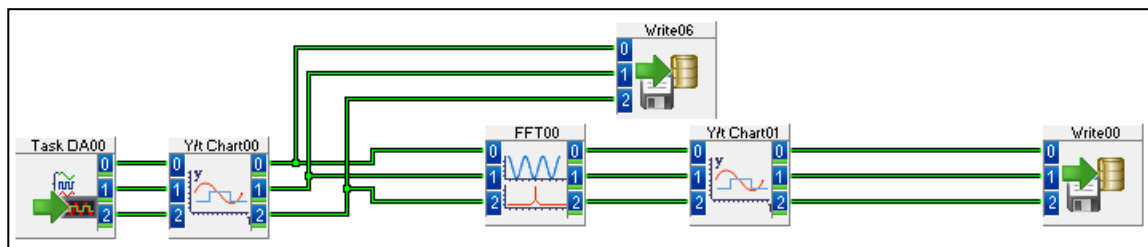


Figure 3.13: DASYLab's layout

From Figure 3.13, vibration signals acquired from NiDAQ were read from the first function ‘Task DA00’ and a ‘Y/t Chart00’ were used to plot a time-domain graph. The data was saved into hard disk drive (HDD) by using ‘Write06’ function. The time-domain graph was converted into FFT by using the ‘FFT00’ function and a ‘Y/tChart01’ to monitor the process. FFT data was written into HDD by using function ‘Write06’.

3.5 DATA PROCESSING ALGORITHM

For this project, MATLAB[®] software was used to develop an algorithm to analyze the failure data. Algorithm developed includes analysis in frequency domain, and time-frequency domain.

3.5.1 Discrete Wavelet Transform

Figure 3.14 shows the flow chart for decomposition process by using MATLAB[®]'s command. In wavelet analysis, it is often speak of approximation and details. The ‘*approximation*’ is the high-scale, low frequency components of the signals. While the ‘*detail*’ are the low-scale, high frequency components (Misiti M. *et al.*, 2009).

Figure 3.15 shows the filtering process at its most basic level. The input signal passes through the filter and emerges as two signals. Unfortunately, if the process were done by using a real digital signal, it will result to twice as much data as the input. Assuming the input; S, consist of 1000 data, the result after the filtration will each have 1000 samples producing a total of 2000 samples of data. By looking carefully at the computation, only one data may be kept in each two 2000-length samples to get the complete information where it is known as down-sampling. Two sequences were produced called cA and cD.

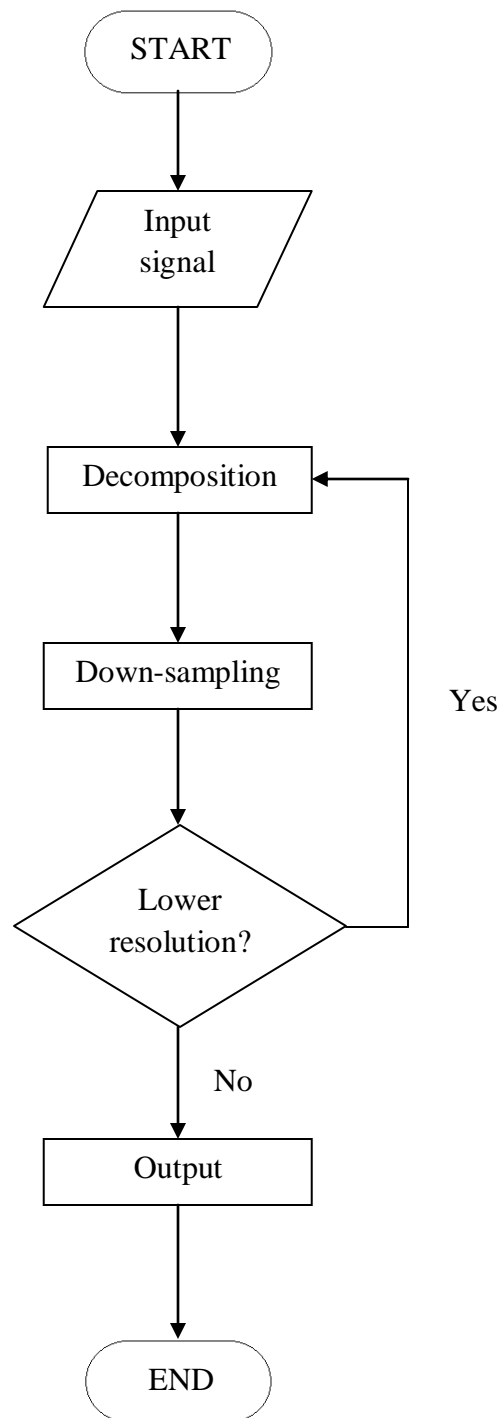


Figure 3.14: Flow chart for decomposition process by using MATLAB[®]'s command

Source: MATLAB[®] ToolBox

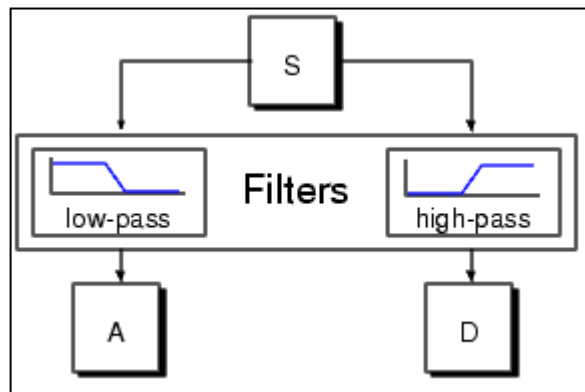


Figure 3.15: Filtering process at its most basic level

Source: Misiti M. *et al.*, 2009

The process on the right of Figure 3.16 which includes the down-sampling produces DWT coefficients. The MATLAB[®] code needed to generate s , cD , and cA is:

```

s = sin(20.*linspace(0,pi,1000)) + 0.5.*rand(1,1000);
[cA,cD] = dwt(s,'db2');

```

where $db2$ is the name of the wavelet for the analysis.

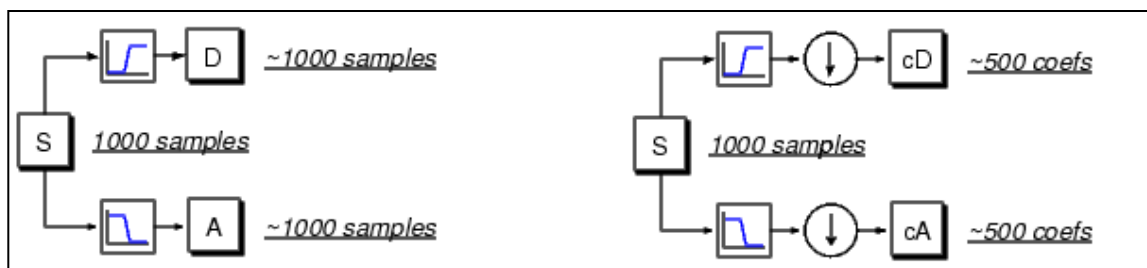


Figure 3.16: Down-sampling process from left to right

Source: Misiti M. *et al.*, 2009

Notice that the detail coefficients cD are small and consist mainly of high-frequency noise, while the approximation coefficient; cA , contain much less noise than the original signal.

```
[length(cA) length(cD)]
ans =
501 501
```

Decomposition process may be iterated with successive approximations being decomposed in turn, so that one signal is broken down into many layer resolution components which is called the wavelet decomposition tree as shown in Figure 3.17.

Since the analysis process is iterative, in theory it can be continued indefinitely. In practice, a suitable number of levels need to be selected based on the nature of the signal, or on a suitable criterion such as entropy.

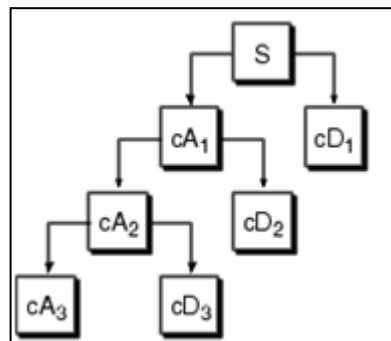


Figure 3.17: Wavelet decomposition tree

Source: Misiti M. *et al.*, 2009

3.5.2 Analysis using Discrete Wavelet Transform Toolbox

Analysis for this project is by using MATLAB[®]'s Discrete Wavelet Transform's Toolbox. The analysis starts off by reading the desired raw data. The MATLAB[®] code needed to load the desired data is:

```
load contaminated_90_04.ASC;
```

where contaminated_90_04.ASC is the name of the file.

After the data has been loaded, click on START on MATLAB[®]'s user interface (UI) and choose Toolbox > Discrete Wavelet Transform. Figure 3.18 shows DWT's Toolbox main menu. Click on "Wavelet 1-D" under the "One-Dimensional" group to proceed.

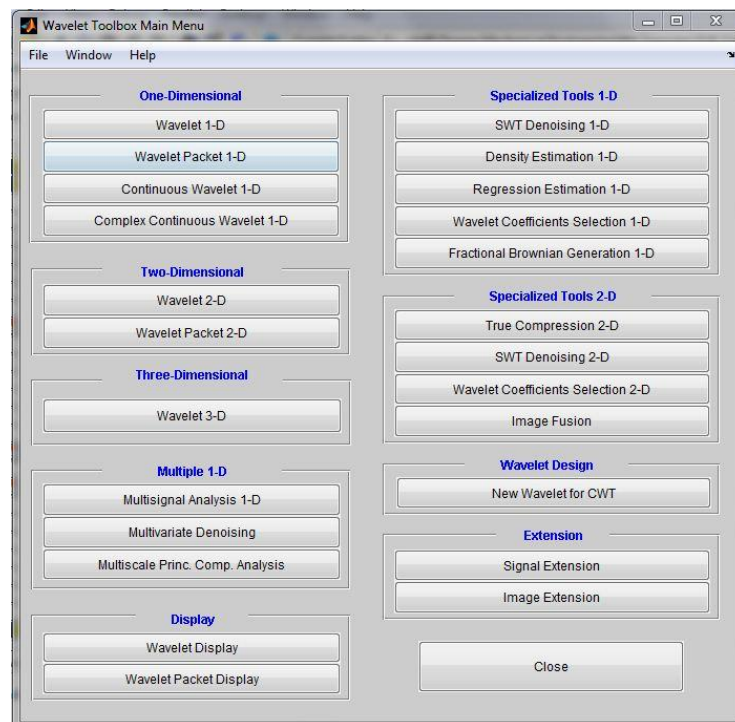


Figure 3.18: Discrete Wavelet Transform's Toolbox main menu

Next is to import the loaded file from previous workspace by clicking OK as shown in Figure 3.19 (a). Select wavelet type as 'db4' with 8 levels of decomposition as shown in Figure 3.19 (b) and click 'Analyze' to proceed (Kim *et al.*, 2007). After the toolbox completed analyzing the input, change the 'display mode' to 'Separated Mode' as shown in Figure 3.19 (c). Figure 3.20 shows the output of MATLAB® DWT's Toolbox.

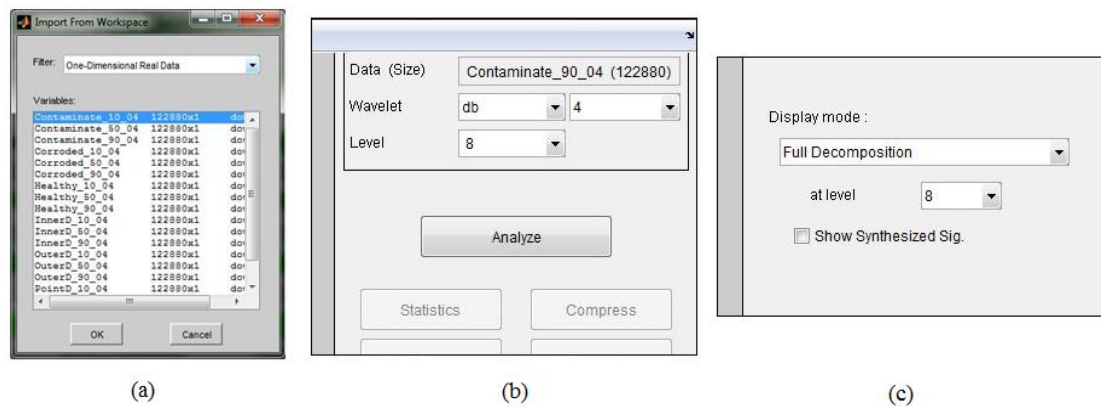


Figure 3.19: Selecting data (a), choosing wavelet type (b), and changing display mode (c)

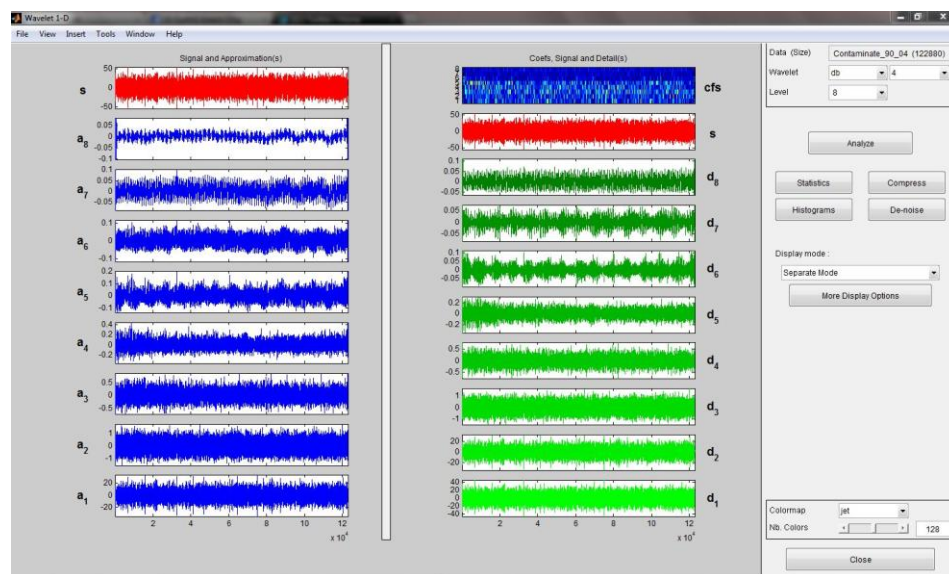


Figure 3.20: Output for MATLAB® Discrete Wavelet Transform's Toolbox

CHAPTER 4

RESULTS & DISCUSSION

4.1 INTRODUCTION

This chapter presents the results of the experiment and further discusses the outcome of the analysis. For the purpose of vibration signals collection, six groups of vibration signals were collected. They consist of a healthy group, corroded group, contaminated group, point defect group, outer race defect group, and inner race defect group. Each group contains vibration signals of three level of speed depending on the capacity of the motor. 287 rpm as the lowest speed, 1,466 rpm as the medium speed, and 2,664 rpm as the highest speed. The total data of each vibration signal is 122,880 data per six seconds.

4.2 DATA ACQUISITION

Figure 4.1 shows the vibration reading for the test rig running on 287 rpm with respect to each types of bearing defects and a healthy one. The data seems to be constant throughout the whole six seconds of data acquisition but OR defect from Figure 4.1 (c) and IR defect Figure 4.1 (d) seems to yield consistent spiking. While CN defect from Figure 4.1 (e) and CB defect from Figure 4.1 (f) is starting to yield high frequency reading compared to the others.

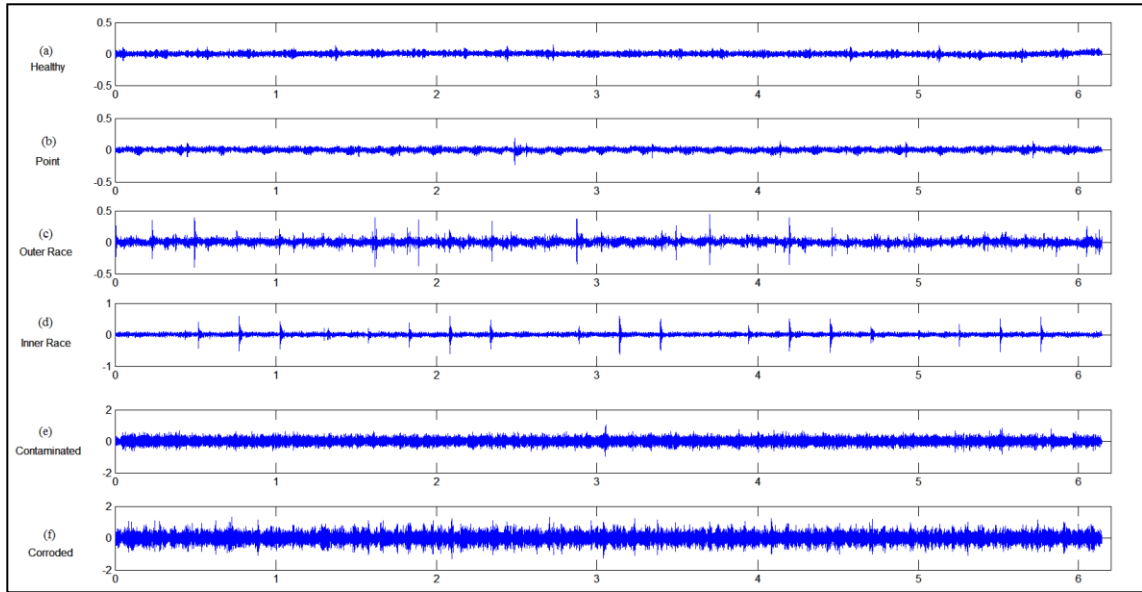


Figure 4.1: Vibration reading when running on 287 rpm for healthy bearing (a), PD (b), OR defect (c), IR defect (d), CN defect (e), and CB defect (f)

Figure 4.2 shows the vibration reading for the test ring running on 1466 rpm with respect to each types of bearing defects and a healthy one. From Figure 4.2 (a), Figure 4.2 (b), Figure 4.2 (c), and Figure 4.2 (d); healthy bearing, PD, OR defect, and IR defect is producing constant reading while CB defect and CN defect in Figure 4.2 (e) and Figure 4.2 (f) starting to produce high vibratory reading as its frequency is increasing up to more than 20 Hz compared to the others.

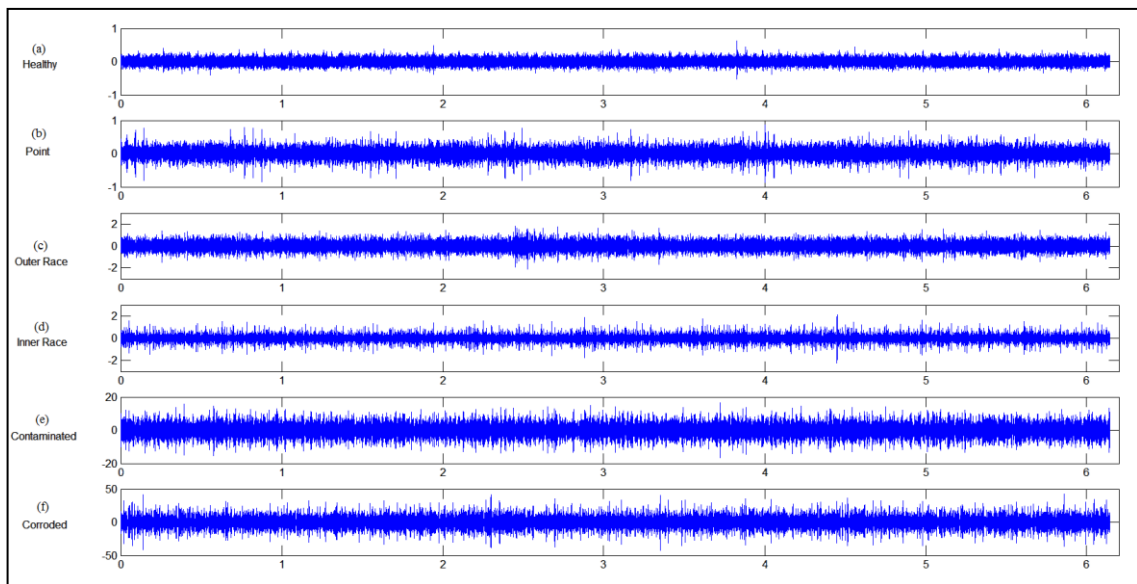


Figure 4.2: Vibration reading when running on 1466 rpm for healthy bearing (a), PD (b), OR defect (c), IR defect (d), CN defect (e), and CB defect (f)

Figure 4.3 shows the vibration reading for the test rig running on 2664 rpm with respect to each types of bearing defects and a healthy one. Again, healthy bearing; from Figure 4.3 (a), is producing constant reading similar to PD in Figure 4.3 (b). However, CB defect and CN defect; in Figure 4.3 (e) and Figure 4.3 (f), produces high vibratory reading especially CB defect at nearly 100 Hz of frequency.

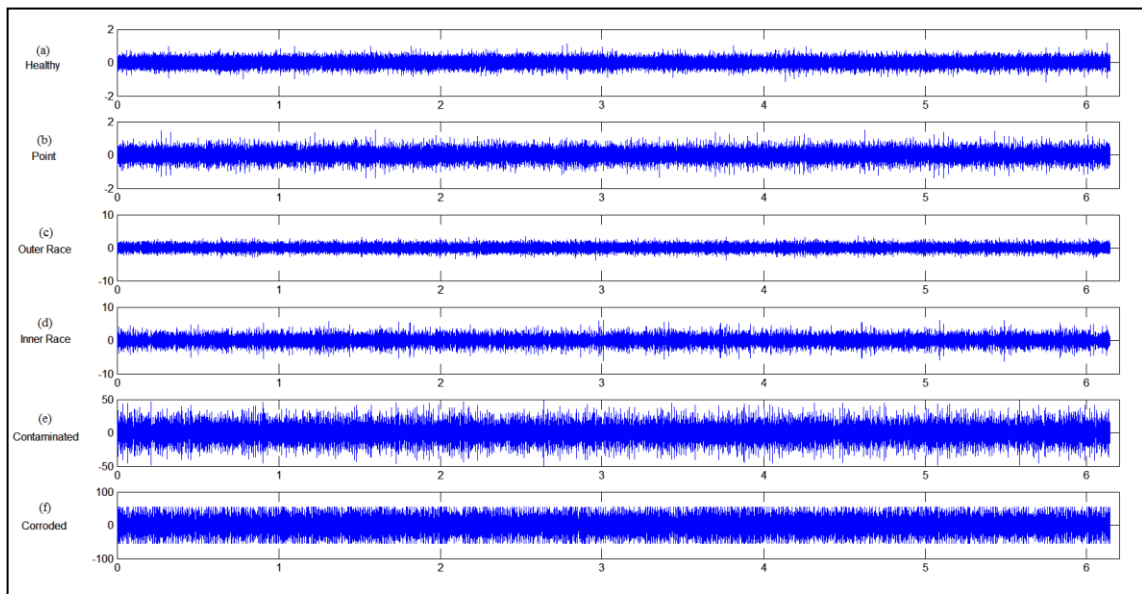


Figure 4.3: Vibration reading when running on 2664 rpm for healthy bearing (a), PD (b), OR defect (c), IR defect (d), CN defect (e), and CB defect (f)

4.3 DECOMPOSITION RESULT

Figure 4.4 to Figure 4.21 shows the decomposition result for all type of tested bearings including the healthy ones. From the result generated, detectable defect feature obviously appears from corroded bearing running at 2664 rpm in Figure 4.15 at level 6, 7, and 8. Other result of decomposition appears to be weakly observed throughout the decomposition process for speed 2446 rpm and 1446 rpm in Figure 4.8, Figure 4.9, Figure 4.11, Figure 4.12, Figure 4.14, Figure 4.17, Figure 4.18, Figure 4.20, and Figure 4.21. This is probably because of the frequency excitation generated from the bearing is not sufficient enough for DWT to detect its defect features as proven by Tandon & Choudhury (1999) where it was found out that the direct vibration spectrum from a defective bearing may not indicate the defect at the initial stage.

Result of decomposition for 287 rpm (Figure 4.4, Figure 4.7, Figure 4.10, Figure 4.13, Figure 4.16, and Figure 4.19) bearings yields similar outcome with results of decomposition for 1446 rpm where it is also may be due to insufficient frequency excitation generated from the bearing.

This shows that DWT will only be efficient for online monitoring method when there's enough frequency excitation by applying DWT on a system running on high speed of at least 2664 rpm.

However, further research was done in order to enhance DWT result for lower speed system. It seems that by using a statistical tool known as Root Mean Square (RMS), it would further support the result for DWT under high or medium speed system.

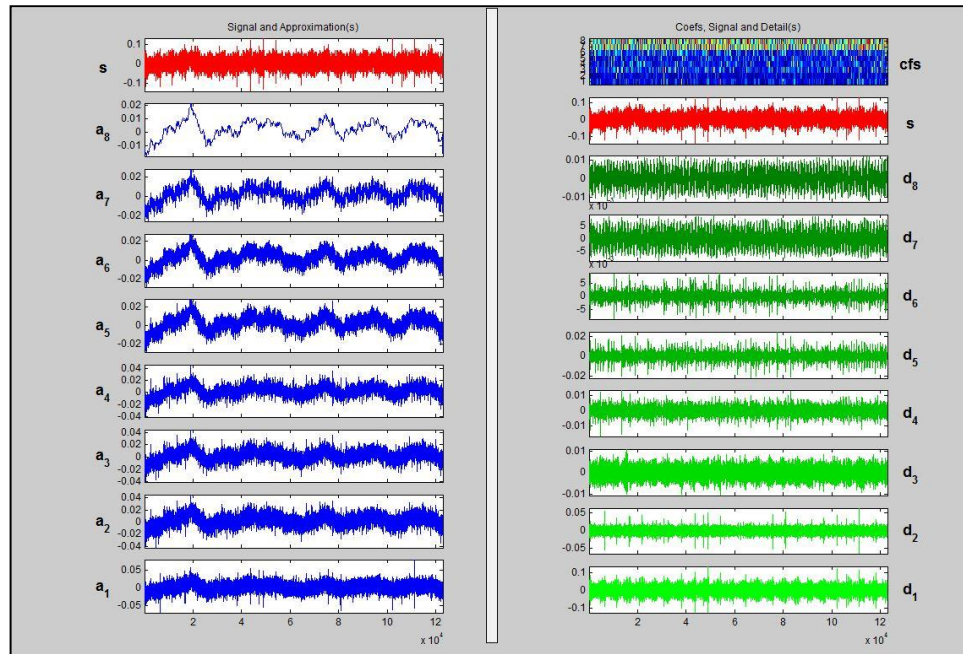


Figure 4.4: Decomposition result for healthy bearing at 287 rpm

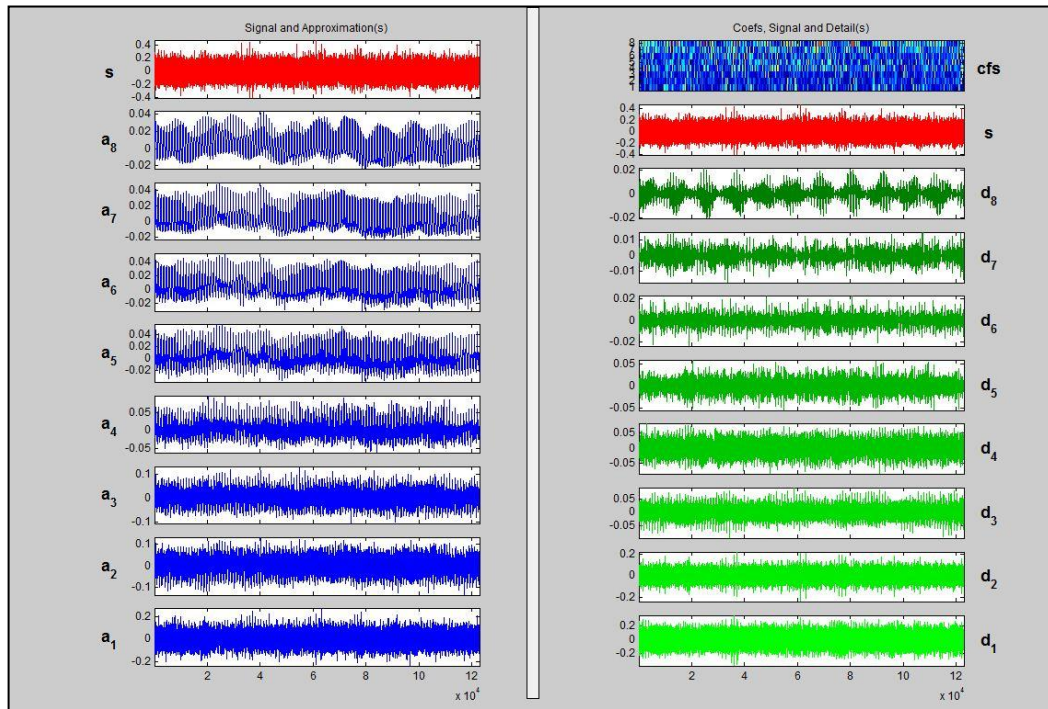


Figure 4.5: Decomposition result for healthy bearing at 1466 rpm

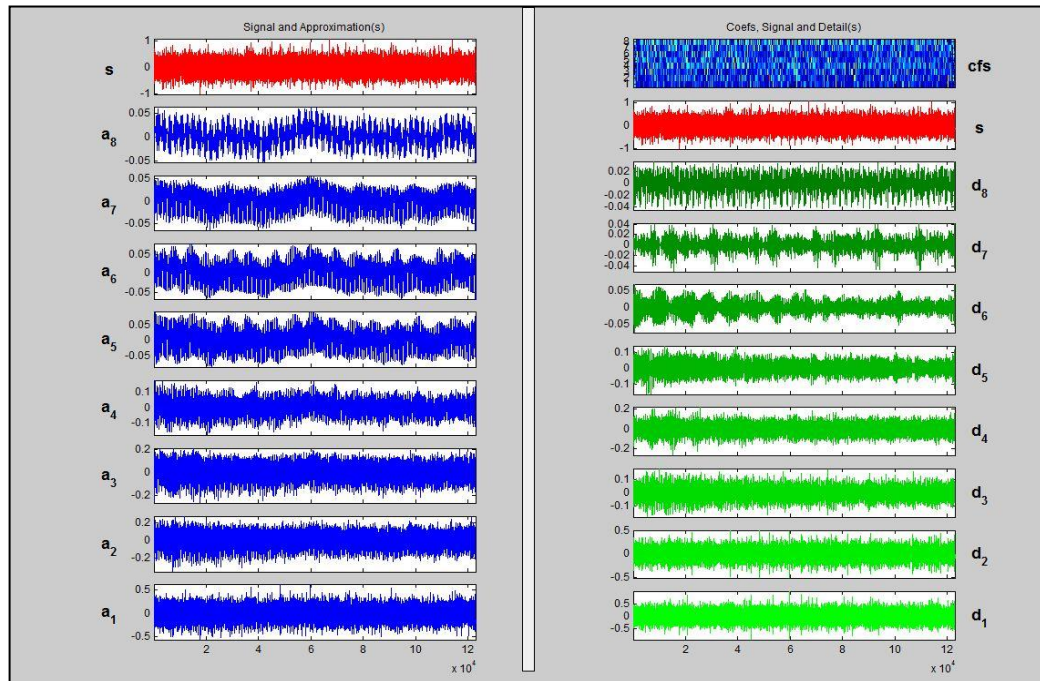


Figure 4.6: Decomposition result for healthy bearing at 2664 rpm

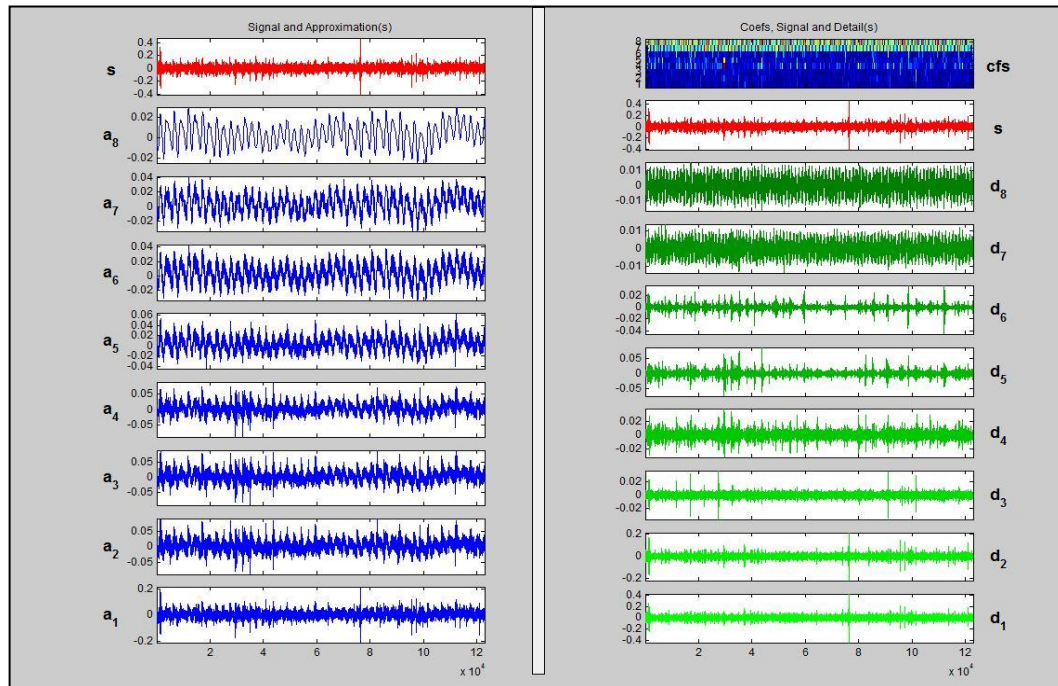


Figure 4.7: Decomposition result for outer race defect at 287 rpm

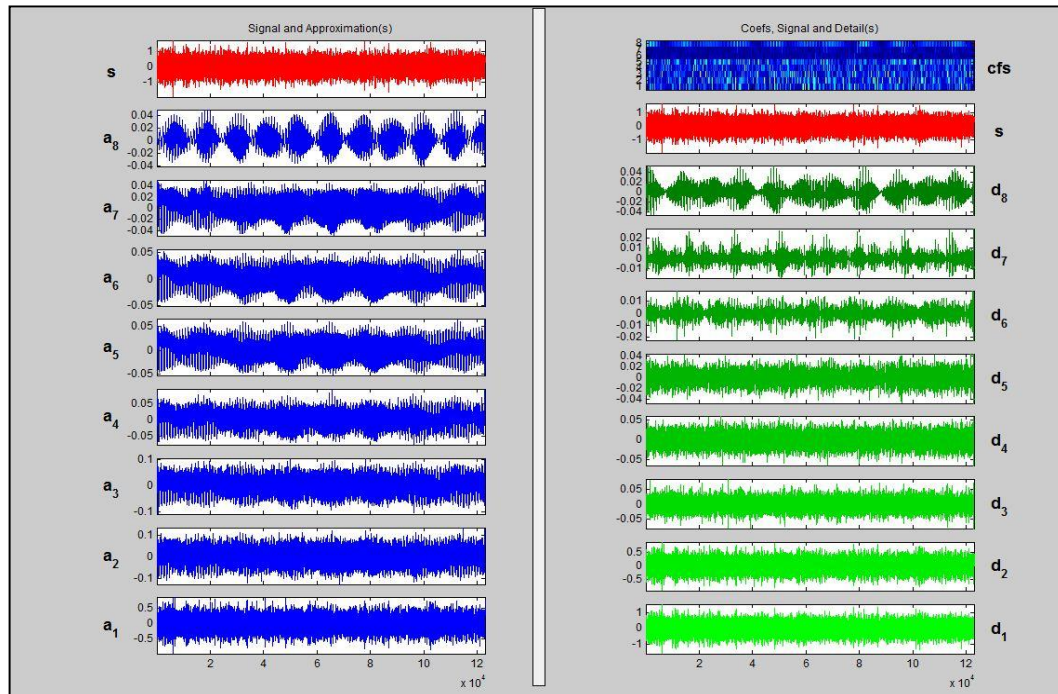


Figure 4.8: Decomposition result for outer race defect at 1466 rpm

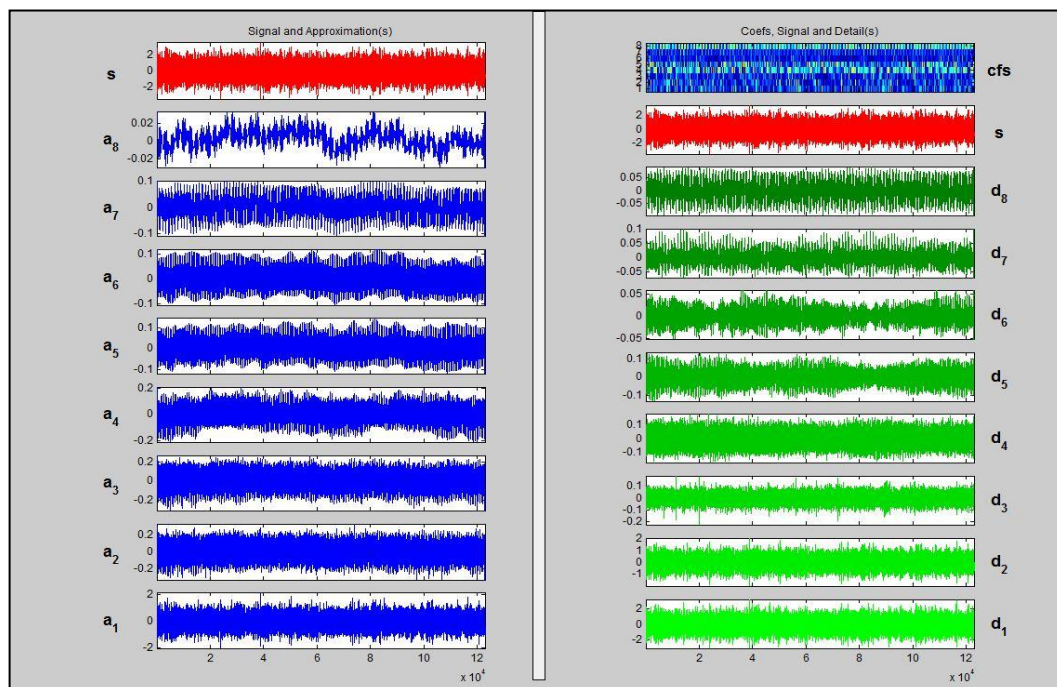


Figure 4.9: Decomposition result for outer race defect at 2664 rpm

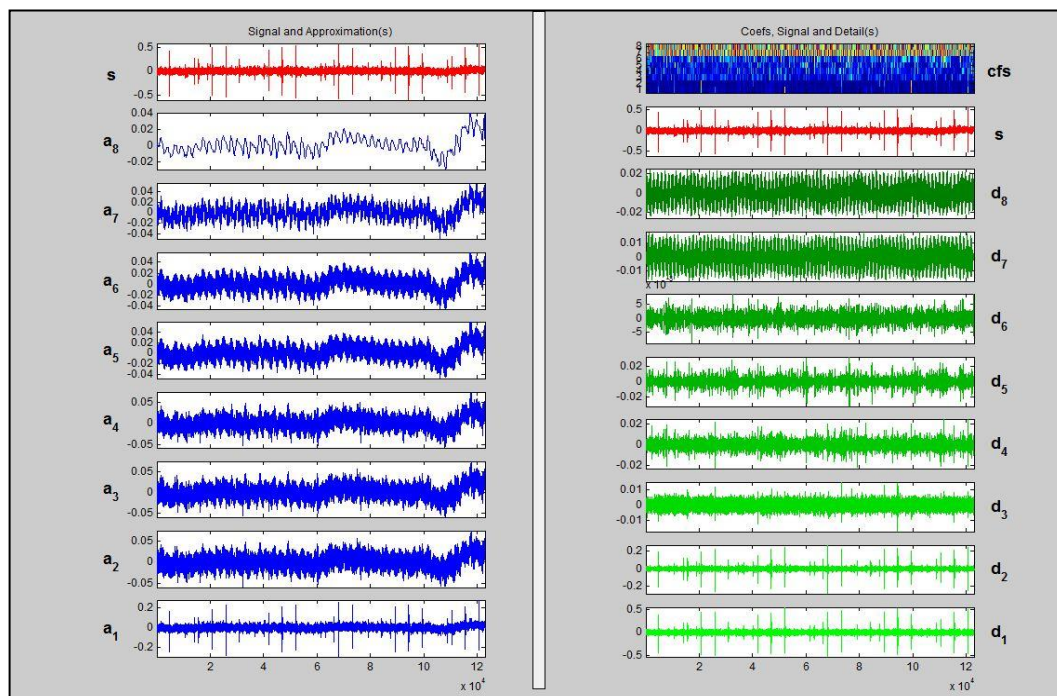


Figure 4.10: Decomposition result for inner race defect 287 rpm

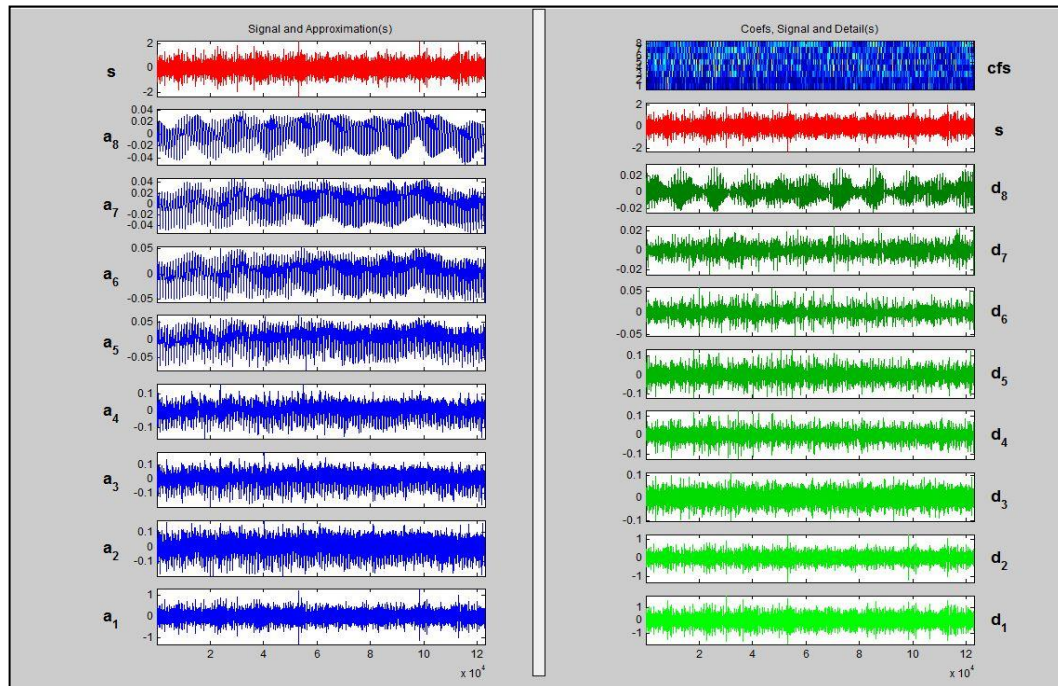


Figure 4.11: Decomposition result for inner race defect at 1466 rpm

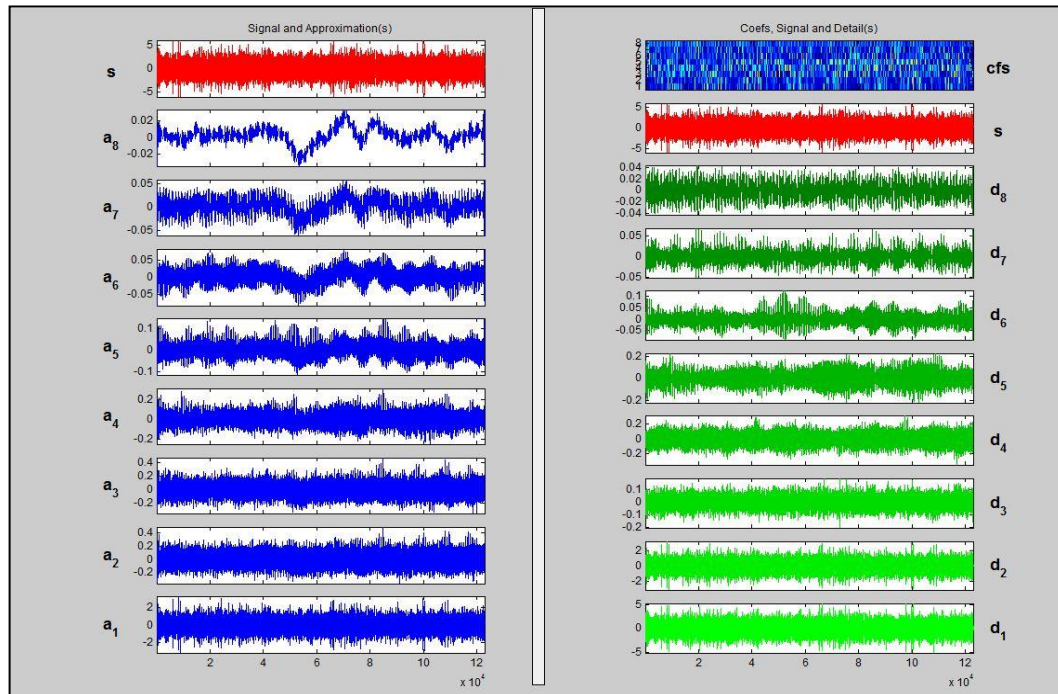


Figure 4.12: Decomposition result for inner race defect at 2664 rpm

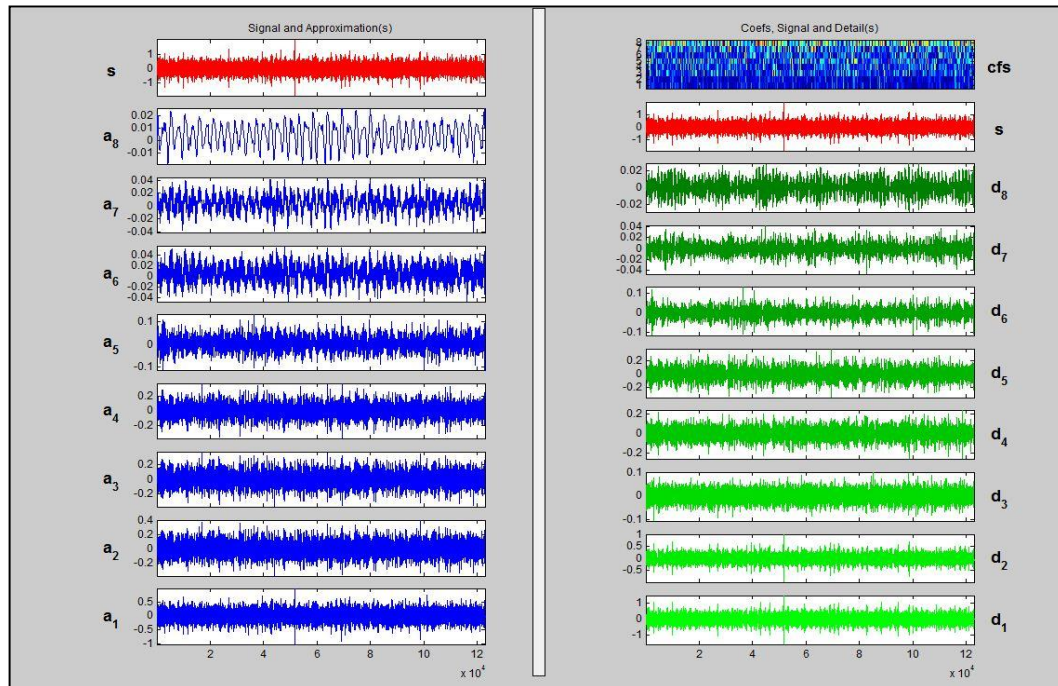


Figure 4.13: Decomposition result for corroded defect at 287 rpm

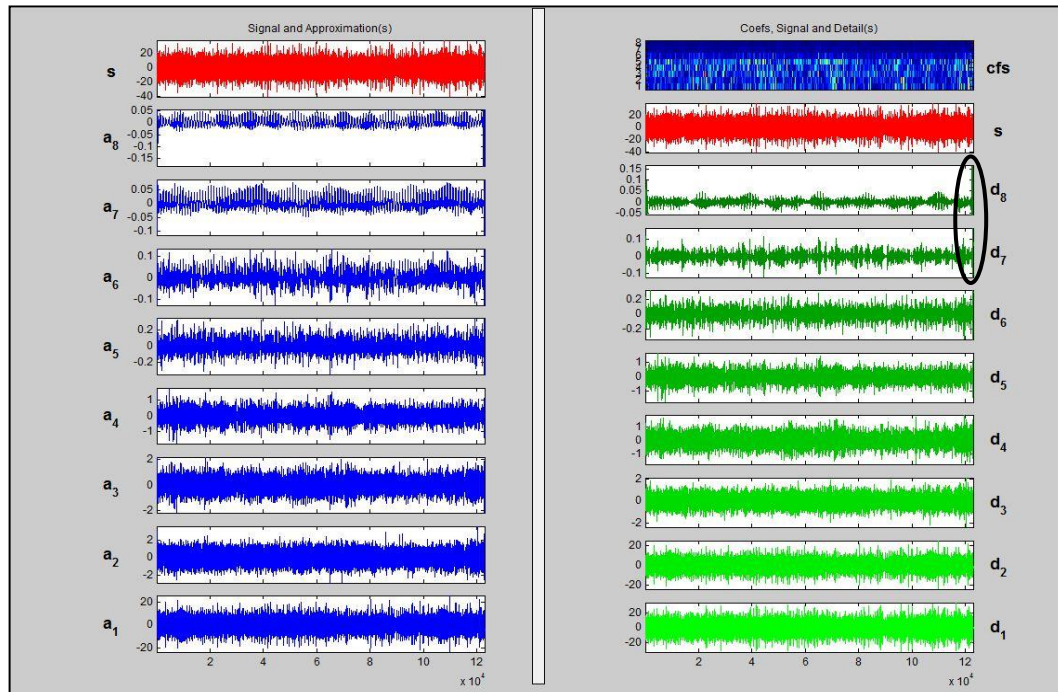


Figure 4.14: Decomposition result for corroded defect at 1466 rpm

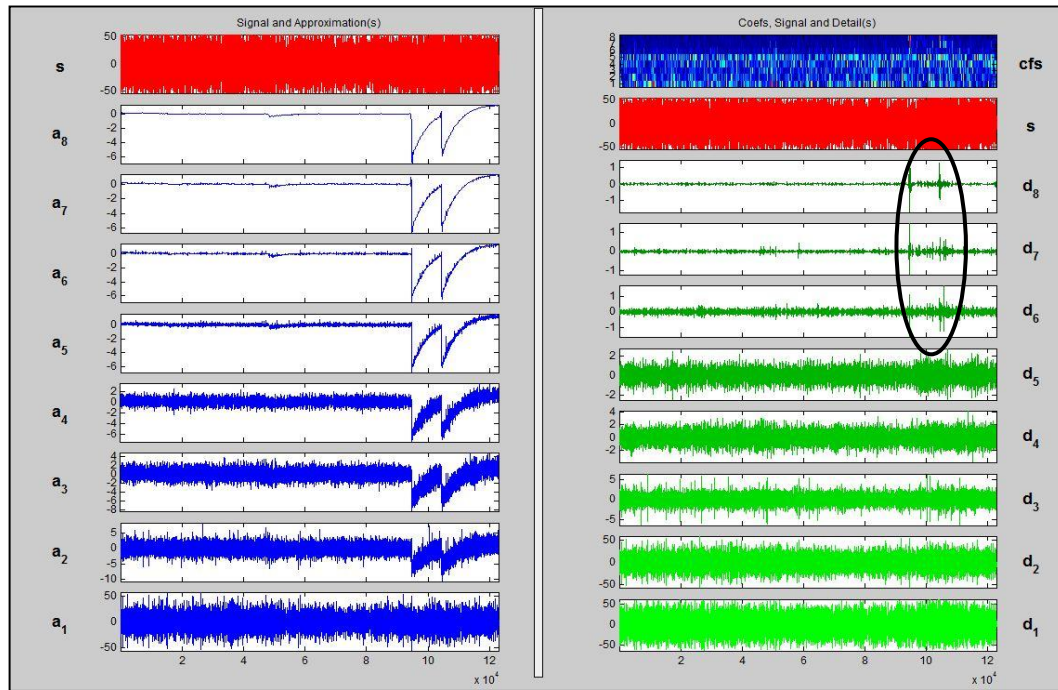


Figure 4.15: Decomposition result for corroded defect at 2664 rpm

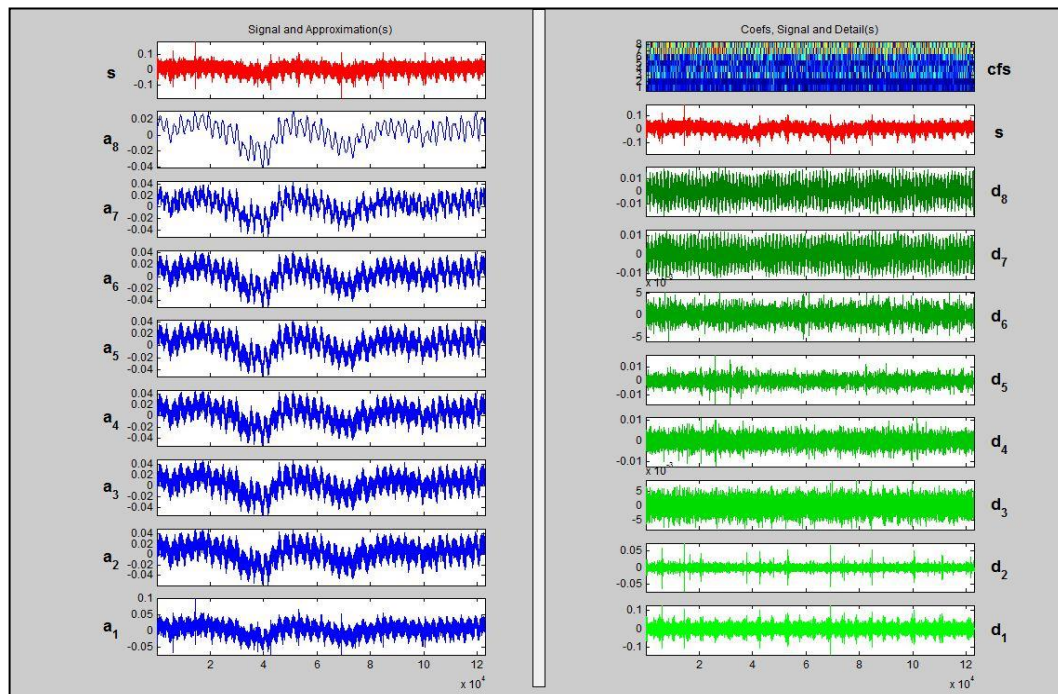


Figure 4.16: Decomposition result for point defect at 287 rpm

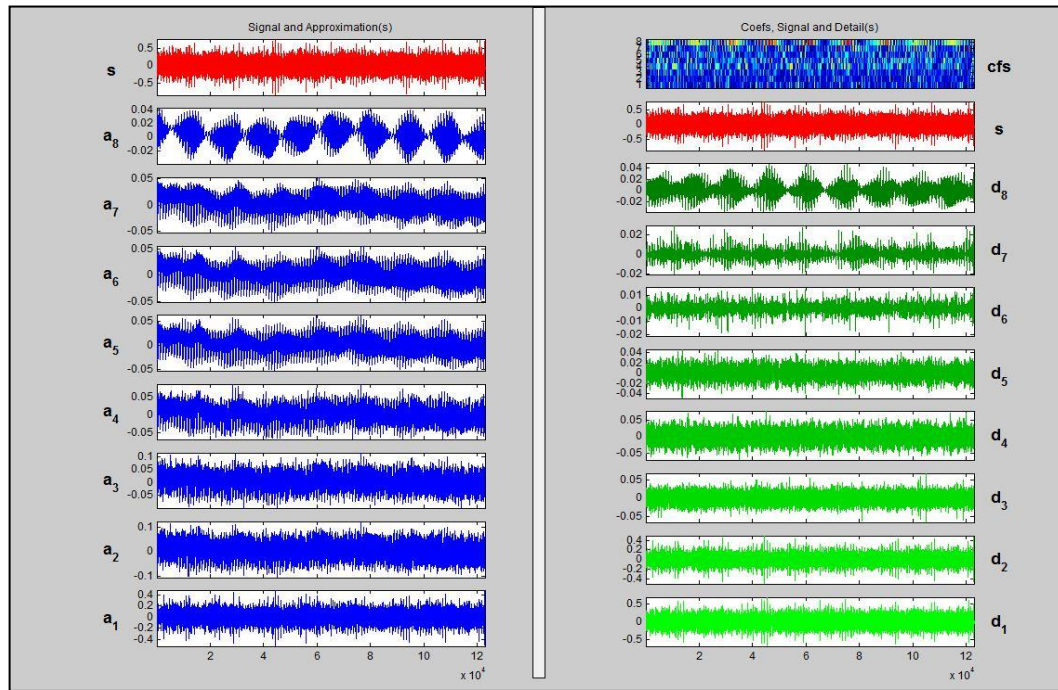


Figure 4.17: Decomposition result for point defect at 1466 rpm

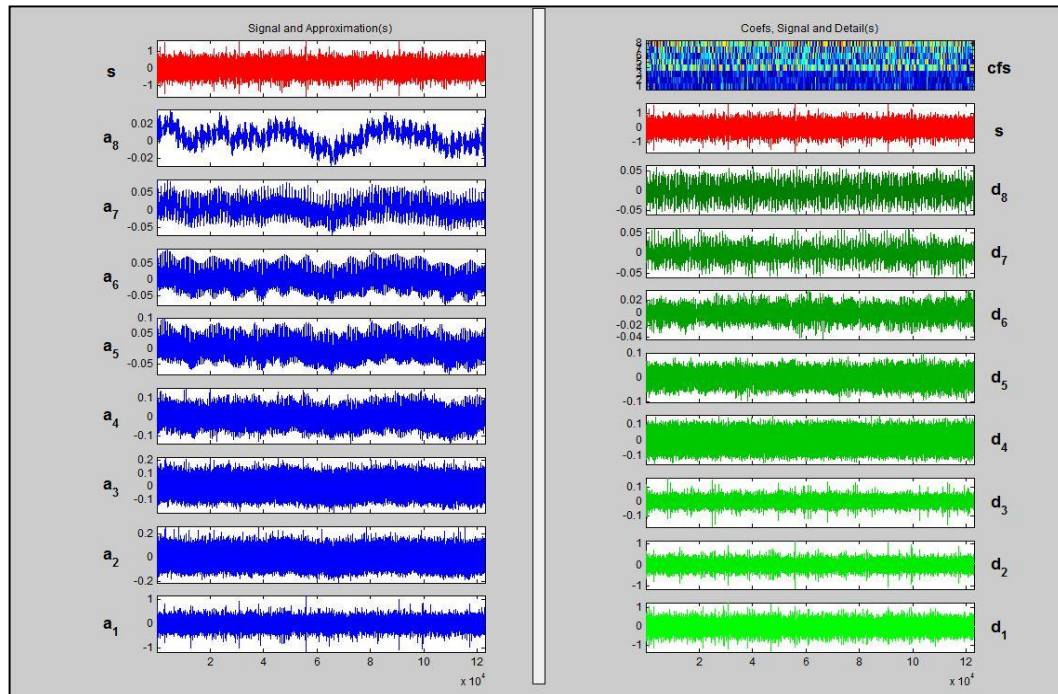


Figure 4.18: Decomposition result for point defect at 2664 rpm

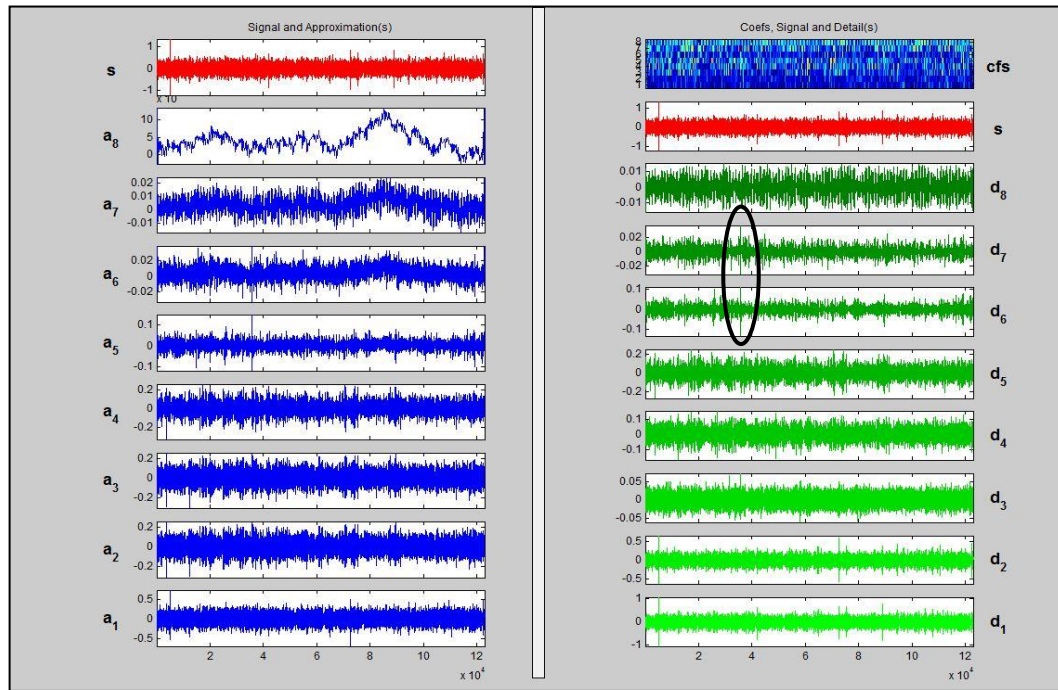


Figure 4.19: Decomposition result for contaminated defect at 287 rpm

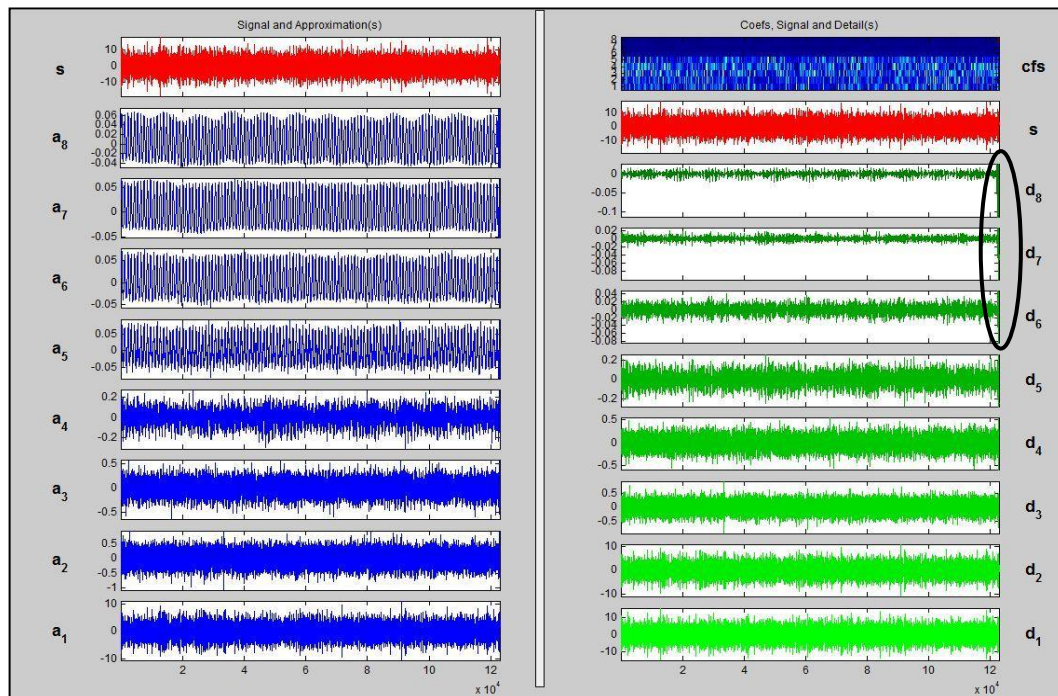


Figure 4.20: Decomposition result for contaminated defect at 1466 rpm

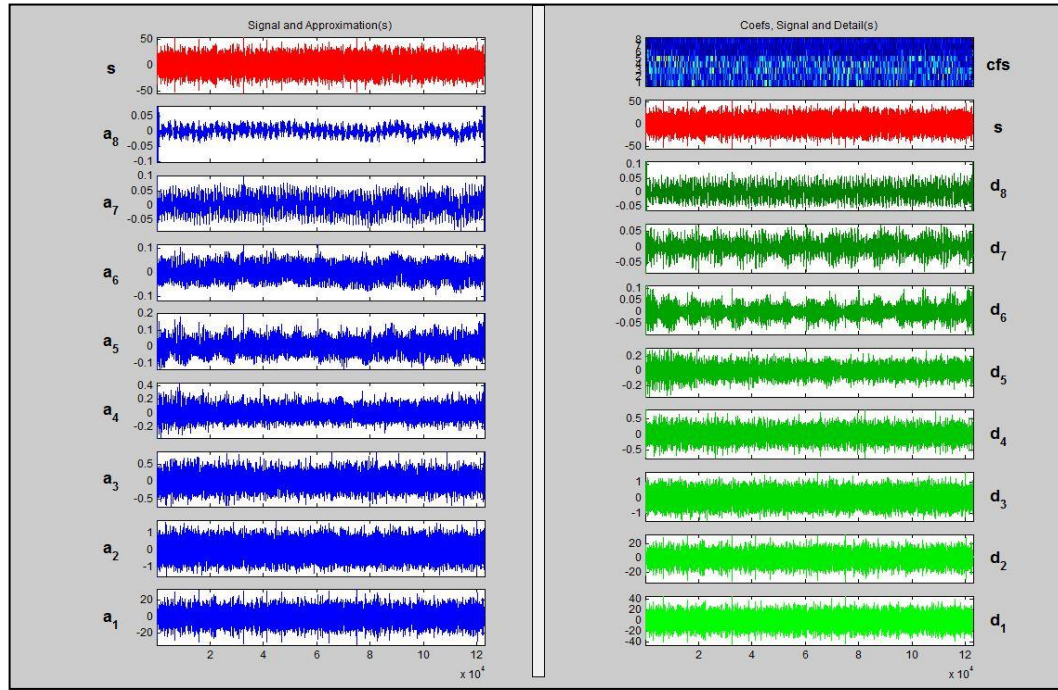


Figure 4.21: Decomposition result for contaminated defect at 2664 rpm

4.4 ROOT MEAN SQUARE PERCENTAGE ANALYSIS

For data of insufficient frequency excitation, calculating the RMS value for each decomposition level and finding the percentage towards the original input seems to yield understandable trend when a graph is plotted. Cartwright (2007) proved in his paper the effectiveness of RMS by simple means without calculus. This method uses the definition of RMS of a waveform which is found simply by squaring that waveform, taking the mean of that squared form, and then computing the square root.

Any percentage value or graph plotted that is below the healthy line may be considered defected. This is because; decomposition process is where the frequency amount of each level gets smaller as the decomposition level increases. So, if the RMS value of the next level declines at an irregular rate or stays flat on its line, the bearing may be considered as defected.

4.4.1 RMS Data for 2664 rpm

Table 4.1 shows the tabulated data of RMS percentage value for each level of decomposition with respect to the input's RMS value for data of 2664 rpm.

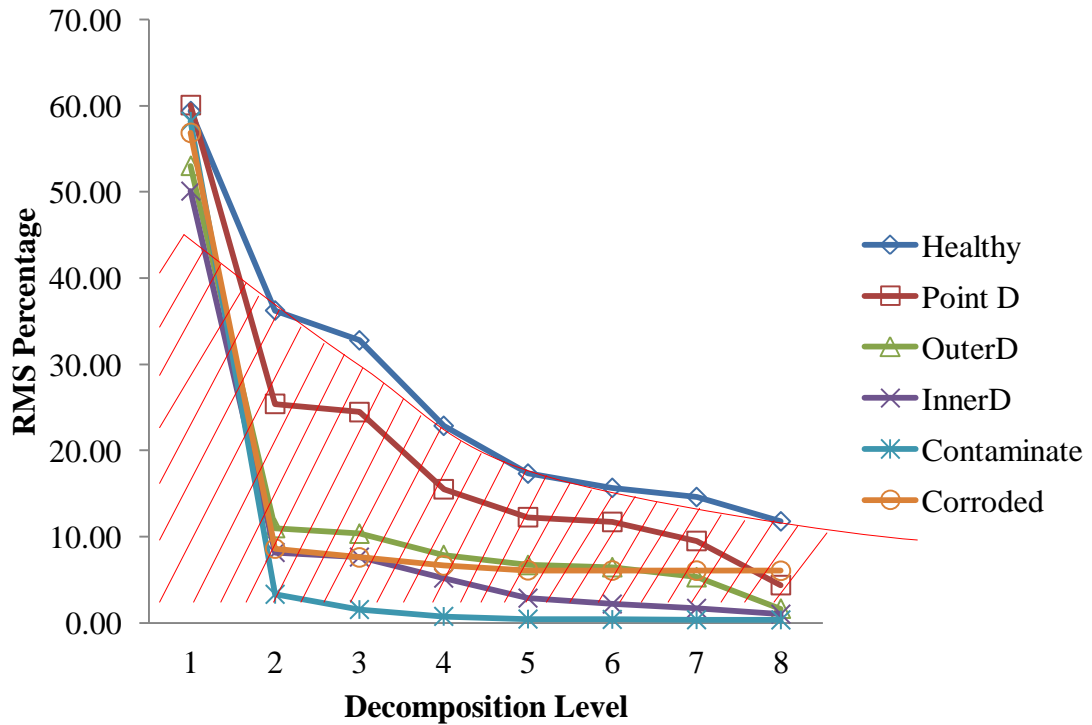
Figure 4.22 shows the trend generated by the RMS percentage value of each decomposition level. From the plotted graph, it seems that all of the defected bearing's RMS values for each decomposition level are below the healthy line (red region) thus proving that RMS is an excellent statistical tool to support DWT decomposition result during speed-up (2800 rpm) was sufficiently useful as also proven by Kim *et al*, (2007).

Table 4.1: RMS percentage value for each level of decomposition at 2664 rpm

D. Level	Healthy		Point Defect		Outer Defect	
	RMS	%	RMS	%	RMS	%
Input	0.1876	100.00	0.2715	100.00	0.7561	100.00
1	0.1114	59.38	0.1531	56.39	0.4010	53.04
2	0.0680	36.25	0.0690	25.41	0.0832	11.00
3	0.0615	32.78	0.0664	24.46	0.0783	10.36
4	0.0429	22.87	0.0421	15.51	0.0596	7.88
5	0.0325	17.32	0.0333	12.27	0.0508	6.72
6	0.0294	15.67	0.0318	11.71	0.0489	6.47
7	0.0274	14.61	0.0258	9.50	0.0401	5.30
8	0.0221	11.78	0.0119	4.38	0.0125	1.65

Table 4.1: Continued

D. Level	Inner Defect		Contaminated		Corroded	
	RMS	%	RMS	%	RMS	%
Input	1.0923	100.00	10.182	100.00	18.771	100.00
1	0.5472	50.10	5.9261	58.20	10.6721	56.85
2	0.0892	8.17	0.3377	3.32	1.6194	8.63
3	0.0834	7.64	0.1580	1.55	1.4258	7.60
4	0.0567	5.19	0.0771	0.76	1.2504	6.66
5	0.0314	2.87	0.0452	0.44	1.1460	6.11
6	0.0239	2.19	0.0408	0.40	1.1404	6.08
7	0.0185	1.69	0.0377	0.37	1.1382	6.06
8	0.0111	1.02	0.0354	0.35	1.1349	6.05

**Figure 4.22:** RMS percentage vs. decomposition level for speed of 2664 rpm

4.4.2 RMS Data for 1466 rpm

Table 4.2 shows the tabulated data of RMS percentage value for each level of decomposition with respect to the input's RMS value for data of 1466 rpm.

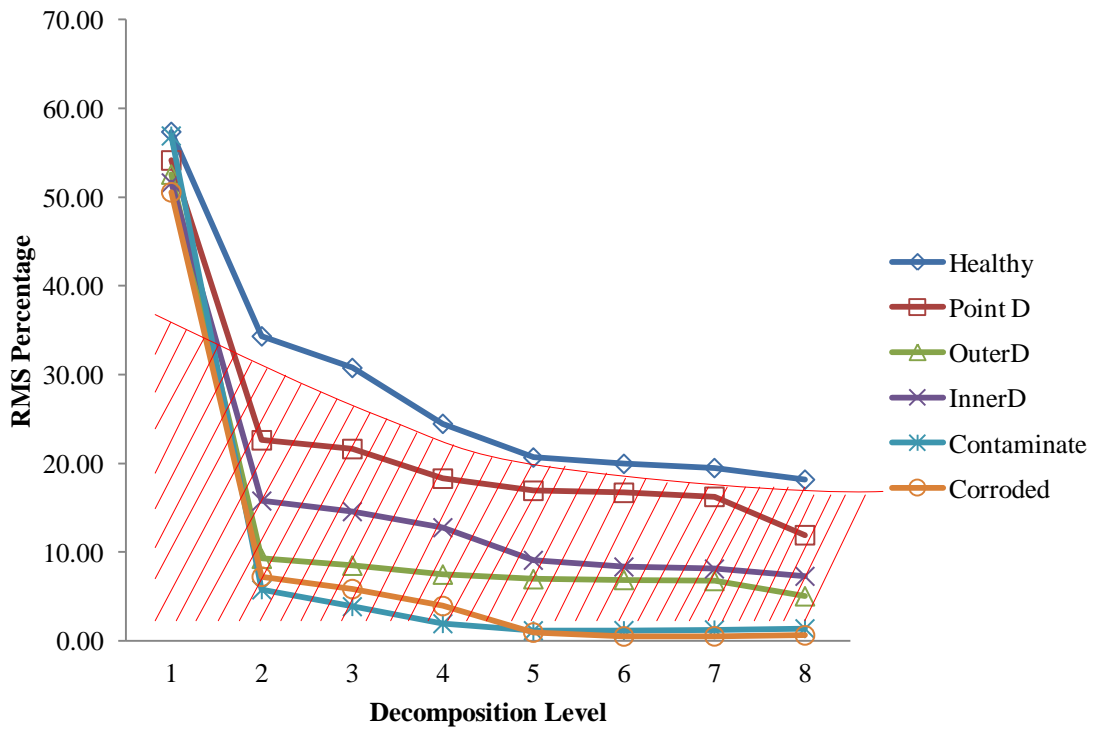
Figure 4.23 shows the trend generated by the RMS percentage value of each decomposition level. From the plotted graph, it seems that all of the defected bearing's RMS values for each decomposition level are below the healthy line (red region) thus proving that RMS is an excellent statistical tool to support DWT decomposition result for speed at 1466 rpm and above.

Table 4.2: RMS percentage value for each level of decomposition at 1466 rpm

D. Level	Healthy		Point Defect		Outer Defect	
	RMS	%	RMS	%	RMS	%
Input	0.0842	100.00	0.1318	100.00	0.3476	100.00
1	0.0483	57.36	0.0714	54.14	0.1827	52.56
2	0.0289	34.32	0.0298	22.61	0.0322	9.26
3	0.0259	30.76	0.0285	21.62	0.0295	8.49
4	0.0206	24.47	0.0241	18.29	0.0260	7.48
5	0.0174	20.67	0.0223	16.92	0.0242	6.96
6	0.0168	19.95	0.0220	16.69	0.0239	6.88
7	0.0164	19.48	0.0214	16.24	0.0235	6.76
8	0.0153	18.17	0.0157	11.91	0.0175	5.03

Table 4.2: Continued

D. Level	Inner Defect		Contaminated		Corroded	
	RMS	%	RMS	%	RMS	%
Input	0.2664	100.00	3.2802	100.00	7.7067	100.00
1	0.1375	51.61	1.8667	56.91	3.8960	50.55
2	0.0420	15.77	0.1888	5.76	0.5572	7.23
3	0.0388	14.56	0.1266	3.86	0.4499	5.84
4	0.0340	12.76	0.0637	1.94	0.3028	3.93
5	0.0242	9.08	0.0379	1.16	0.0727	0.94
6	0.0222	8.33	0.0385	1.17	0.0389	0.50
7	0.0216	8.11	0.0411	1.25	0.0399	0.52
8	0.0194	7.28	0.0449	1.37	0.0482	0.63

**Figure 4.23:** RMS percentage vs. decomposition level for speed of 1466 rpm

4.4.3 RMS Data for 287 rpm

Table 4.3 shows the tabulated data of RMS percentage value for each level of decomposition with respect to the input's RMS value for data of 287 rpm.

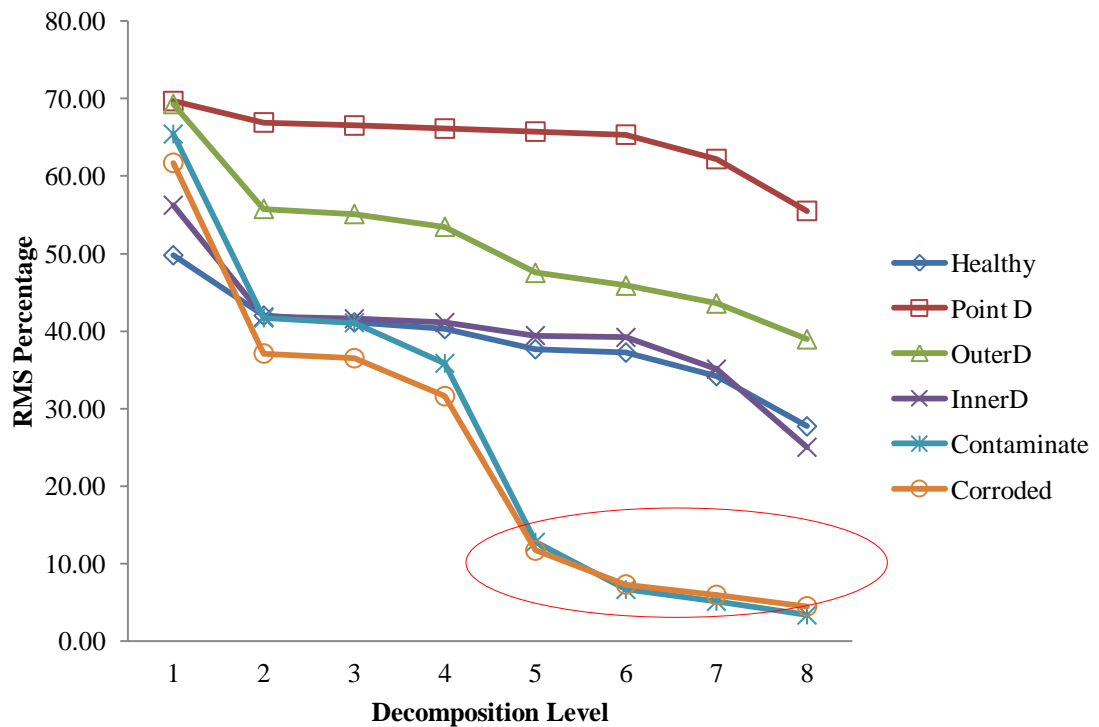
Figure 4.24 shows the trend generated by the RMS percentage value of each decomposition level. From the plotted graph, it seems that data from point defect, outer race defect and inner race defect is above the healthy line. This is probably due to low frequency excitation. Even though RMS was able to enhance DWT result for 1466 rpm's data, but 287 rpm is operating too slow thus RMS weren't able to clearly enhance the result of DWT analysis.

Table 4.3: RMS percentage value for each level of decomposition at 287 rpm

D. Level	Healthy		Point Defect		Outer Defect	
	RMS	%	RMS	%	RMS	%
Input	0.0231	100.00	0.0254	100.00	0.0303	100.00
1	0.0115	49.78	0.0177	69.69	0.0210	69.31
2	0.0097	41.99	0.0170	66.93	0.0169	55.78
3	0.0095	41.13	0.0169	66.54	0.0167	55.12
4	0.0093	40.26	0.0168	66.14	0.0162	53.47
5	0.0087	37.66	0.0167	65.75	0.0144	47.52
6	0.0086	37.23	0.0166	65.35	0.0139	45.87
7	0.0079	34.20	0.0158	62.20	0.0132	43.56
8	0.0064	27.71	0.0141	55.51	0.0118	38.94

Table 4.3: Continued

D. Level	Inner Defect		Contaminate		Corroded	
	RMS	%	RMS	%	RMS	%
Input	0.0416	100.00	0.1490	100.00	0.2304	100.00
1	0.0234	56.25	0.0975	65.44	0.1422	61.72
2	0.0174	41.83	0.0621	41.68	0.0855	37.11
3	0.0173	41.59	0.0612	41.07	0.0841	36.50
4	0.0171	41.11	0.0534	35.84	0.0728	31.60
5	0.0164	39.42	0.0190	12.75	0.0269	11.68
6	0.0163	39.18	0.0099	6.64	0.0168	7.29
7	0.0146	35.10	0.0076	5.10	0.0137	5.95
8	0.0104	25.00	0.0050	3.36	0.0103	4.47

**Figure 4.24:** RMS percentage vs. decomposition level for speed of 287 rpm

However, the most defected bearings; contaminated and corroded, are still below the lines of healthy (red circle) where this is most probably due to giving enough frequency excitation. This is because of how DWT itself decomposes the data. As shown previously in Figure 3.14, the input was divided into approximate (cA) and detailed (cD) output at each level of decomposition. By referring to raw data transformed into FFT graph of 10,000 Hz in Figure 4.25; at first level of decomposition, 10,000-length of data were decomposed to 5,000-length data of cA_1 and 5,000-length data of cD_1 . As the DWT proceeds with decomposition process, cA_1 was then divided into two parts again leaving 2,500-length data each for cA_2 and cD_2 at level 2. At level 1's decomposition, the energy was divided with most of it towards cD_1 rather than cA_1 . While at level 2's decomposition, most of the energy were left at cA_2 and low amount of energy are seen at cD_2 . As the decomposition process continues up to level 8, the energy left at cA_8 would be the lowest thus making it having a low value RMS.

The same theory applies for corroded defect at speed of 287 rpm. Research by Tandon & Choudhury (1999) yields similar result where it was found out that the direct vibration spectrum from a defective bearing may not indicate the defect at the initial stage.

FFT graphs for other speeds may be referred at Appendix D throughout Figure 4.26 until Figure 4.42.

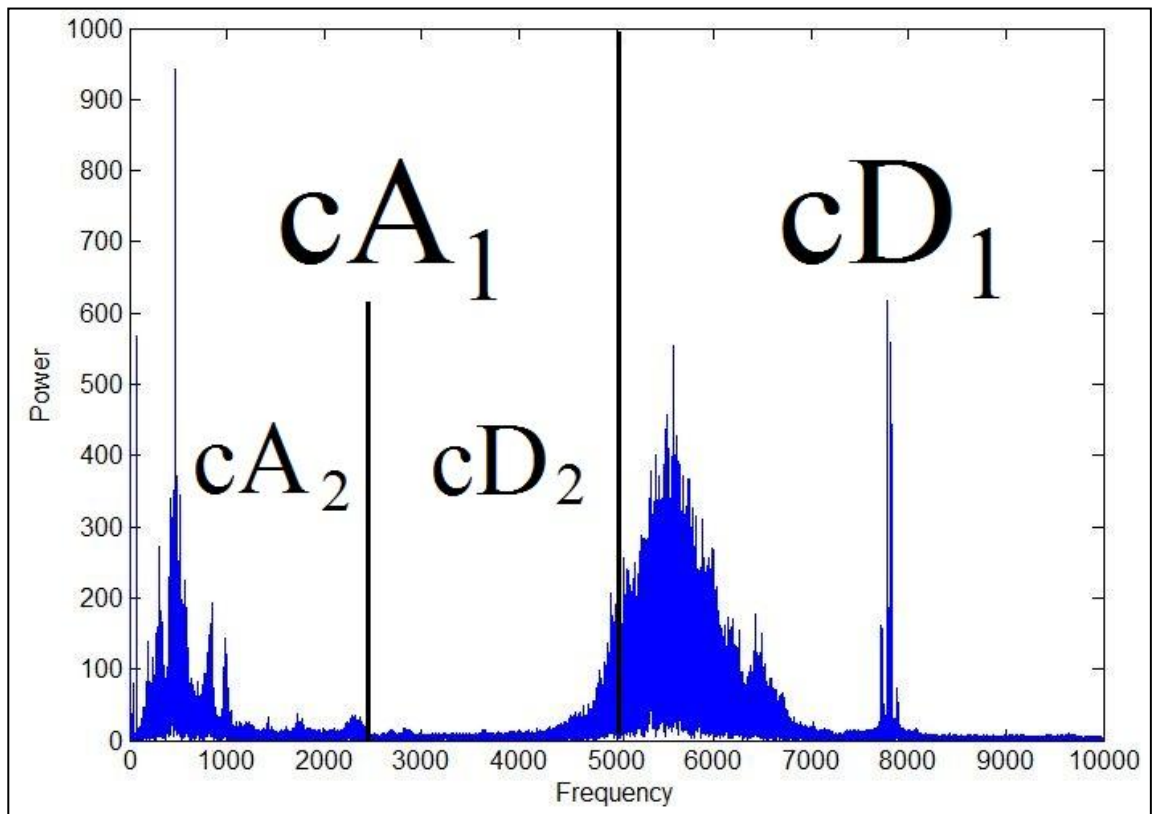


Figure 4.25: FFT result for contaminated defect at speed of 287 rpm

CHAPTER 5

CONCLUSION & RECOMMENDATIONS

5.1 CONCLUSION

The designed and fabricated test rig was proven to be effective in collecting vibration signals produced from tested bearings as constant vibration signals was harnessed throughout the whole experimental procedure.

From the experiment, Discrete Wavelet Transform (DWT) was used to detect defect features from defected bearings as they produce vibration signals. Fast Fourier Transform (FFT) and Root Mean Square (RMS) plays an important role in supporting results analyzed by using DWT from MATLAB[®] Toolbox.

From the analysis, it shows that a system with low operating speed yields unsystematic results due to low excitation from the defect. As the system's speed were increased to a higher speed of more than 1446 rpm, the output yields more systematic results and they start to appear in a consistent manner. Once the speed reaches 2664 rpm, corroded bearing yields the highest amplitude reading and defect features appears at level 6, 7, and 8 while in other defected bearings with similar speed were weakly observed throughout the decomposition processes.

For data of insufficient excitation, even though the defect features were weakly observed throughout the decomposition processes, defect features still may be discovered by calculating and plotting graph for the percentage of RMS value of each

decomposition level compared to the original input. By using the same concept, RMS percentage of a healthy bearing were used as an indication to other defected bearings. Defect feature were shown on the RMS Percentage graph if the RMS percentage suddenly declines at an irregular rate compared to the healthy bearing. This shows that DWT appears to be effective in pointing out the location and frequency of defect when the excitation is high enough. If the excitation is low, it won't affect the bearing and the machine's structure much.

Using DWT is indeed appropriate as an effective tool in detecting defect features in bearings. However, on systems of low speed, it is recommended for the DWT results to be enhanced by using RMS value of each decomposition level.

All of these are possible for online monitoring without shutting down the machine for maintenance purpose. Therefore, this method is suggested as an alternative technique in bearing fault detection online monitoring, especially for system running on high speed.

5.2 RECOMMENDATIONS

Recommendation to further improve the result of this project is firstly to increase the speed range with the lowest speed at 3,000 rpm. Next is to vary the kind of defected bearings since there are numbers of types of bearing defects. Other than that is to use different type of bearings other than caged-ball bearings. Not only that, the positioning of bearing should be changed to vertical type bearing as this may be done simply by redesigning the test rig. Lastly is to use Envelope Analysis and to compare its result with Discrete Wavelet Transform's result.

REFERENCES

- Braun S., Datner B., 1977. Analysis of roller/ball bearing vibrations. *ASME paper 77-WA/DE-5*. pp.1-8.
- Catwright Kenneth V., 2007. Determining the effective or rms voltage of various waveforms without calculus. *The Technology Interface*. **Fall-2007**.
- Chaturvedi GK, Thomas DW, 1981. Bearing fault detection using adaptive noise cancelling. *ASME paper 91-DET-7*. pp.1-10.
- Cristalli C., N. Paone, and R.M. Rodriguez, 2006. Mechanical fault detection of electric motors by laser vibrometer and accelerometer measurements. *Mechanical Systems and Signal Processing*. pp.1350-1361.
- Djebala Abderrazek, Nouredine Ouelaa, and Nacer Hamzaoui, 2007. Detection of rolling bearing defects using discrete wavelet analysis. *Meccanica*. pp.339-348.
- Eschmann P., Hasbargen L., Weigand K, 1958. Ball and roller bearings: Their theory, design, and application. *London: K.G Heyden*.
- Igarashi T, Hamada H, 1982. Studies on the vibration and sound of defective rolling bearings (first report: vibration of ball bearings with one defect). *Bull JSME* **25(204)**. pp.994-1001.
- Khalid F, 2007. Rolling element fault diagnosis using Laplace-wavelet envelope power spectrum. *EURASIP Journal on Advances in Signal Processing*. pp.1-14.
- Kim P.Y., 1984a. A review of rolling element bearing health monitoring (II): preliminary test results on current technologies. In: *Proceedings of Machinery Vibration Monitoring and Analysis Meeting, Vibration Institute, New Orleans, LA*. 26-28 June. pp.127-32.
- Kim P.Y., 1984b. A review of rolling element bearing health monitoring (III): preliminary test results on eddy current proximity transducer technique. In: *Proceedings of 3rd International Conference on Vibration in Rotating Machinery, York, UK*. 11-13 September. pp.119-25.
- Kun Feng, Zhinong Jiang, Wei He, and Qiang Qin, 2011. Rolling element bearing fault detection based on optimal antisymmetric real Laplace wavelet. *Measurement*. pp.1582-1591.

- Kim B.S., S.H. Lee, M.G. Lee, J. Ni, J.Y. Song, and C.W. Lee, 2007. A comparative study on damage detection in speed-up and coast-down process of grinding spindle-typed rotor-bearing system. *Journal of Materials Processing Technology*. pp30-36
- Lou X. and K.A.K.A. Loparo, 2004. Bearing fault diagnosis based on wavelet transform and fuzzy inference. *Mechanical System and Signal Processing* **18**. pp.1077-95
- Lyon R.H., 1986. Machinery Noise and Diagnostics. Butterworth, Stoneham, MA.
- Mallat S.G., 1989. A theory for multiresolution signal decomposition: the wavelet representation. *IEEE Transaction on pattern analysis and machine intelligence* **11(7)**. pp.674-93.
- Mathew J, Alfredson R.J., 1984. The condition monitoring of rolling element bearings using vibration analysis. *Trans ASME, J Vibr, Acoust, Stress Reliab Design*. **106**:447-53.
- McFadden P.D., Smith J.D., 1984(1). Vibration monitoring of rolling element bearings by the high frequency resonance technique – a review. *Tribology International*. pp.3-10.
- McFadden P.D and Smith J.D., 1984(2). Model for the vibration produced by a single point defect in a rolling element bearing. *Journal of Sound and Vibration* **96(1)**. pp.69-82.
- McFadden P.D. and Smith J.D., 1985. The vibration produced by multiple point defects in a rolling element bearing. *Journal of Sound and Vibration* **98(2)**. pp.263-73.
- Misiti M., Misiti Y, Oppenheim G., Poggi J.M., 2009. Wavelet Toolbox™ 4 User's Guide (Version 4.4. The MathWorks Inc.
- Mori K, Kasashima N, Yoshioda T, and Ueno Y, 1996. Prediction of spalling on a ball bearing by applying discrete wavelet transform to vibration signals. *Wear* **8**, pp.195-162.
- Nikolaou N. and I. Antoniadis, 2002. Demodulation of vibration signals generated by defects in rolling element bearings using complex shifted Morlet wavelets. *Mechanical Systems and Signal Processing* **16**. pp.677-694.
- Nizwan C.K.E., M.N. Hisyam, and N. Ismail, 2010. A time-frequency localization analysis of vibration data for bearing fault detection. *Malaysian Technical Universities International Conference of Engineering & Technology 2011*.
- Othman O-Khalifa, 2009. Wavelet theory and applications. Electrical and Computer Engineering Department. International Islamic University Malaysia.

- Prabhakar S., A.R. Mohanty, and A.S. Sekhar, 2002. Application of discrete wavelet transform for detection of ball bearing race faults. *Tribology International*. pp.793-800.
- Prasad H, Ghosh M, Biswas S, 1984. Diagnostic monitoring of rolling element bearings by High Frequency Resonance Technique. *ASLE paper* **84-LC-3c3**. pp1-9.
- Prasad H, 1987. The effect of cage and roller slip on the measured defect frequency response of rolling element bearings. *ASLE Trans* **30(3)**. pp.350-7.
- Purushotham V., S. Narayanan, and Surayanarayana A.N. Prasad, 2005. Multi-fault diagnosis of rolling bearing elements using wavelet analysis and hidden Markov model based fault recognition. *NDT&E International*. pp.654-664.
- Riddle J., 1955. Ball bearing maintenance. *Norman, OK: Univ. of Oklahoma Press*.
- Schoen R.R, T.G. Habetler, F. Kamran, R.G. Barthheld, 1995. Motor bearing damage detection using stator current monitoring. *IEEE Transactions on Industry Applications* **31 (6)** (1995). pp.271-282.
- SKF, 1994. SKF Handbook: Bearing failures and their causes. *Palmeblads Tryckeri AB*. Publication PI 401 E.
- Staszewski W.J., 1998. Structural and mechanical damage detection using wavelets. *The Shock and Vibration Digest* **30(6)**. pp.457-72.
- Sunnersjo C.S., 1978. Varying compliance vibrations of rolling bearings. *J Sound Vibration* **58(3)**, pp.363-73.
- Tandon N. and A. Choudhury, 1999. A review of vibration and acoustic measurement methods for the detection of defects in rolling element bearings. *Tribology International*. pp.469-480.
- Tandon N., G.S. Yadava, and K.M. Ramakrishna, 2005. A comparison of some condition monitoring techniques for the detection of defect in induction motor ball bearings. *Mechanical Systems and Signal Processing*. pp.244-256.
- Tandon N, Nakra BC, 1992. Vibration and acoustic monitoring techniques for the detection of defects in rolling element bearings – a review. *Shock Vibration Digest* **24(3)**. pp.3-11.
- The Timken Company – Where You Turn. Retrieved from <http://www.timken.com/en-us/products/Pages/Catalogs.aspx> online at 16 October 2011

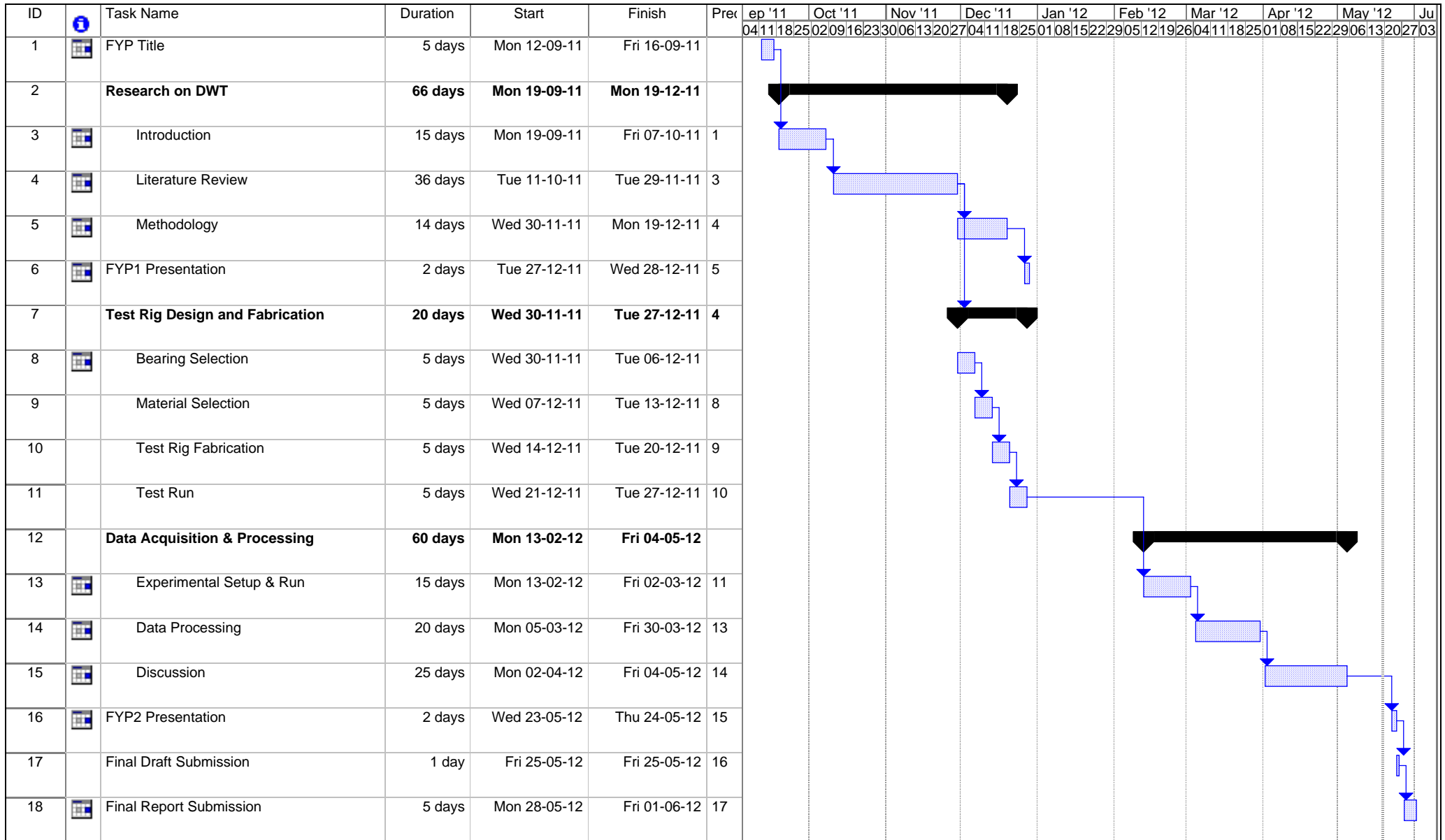
APPENDIX A
PROJECT GANTT CHART

APPENDIX B
TECHNICAL DRAWINGS

APPENDIX C
CNC MACHINE CODING

APPENDIX D

FFT GRAPH



Project: FYP1 Gantt Chart
Date: Sat 19-05-12

Task

Split

Progress

Milestone

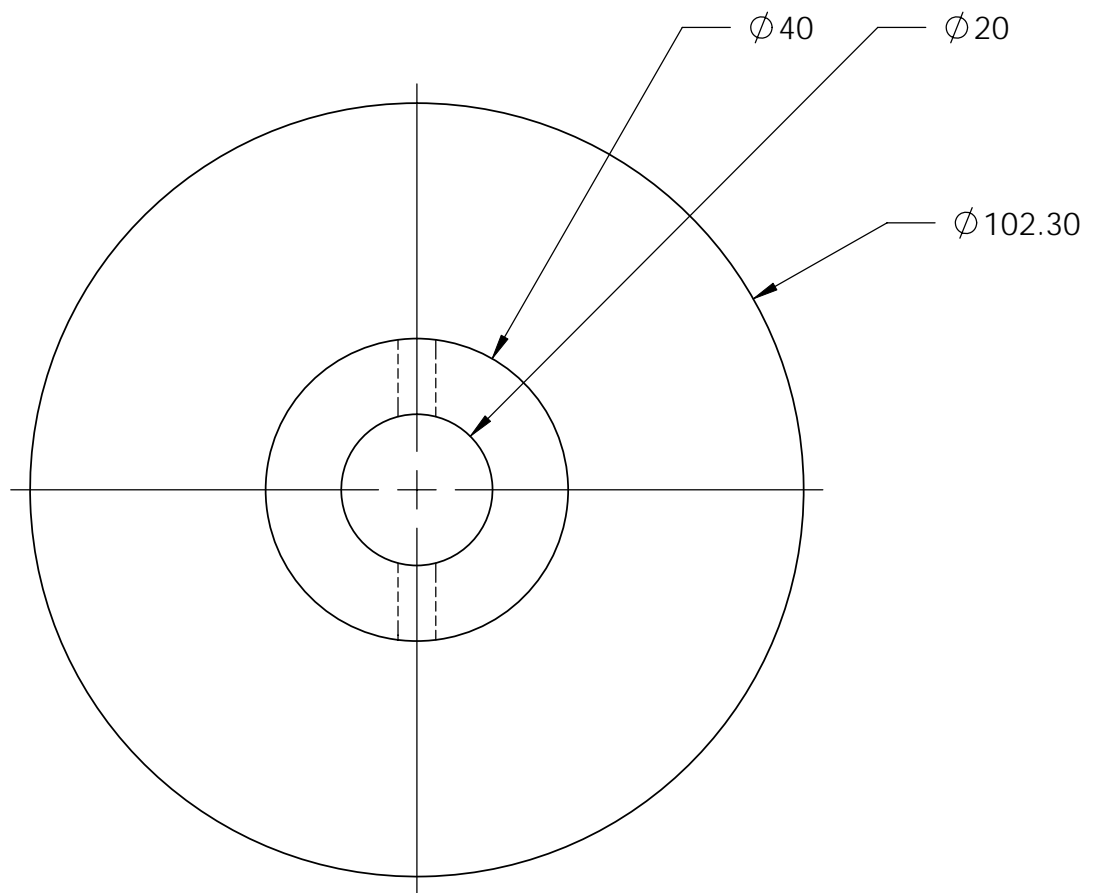
Summary

Project Summary

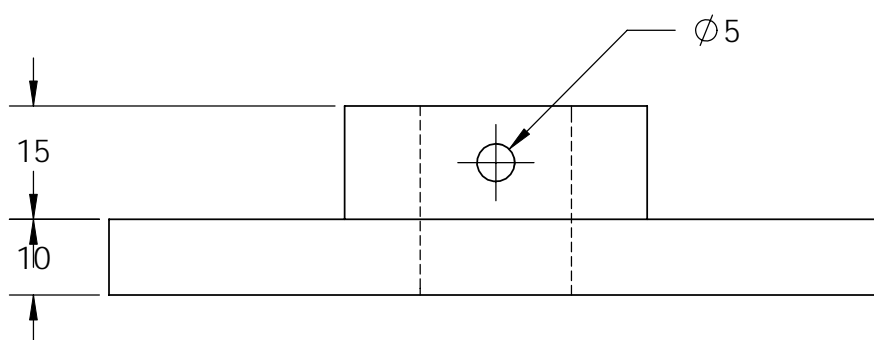
External Tasks

External Milestone


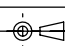
Deadline

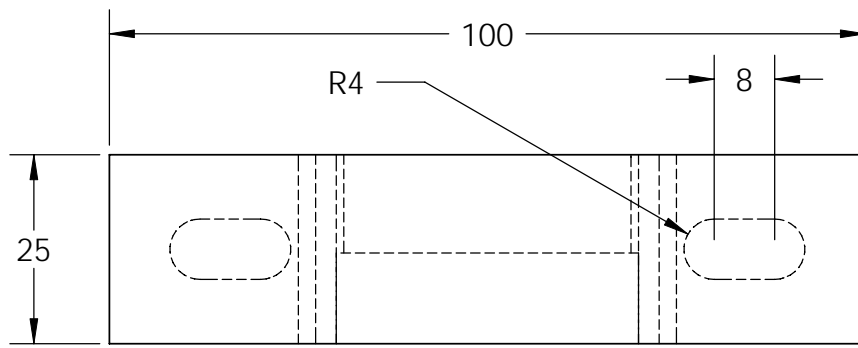


TOP VIEW

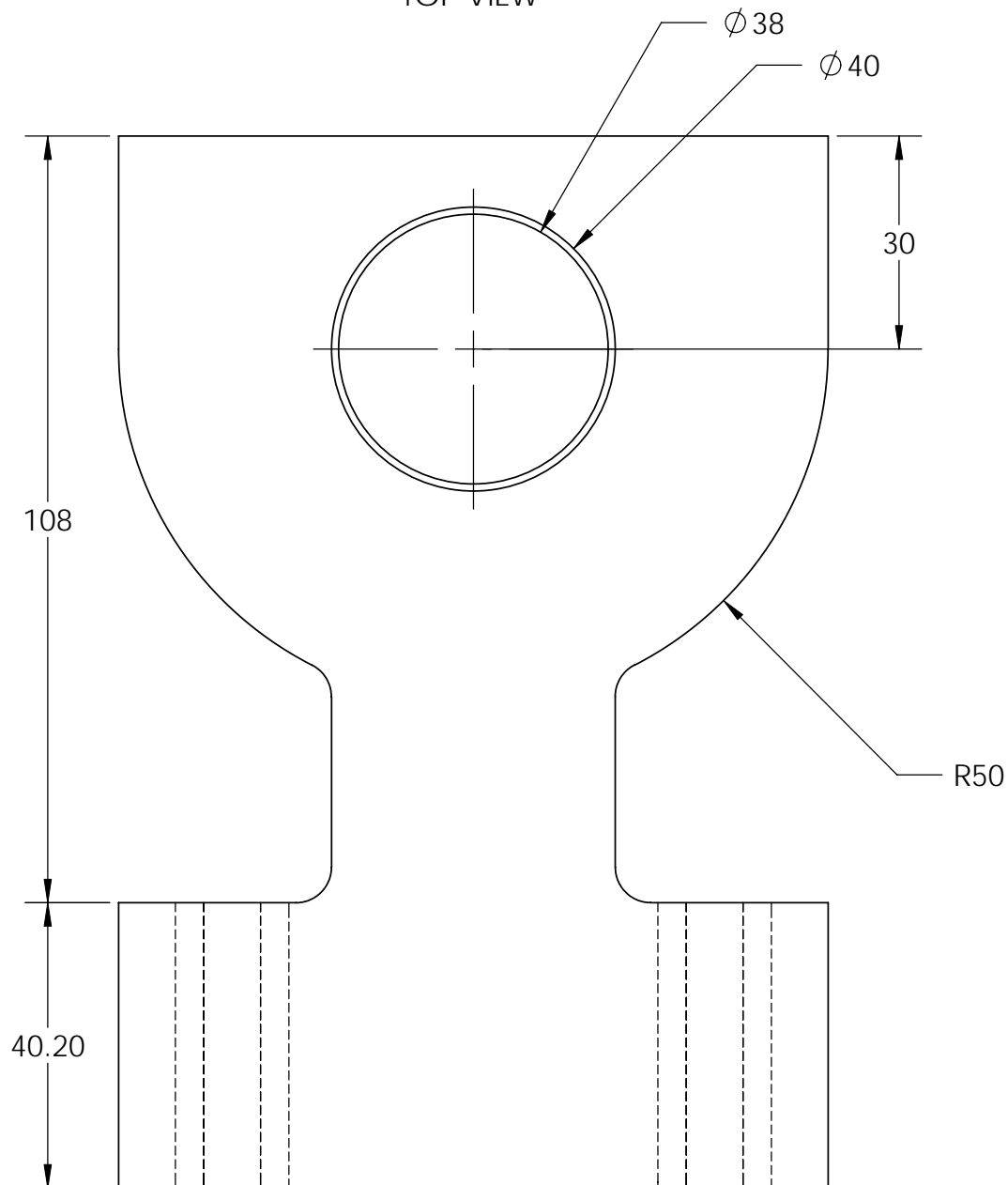


FRONT VIEW

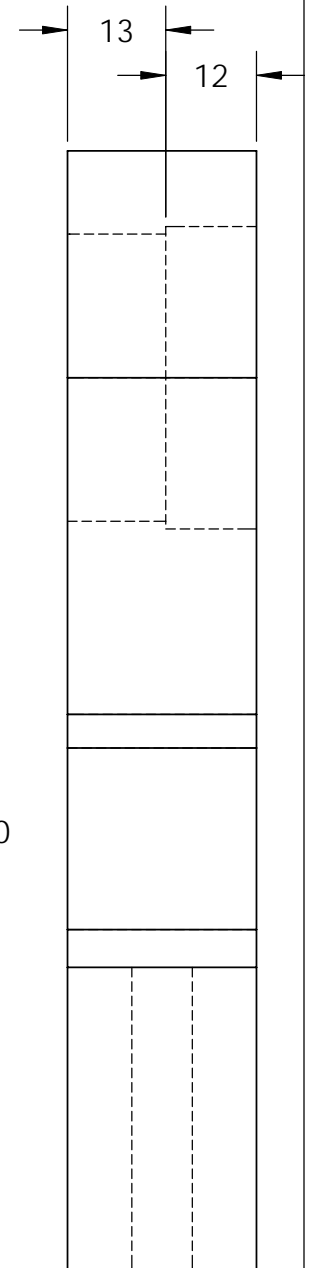
ALL DIMENSIONS ARE IN MILLIMETRES (mm) UNLESS OTHERWISE SPECIFIED		NAME	DATE	<div>FLY WHEEL</div>			
	DRAWN	S.AZEEM ONG	10/11/11				
	CHECKED	C.K.E NIZWAN	12/11/11				
	APPROVED	C.K.E NIZWAN	12/11/11				
MATERIAL	<div><div>Universiti Malaysia PAHANG</div><div>flywheeling • Add This Logo • Creativity</div></div>						
ALUMINUM							
FACULTY OF MECHANICAL ENGINEERING					SIZE	DWG. NO.	
DO NOT SCALE DRAWING					A	flywheel	
				SCALE:1:2	WEIGHT:	SHEET 1 OF 1	




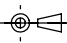
TOP VIEW

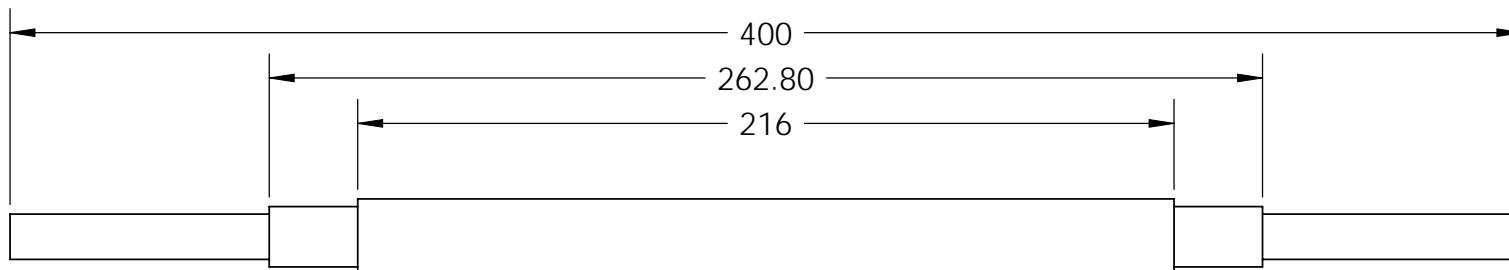
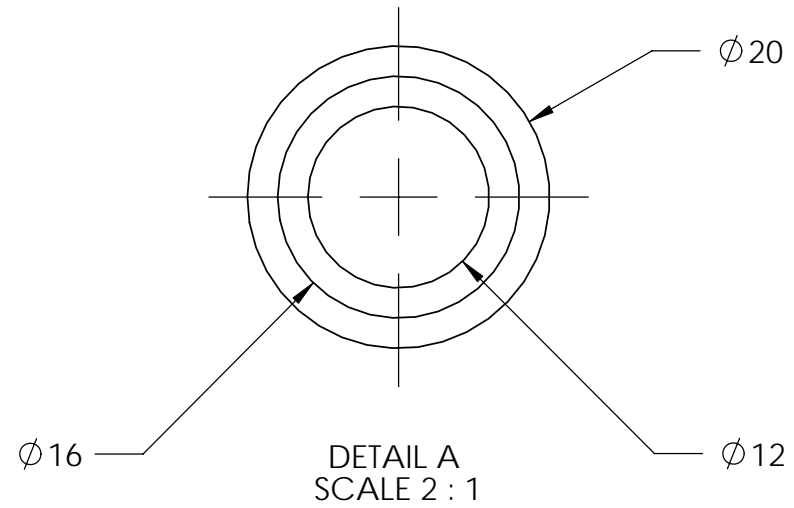


FRONT VIEW

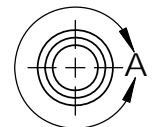


SIDE VIEW

ALL DIMENSIONS ARE IN MILLIMETRES (mm) UNLESS OTHERWISE SPECIFIED		NAME		DATE		BEARING HOUSING				
		DRAWN	S.AZEEM ONG	10/11/11						
		CHECKED	C.K.E NIZWAN	12/11/11						
		APPROVED	C.K.E NIZWAN	12/11/11						
MATERIAL	ALUMINUM			SIZE		DWG. NO.				
FACULTY OF MECHANICAL ENGINEERING				A		housing tech				
DO NOT SCALE DRAWING				SCALE:1:1		WEIGHT:			SHEET 1 OF 1	



FRONT VIEW



SIDE VIEW

DIMENSIONS ARE IN
MILLIMETRES (mm) UNLESS
OTHERWISE SPECIFIED

MATERIAL
ALUMINUM

FACULTY OF
MECHANICAL ENGINEERING

DO NOT SCALE DRAWING

	NAME	DATE
DRAWN	S.AZEEM ONG	11/11/11
CHECKED	C.K.E NIZWAN	12/11/11
APPROVED	C.K.E NIZWAN	12/11/11



TITLE:

SHAFT

SIZE	DWG. NO.	
A	shaft - tech	

SCALE: 1:2	WEIGHT:	SHEET 1 OF 1
------------	---------	--------------

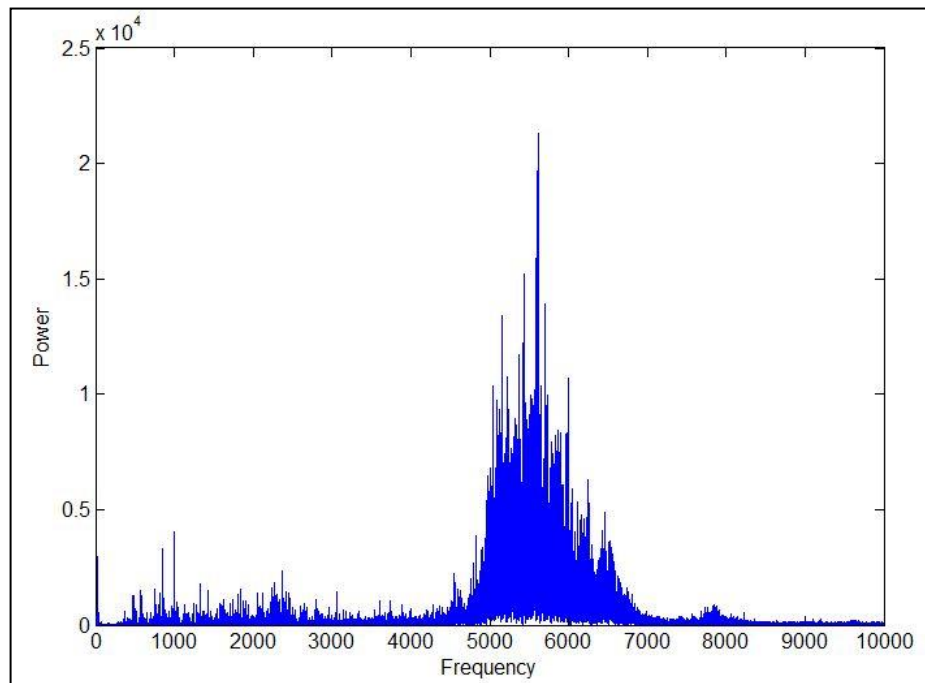


Figure 4.26: FFT result for contaminated defect at speed 1466

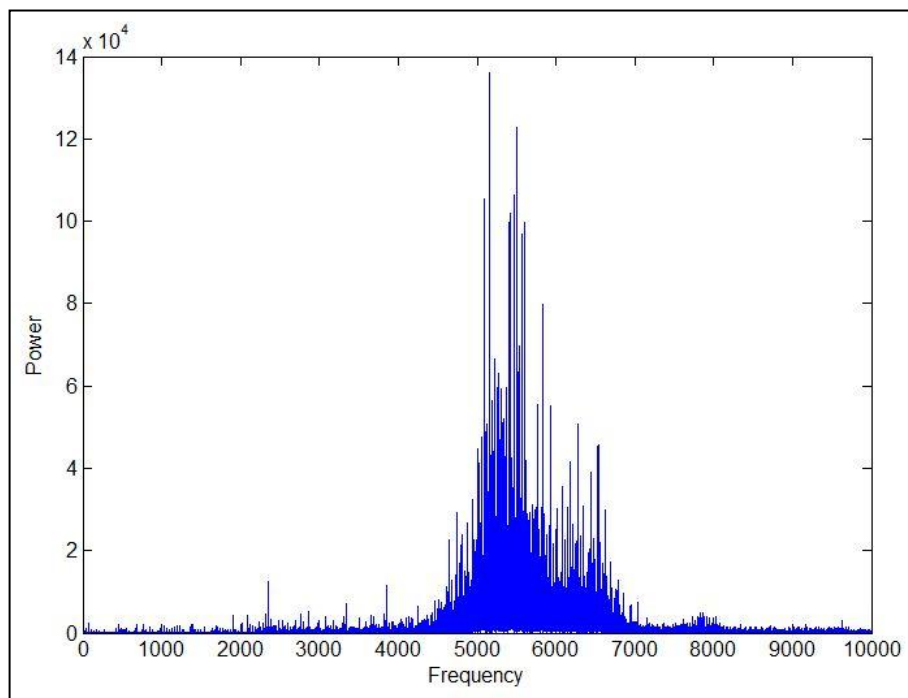


Figure 4.27: FFT result for contaminated defect at speed 2664

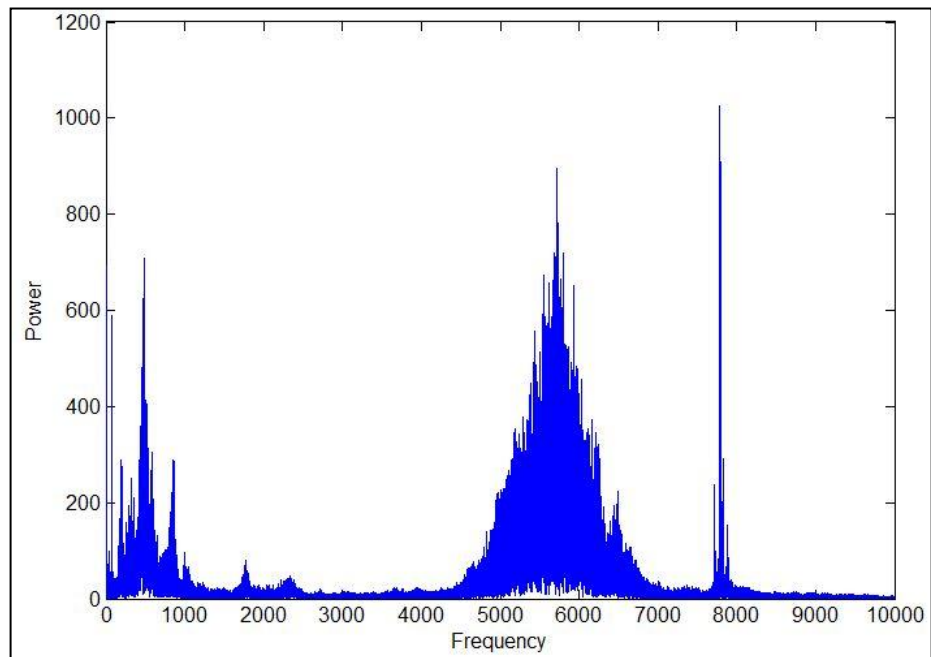


Figure 4.28: FFT result for corroded defect at speed 287

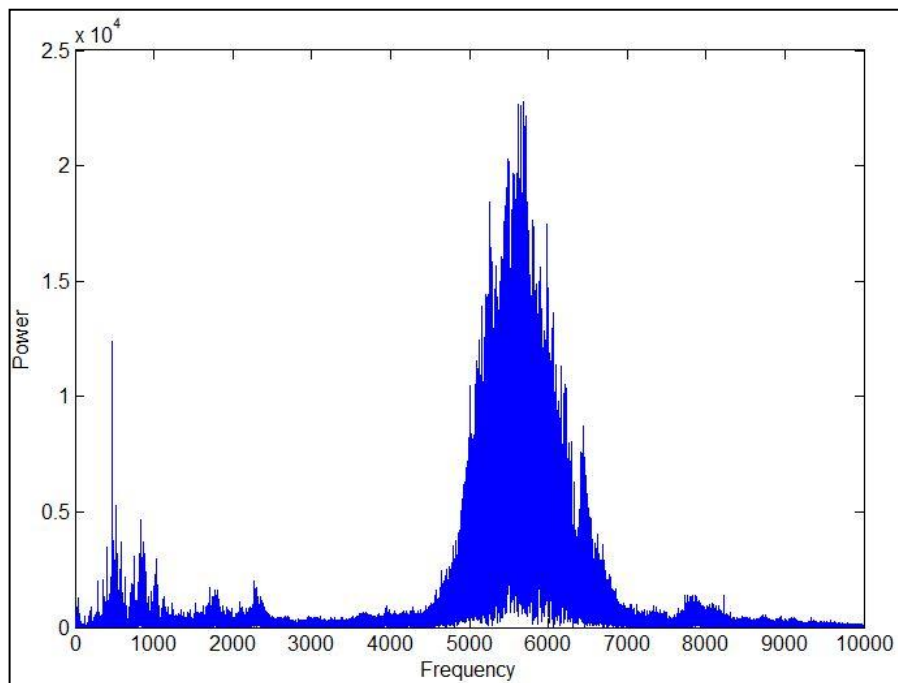


Figure 4.29: FFT result for corroded defect at speed 1466

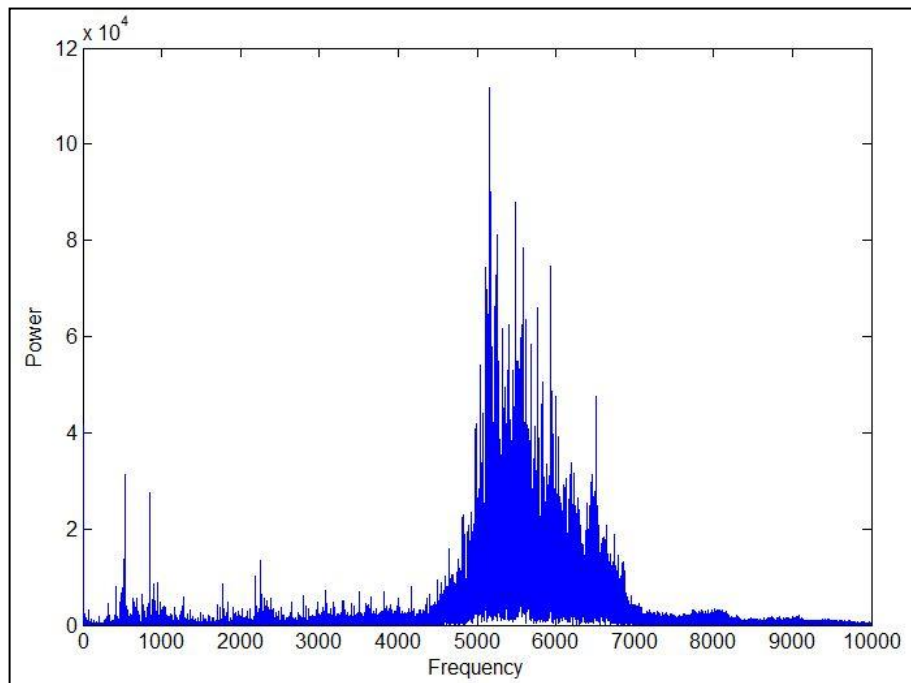


Figure 4.30: FFT result for corroded defect at speed 2664

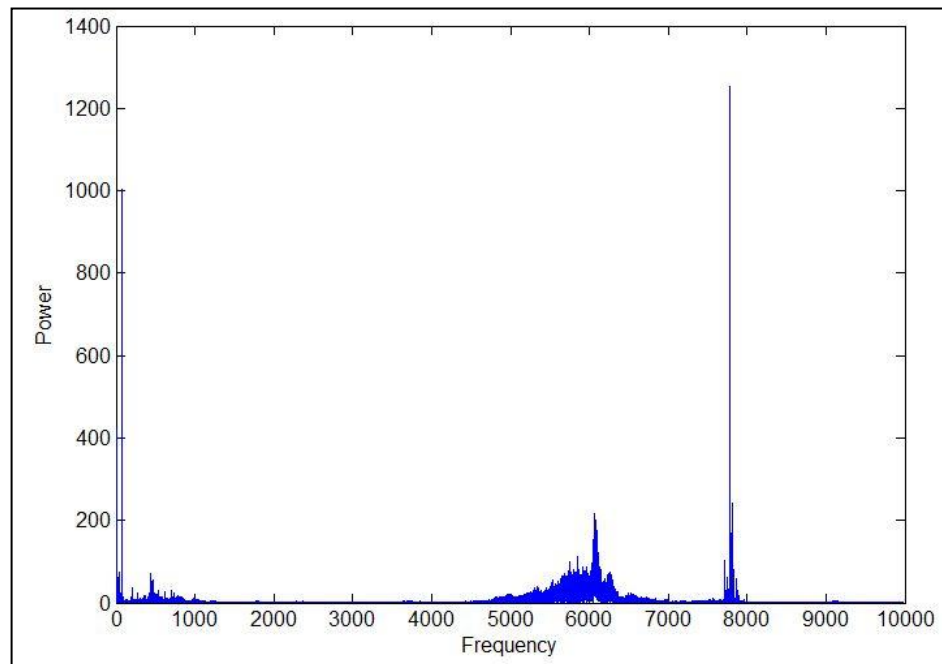


Figure 4.31: FFT result for inner race defect at speed 287

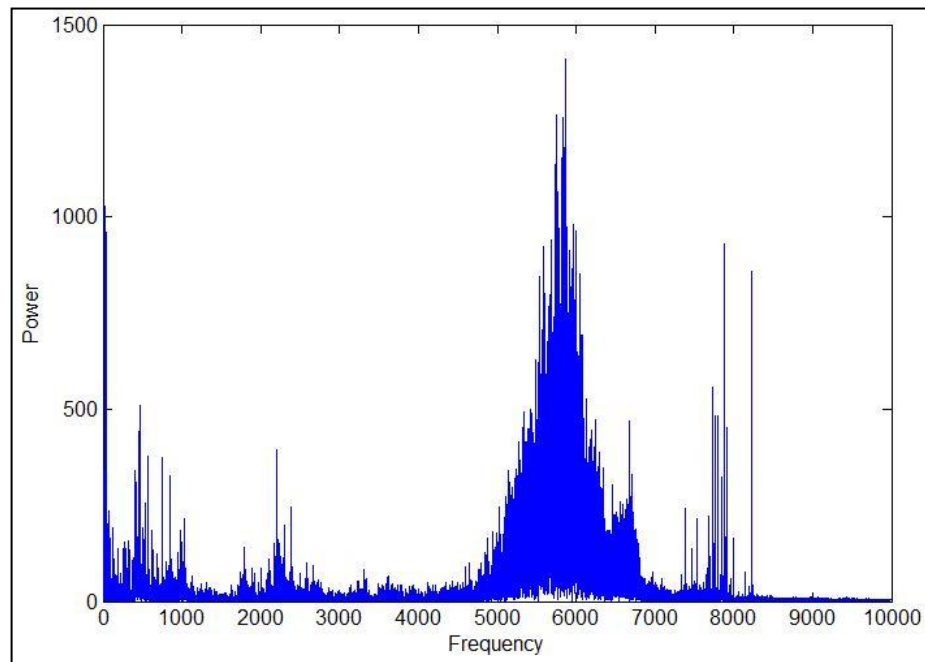


Figure 4.32: FFT result for inner race defect at speed 1466

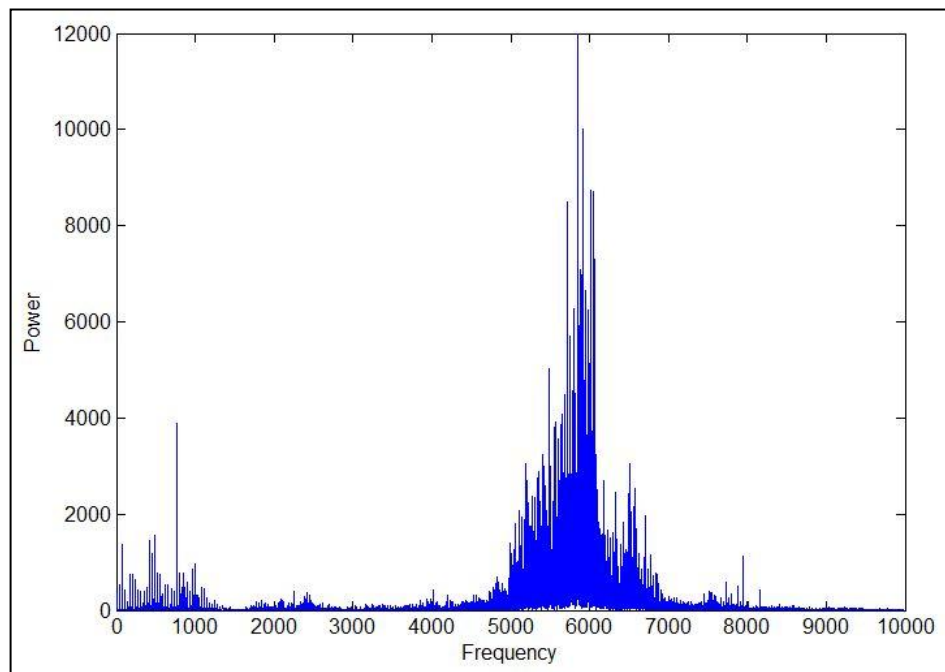


Figure 4.33: FFT result for inner race defect at speed 2664

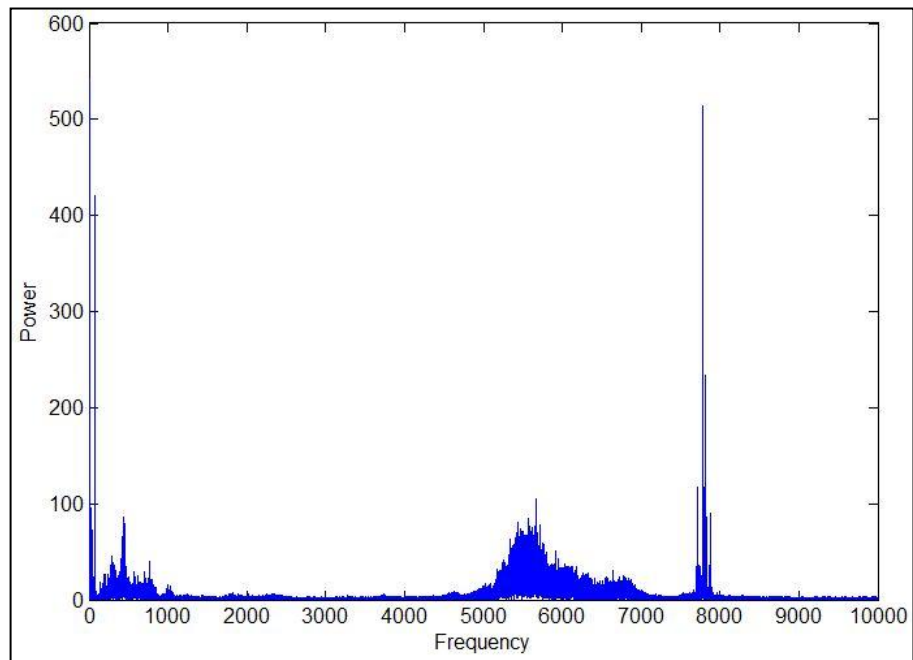


Figure 4.34: FFT result for outer race defect at speed 287

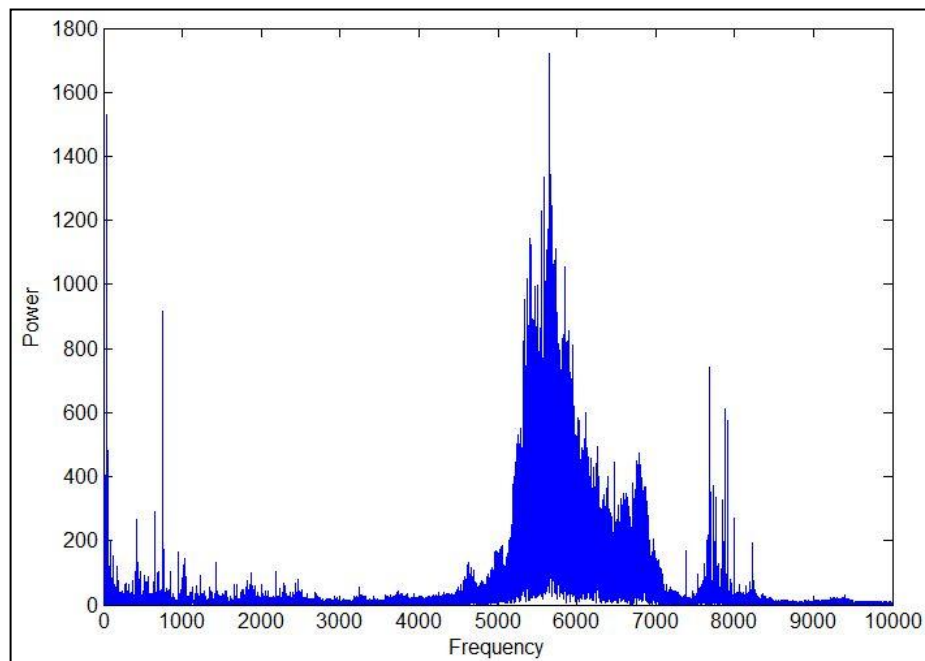


Figure 4.35: FFT result for outer race defect at speed 1466

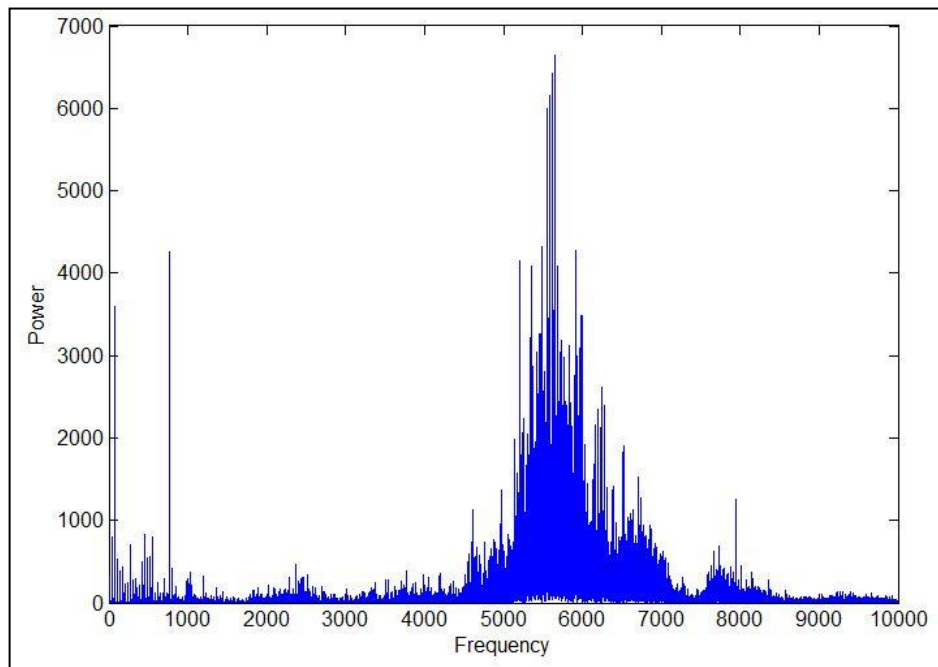


Figure 4.36: FFT result for outer race defect at speed 2664

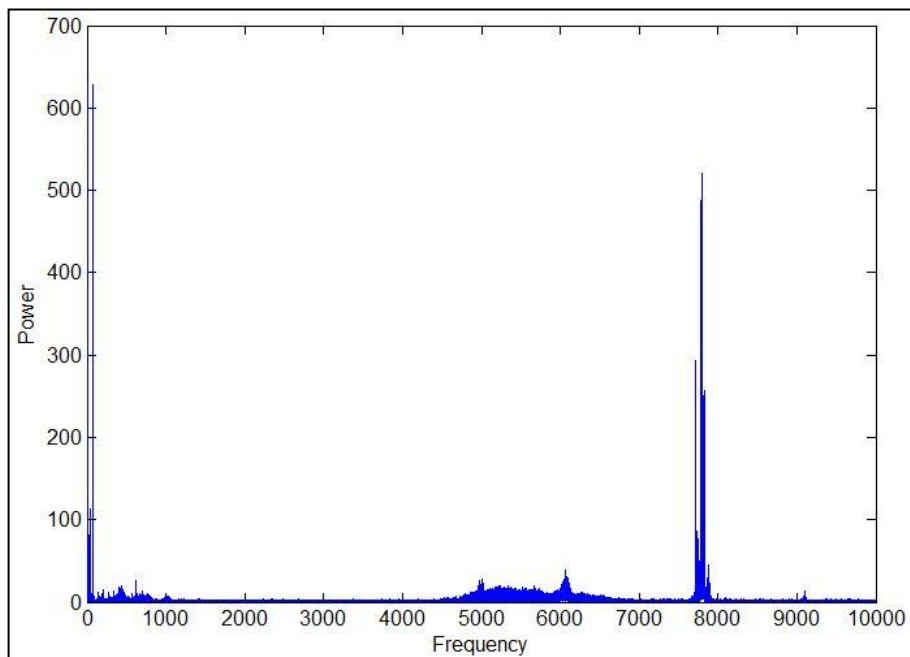


Figure 4.37: FFT result for point defect at speed 287

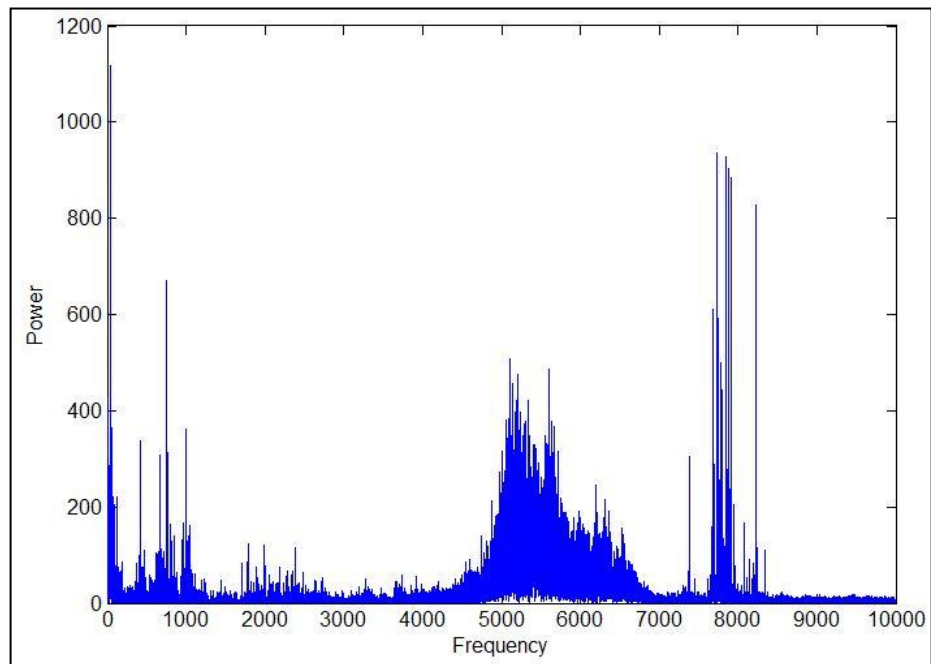


Figure 4.38: FFT result for point defect defect at speed 1466

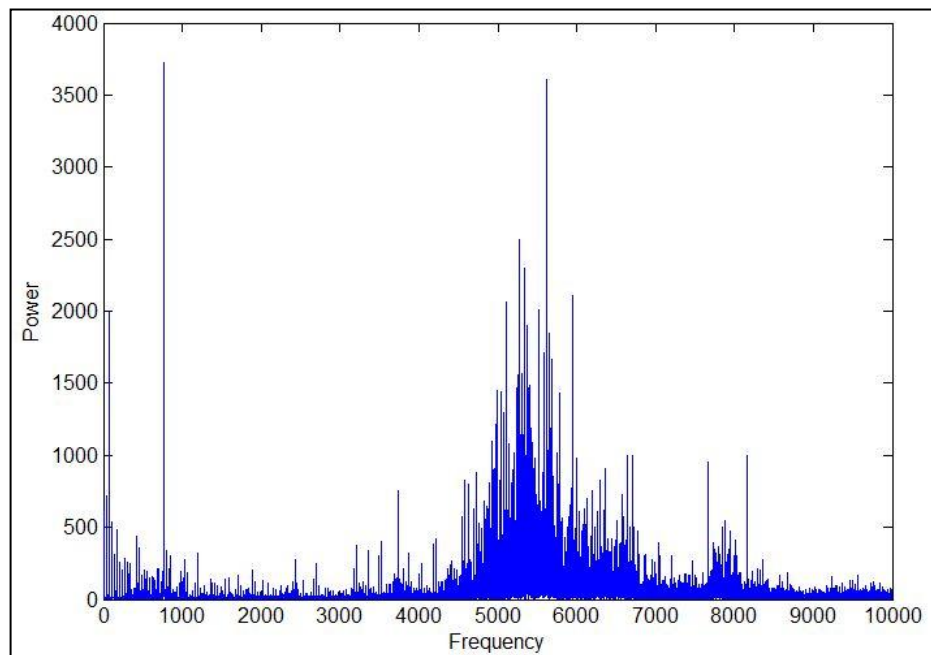


Figure 4.39: FFT result for point defect defect at speed 2664

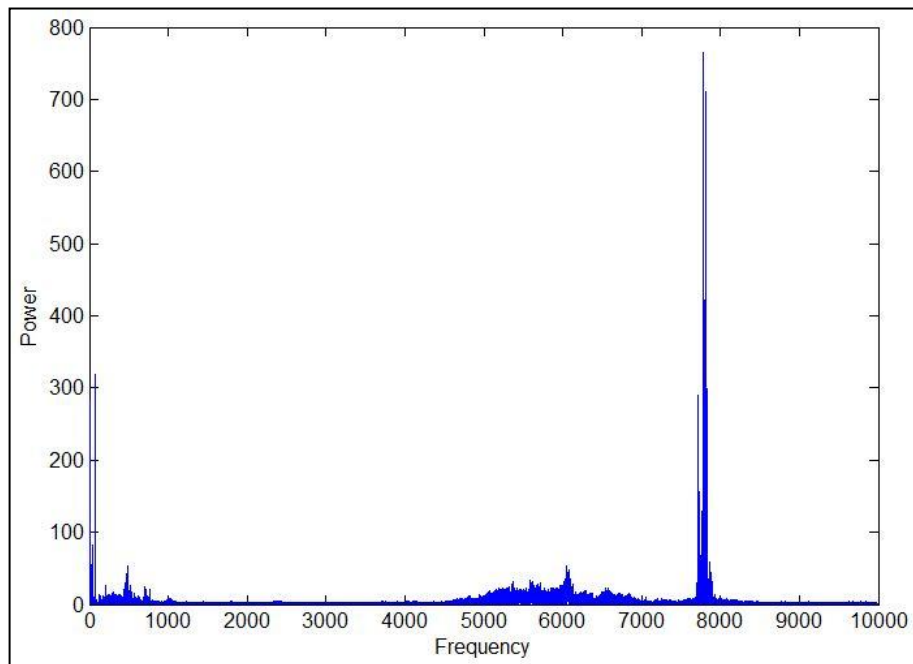


Figure 4.40: FFT result for healthy bearing at speed 287

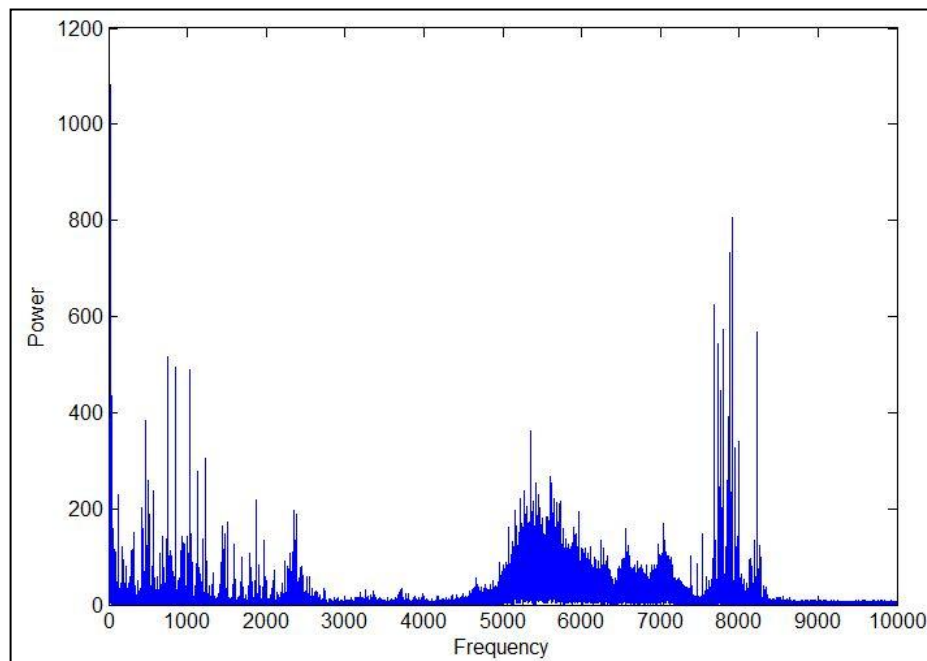


Figure 4.41: FFT result for healthy bearing at speed 1466

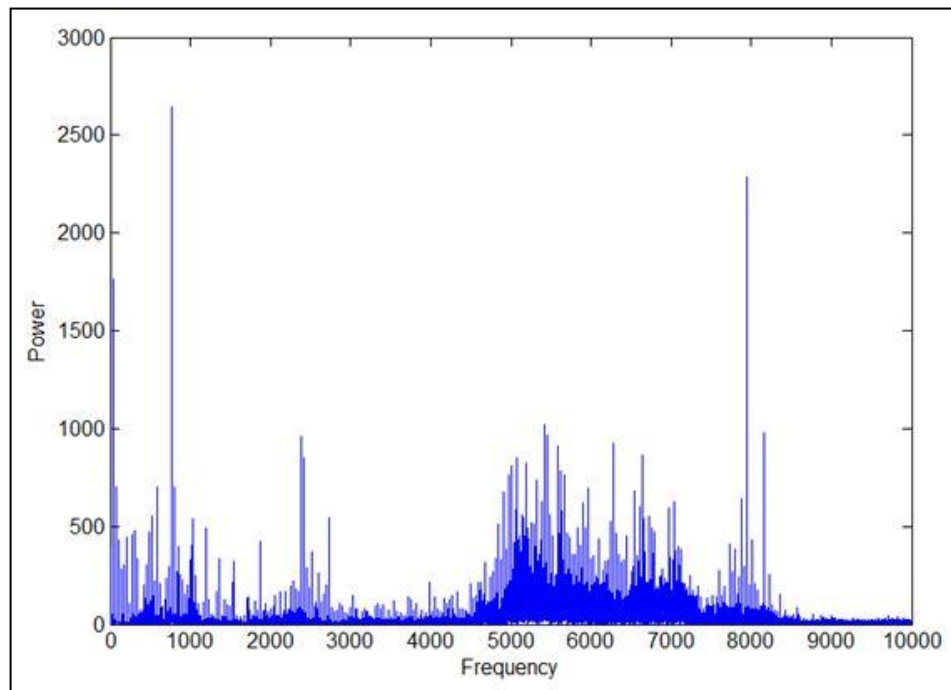


Figure 4.42: FFT result for healthy bearing at speed 2664

%
O0003
(PROGRAM NAME - BEARING
HOUSING)
(=DATE=DD-MM-YY - 04-01-12
TIME=HH:MM - 11:39)
N100 G21
N102 G0 G17 G40 G49 G80 G90
(20. FLAT ENDMILL TOOL
- 1 DIA. OFF. - 1 LEN. - 1
DIA. - 20.)
N104 T1 M6
N106 G0 G90 G54 X-8.5 Y-
23.78 A0. S1200 M3
N108 G43 H1 Z25.
N110 Z5.
N112 G1 Z-.5 F10.
N114 G3 X8.5 R8.5 F120.
N116 X-8.5 R8.5
N118 G1 Z-1. F10.
N120 G3 X8.5 R8.5 F120.
N122 X-8.5 R8.5
N124 G1 Z-1.5 F10.
N126 G3 X8.5 R8.5 F120.
N128 X-8.5 R8.5
N130 G1 Z-2. F10.
N132 G3 X8.5 R8.5 F120.
N134 X-8.5 R8.5
N136 G1 Z-2.5 F10.
N138 G3 X8.5 R8.5 F120.
N140 X-8.5 R8.5
N142 G1 Z-3. F10.
N144 G3 X8.5 R8.5 F120.
N146 X-8.5 R8.5
N148 G1 Z-3.5 F10.
N150 G3 X8.5 R8.5 F120.
N152 X-8.5 R8.5
N154 G1 Z-4. F10.
N156 G3 X8.5 R8.5 F120.
N158 X-8.5 R8.5
N160 G1 Z-4.5 F10.
N162 G3 X8.5 R8.5 F120.
N164 X-8.5 R8.5
N166 G1 Z-5. F10.
N168 G3 X8.5 R8.5 F120.
N170 X-8.5 R8.5
N172 G1 Z-5.5 F10.
N174 G3 X8.5 R8.5 F120.
N176 X-8.5 R8.5
N178 G1 Z-6. F10.
N180 G3 X8.5 R8.5 F120.
N182 X-8.5 R8.5
N184 G1 Z-6.5 F10.
N186 G3 X8.5 R8.5 F120.
N188 X-8.5 R8.5
N190 G1 Z-7. F10.
N192 G3 X8.5 R8.5 F120.
N194 X-8.5 R8.5
N196 G1 Z-7.5 F10.
N198 G3 X8.5 R8.5 F120.
N200 X-8.5 R8.5
N202 G1 Z-8. F10.
N204 G3 X8.5 R8.5 F120.
N206 X-8.5 R8.5
N208 G1 Z-8.5 F10.
N210 G3 X8.5 R8.5 F120.
N212 X-8.5 R8.5
N214 G1 Z-9. F10.
N216 G3 X8.5 R8.5 F120.
N218 X-8.5 R8.5

N220 G1 Z-9.5 F10.
N222 G3 X8.5 R8.5 F120.
N224 X-8.5 R8.5
N226 G1 Z-10. F10.
N228 G3 X8.5 R8.5 F120.
N230 X-8.5 R8.5
N232 G1 Z-10.5 F10.
N234 G3 X8.5 R8.5 F120.
N236 X-8.5 R8.5
N238 G1 Z-11. F10.
N240 G3 X8.5 R8.5 F120.
N242 X-8.5 R8.5
N244 G1 Z-11.5 F10.
N246 G3 X8.5 R8.5 F120.
N248 X-8.5 R8.5
N250 G1 Z-12. F10.
N252 G3 X8.5 R8.5 F120.
N254 X-8.5 R8.5
N256 G1 Z-12.5 F10.
N258 G3 X8.5 R8.5 F120.
N260 X-8.5 R8.5
N262 G1 Z-13. F10.
N264 G3 X8.5 R8.5 F120.
N266 X-8.5 R8.5
N268 G1 Z-13.5 F10.
N270 G3 X8.5 R8.5 F120.
N272 X-8.5 R8.5
N274 G1 Z-14. F10.
N276 G3 X8.5 R8.5 F120.
N278 X-8.5 R8.5
N280 G1 Z-14.5 F10.
N282 G3 X8.5 R8.5 F120.
N284 X-8.5 R8.5
N286 G1 Z-15. F10.
N288 G3 X8.5 R8.5 F120.
N290 X-8.5 R8.5
N292 G1 Z-15.5 F10.
N294 G3 X8.5 R8.5 F120.
N296 X-8.5 R8.5
N298 G1 Z-16. F10.
N300 G3 X8.5 R8.5 F120.
N302 X-8.5 R8.5
N304 G1 Z-16.5 F10.
N306 G3 X8.5 R8.5 F120.
N308 X-8.5 R8.5
N310 G1 Z-17. F10.
N312 G3 X8.5 R8.5 F120.
N314 X-8.5 R8.5
N316 G1 Z-17.5 F10.
N318 G3 X8.5 R8.5 F120.
N320 X-8.5 R8.5
N322 G1 Z-18. F10.
N324 G3 X8.5 R8.5 F120.
N326 X-8.5 R8.5
N328 G1 Z-18.5 F10.
N330 G3 X8.5 R8.5 F120.
N332 X-8.5 R8.5
N334 G1 Z-19. F10.
N336 G3 X8.5 R8.5 F120.
N338 X-8.5 R8.5
N340 G1 Z-19.5 F10.
N342 G3 X8.5 R8.5 F120.
N344 X-8.5 R8.5
N346 G1 Z-20. F10.
N348 G3 X8.5 R8.5 F120.
N350 X-8.5 R8.5
N352 G1 Z-20.5 F10.
N354 G3 X8.5 R8.5 F120.
N356 X-8.5 R8.5
N358 G1 Z-21. F10.

N360 G3 X8.5 R8.5 F120.
N362 X-8.5 R8.5
N364 G1 Z-21.5 F10.
N366 G3 X8.5 R8.5 F120.
N368 X-8.5 R8.5
N370 G1 Z-22. F10.
N372 G3 X8.5 R8.5 F120.
N374 X-8.5 R8.5
N376 G1 Z-22.5 F10.
N378 G3 X8.5 R8.5 F120.
N380 X-8.5 R8.5
N382 G1 Z-23. F10.
N384 G3 X8.5 R8.5 F120.
N386 X-8.5 R8.5
N388 G1 Z-23.5 F10.
N390 G3 X8.5 R8.5 F120.
N392 X-8.5 R8.5
N394 G1 Z-24. F10.
N396 G3 X8.5 R8.5 F120.
N398 X-8.5 R8.5
N400 G1 Z-24.5 F10.
N402 G3 X8.5 R8.5 F120.
N404 X-8.5 R8.5
N406 G1 Z-25. F10.
N408 G3 X8.5 R8.5 F120.
N410 X-8.5 R8.5
N412 G1 Z-25.5 F10.
N414 G3 X8.5 R8.5 F120.
N416 X-8.5 R8.5
N418 G1 Z-26. F10.
N420 G3 X8.5 R8.5 F120.
N422 X-8.5 R8.5
N424 G0 Z25.
N426 X-9.985
N428 Z5.
N430 G1 Z-.5 F10.
N432 G3 X9.985 R9.985 F120.
N434 X-9.985 R9.985
N436 G1 Z-1. F10.
N438 G3 X9.985 R9.985 F120.
N440 X-9.985 R9.985
N442 G1 Z-1.5 F10.
N444 G3 X9.985 R9.985 F120.
N446 X-9.985 R9.985
N448 G1 Z-2. F10.
N450 G3 X9.985 R9.985 F120.
N452 X-9.985 R9.985
N454 G1 Z-2.5 F10.
N456 G3 X9.985 R9.985 F120.
N458 X-9.985 R9.985
N460 G1 Z-3. F10.
N462 G3 X9.985 R9.985 F120.
N464 X-9.985 R9.985
N466 G1 Z-3.5 F10.
N468 G3 X9.985 R9.985 F120.
N470 X-9.985 R9.985
N472 G1 Z-4. F10.
N474 G3 X9.985 R9.985 F120.
N476 X-9.985 R9.985
N478 G1 Z-4.5 F10.
N480 G3 X9.985 R9.985 F120.
N482 X-9.985 R9.985
N484 G1 Z-5. F10.
N486 G3 X9.985 R9.985 F120.
N488 X-9.985 R9.985
N490 G1 Z-5.5 F10.
N492 G3 X9.985 R9.985 F120.
N494 X-9.985 R9.985
N496 G1 Z-6. F10.
N498 G3 X9.985 R9.985 F120.

N500 X-9.985 R9.985
N502 G1 Z-6.5 F10.
N504 G3 X9.985 R9.985 F120.
N506 X-9.985 R9.985
N508 G1 Z-7. F10.
N510 G3 X9.985 R9.985 F120.
N512 X-9.985 R9.985
N514 G1 Z-7.5 F10.
N516 G3 X9.985 R9.985 F120.
N518 X-9.985 R9.985
N520 G1 Z-8. F10.
N522 G3 X9.985 R9.985 F120.
N524 X-9.985 R9.985
N526 G1 Z-8.5 F10.
N528 G3 X9.985 R9.985 F120.
N530 X-9.985 R9.985
N532 G1 Z-9. F10.
N534 G3 X9.985 R9.985 F120.
N536 X-9.985 R9.985
N538 G1 Z-9.5 F10.
N540 G3 X9.985 R9.985 F120.
N542 X-9.985 R9.985
N544 G1 Z-10. F10.
N546 G3 X9.985 R9.985 F120.
N548 X-9.985 R9.985
N550 G1 Z-10.5 F10.
N552 G3 X9.985 R9.985 F120.
N554 X-9.985 R9.985
N556 G1 Z-11. F10.
N558 G3 X9.985 R9.985 F120.
N560 X-9.985 R9.985
N562 G1 Z-11.5 F10.
N564 G3 X9.985 R9.985 F120.
N566 X-9.985 R9.985
N568 G1 Z-12. F10.
N570 G3 X9.985 R9.985 F120.
N572 X-9.985 R9.985
N574 G0 Z25.
N576 X-57. Y29.63
N578 Z5.
N580 G1 Z-.5 F10.
N582 X-30. F120.
N584 Y17.36
N586 G3 X-59.558 Y-15.442
R40.
N588 G1 X-70.65 Y-22.096
N590 X-57. Y29.63
N592 Z-1. F10.
N594 X-30. F120.
N596 Y17.36
N598 G3 X-59.558 Y-15.442
R40.
N600 G1 X-70.65 Y-22.096
N602 X-57. Y29.63
N604 Z-1.5 F10.
N606 X-30. F120.
N608 Y17.36
N610 G3 X-59.558 Y-15.442
R40.
N612 G1 X-70.65 Y-22.096
N614 X-57. Y29.63
N616 Z-2. F10.
N618 X-30. F120.
N620 Y17.36
N622 G3 X-59.558 Y-15.442
R40.
N624 G1 X-70.65 Y-22.096
N626 X-57. Y29.63
N628 Z-2.5 F10.
N630 X-30. F120.

N632 Y17.36
N634 G3 X-59.558 Y-15.442
R40.
N636 G1 X-70.65 Y-22.096
N638 X-57. Y29.63
N640 Z-3. F10.
N642 X-30. F120.
N644 Y17.36
N646 G3 X-59.558 Y-15.442
R40.
N648 G1 X-70.65 Y-22.096
N650 X-57. Y29.63
N652 Z-3.5 F10.
N654 X-30. F120.
N656 Y17.36
N658 G3 X-59.558 Y-15.442
R40.
N660 G1 X-70.65 Y-22.096
N662 X-57. Y29.63
N664 Z-4. F10.
N666 X-30. F120.
N668 Y17.36
N670 G3 X-59.558 Y-15.442
R40.
N672 G1 X-70.65 Y-22.096
N674 X-57. Y29.63
N676 Z-4.5 F10.
N678 X-30. F120.
N680 Y17.36
N682 G3 X-59.558 Y-15.442
R40.
N684 G1 X-70.65 Y-22.096
N686 X-57. Y29.63
N688 Z-5. F10.
N690 X-30. F120.
N692 Y17.36
N694 G3 X-59.558 Y-15.442
R40.
N696 G1 X-70.65 Y-22.096
N698 X-57. Y29.63
N700 Z-5.5 F10.
N702 X-30. F120.
N704 Y17.36
N706 G3 X-59.558 Y-15.442
R40.
N708 G1 X-70.65 Y-22.096
N710 X-57. Y29.63
N712 Z-6. F10.
N714 X-30. F120.
N716 Y17.36
N718 G3 X-59.558 Y-15.442
R40.
N720 G1 X-70.65 Y-22.096
N722 X-57. Y29.63
N724 Z-6.5 F10.
N726 X-30. F120.
N728 Y17.36
N730 G3 X-59.558 Y-15.442
R40.
N732 G1 X-70.65 Y-22.096
N734 X-57. Y29.63
N736 Z-7. F10.
N738 X-30. F120.
N740 Y17.36
N742 G3 X-59.558 Y-15.442
R40.
N744 G1 X-70.65 Y-22.096
N746 X-57. Y29.63
N748 Z-7.5 F10.
N750 X-30. F120.

N752 Y17.36
N754 G3 X-59.558 Y-15.442
R40.
N756 G1 X-70.65 Y-22.096
N758 X-57. Y29.63
N760 Z-8. F10.
N762 X-30. F120.
N764 Y17.36
N766 G3 X-59.558 Y-15.442
R40.
N768 G1 X-70.65 Y-22.096
N770 X-57. Y29.63
N772 Z-8.5 F10.
N774 X-30. F120.
N776 Y17.36
N778 G3 X-59.558 Y-15.442
R40.
N780 G1 X-70.65 Y-22.096
N782 X-57. Y29.63
N784 Z-9. F10.
N786 X-30. F120.
N788 Y17.36
N790 G3 X-59.558 Y-15.442
R40.
N792 G1 X-70.65 Y-22.096
N794 X-57. Y29.63
N796 Z-9.5 F10.
N798 X-30. F120.
N800 Y17.36
N802 G3 X-59.558 Y-15.442
R40.
N804 G1 X-70.65 Y-22.096
N806 X-57. Y29.63
N808 Z-10. F10.
N810 X-30. F120.
N812 Y17.36
N814 G3 X-59.558 Y-15.442
R40.
N816 G1 X-70.65 Y-22.096
N818 X-57. Y29.63
N820 Z-10.5 F10.
N822 X-30. F120.
N824 Y17.36
N826 G3 X-59.558 Y-15.442
R40.
N828 G1 X-70.65 Y-22.096
N830 X-57. Y29.63
N832 Z-11. F10.
N834 X-30. F120.
N836 Y17.36
N838 G3 X-59.558 Y-15.442
R40.
N840 G1 X-70.65 Y-22.096
N842 X-57. Y29.63
N844 Z-11.5 F10.
N846 X-30. F120.
N848 Y17.36
N850 G3 X-59.558 Y-15.442
R40.
N852 G1 X-70.65 Y-22.096
N854 X-57. Y29.63
N856 Z-12. F10.
N858 X-30. F120.
N860 Y17.36
N862 G3 X-59.558 Y-15.442
R40.
N864 G1 X-70.65 Y-22.096
N866 X-57. Y29.63
N868 Z-12.5 F10.
N870 X-30. F120.

N872 Y17.36
N874 G3 X-59.558 Y-15.442
R40.
N876 G1 X-70.65 Y-22.096
N878 X-57. Y29.63
N880 Z-13. F10.
N882 X-30. F120.
N884 Y17.36
N886 G3 X-59.558 Y-15.442
R40.
N888 G1 X-70.65 Y-22.096
N890 X-57. Y29.63
N892 Z-13.5 F10.
N894 X-30. F120.
N896 Y17.36
N898 G3 X-59.558 Y-15.442
R40.
N900 G1 X-70.65 Y-22.096
N902 X-57. Y29.63
N904 Z-14. F10.
N906 X-30. F120.
N908 Y17.36
N910 G3 X-59.558 Y-15.442
R40.
N912 G1 X-70.65 Y-22.096
N914 X-57. Y29.63
N916 Z-14.5 F10.
N918 X-30. F120.
N920 Y17.36
N922 G3 X-59.558 Y-15.442
R40.
N924 G1 X-70.65 Y-22.096
N926 X-57. Y29.63
N928 Z-15. F10.
N930 X-30. F120.
N932 Y17.36
N934 G3 X-59.558 Y-15.442
R40.
N936 G1 X-70.65 Y-22.096
N938 X-57. Y29.63
N940 Z-15.5 F10.
N942 X-30. F120.
N944 Y17.36
N946 G3 X-59.558 Y-15.442
R40.
N948 G1 X-70.65 Y-22.096
N950 X-57. Y29.63
N952 Z-16. F10.
N954 X-30. F120.
N956 Y17.36
N958 G3 X-59.558 Y-15.442
R40.
N960 G1 X-70.65 Y-22.096
N962 X-57. Y29.63
N964 Z-16.5 F10.
N966 X-30. F120.
N968 Y17.36
N970 G3 X-59.558 Y-15.442
R40.
N972 G1 X-70.65 Y-22.096
N974 X-57. Y29.63
N976 Z-17. F10.
N978 X-30. F120.
N980 Y17.36
N982 G3 X-59.558 Y-15.442
R40.
N984 G1 X-70.65 Y-22.096
N986 X-57. Y29.63
N988 Z-17.5 F10.
N990 X-30. F120.

N992 Y17.36
N994 G3 X-59.558 Y-15.442
R40.
N996 G1 X-70.65 Y-22.096
N998 X-57. Y29.63
N1000 Z-18. F10.
N1002 X-30. F120.
N1004 Y17.36
N1006 G3 X-59.558 Y-15.442
R40.
N1008 G1 X-70.65 Y-22.096
N1010 X-57. Y29.63
N1012 Z-18.5 F10.
N1014 X-30. F120.
N1016 Y17.36
N1018 G3 X-59.558 Y-15.442
R40.
N1020 G1 X-70.65 Y-22.096
N1022 X-57. Y29.63
N1024 Z-19. F10.
N1026 X-30. F120.
N1028 Y17.36
N1030 G3 X-59.558 Y-15.442
R40.
N1032 G1 X-70.65 Y-22.096
N1034 X-57. Y29.63
N1036 Z-19.5 F10.
N1038 X-30. F120.
N1040 Y17.36
N1042 G3 X-59.558 Y-15.442
R40.
N1044 G1 X-70.65 Y-22.096
N1046 X-57. Y29.63
N1048 Z-20. F10.
N1050 X-30. F120.
N1052 Y17.36
N1054 G3 X-59.558 Y-15.442
R40.
N1056 G1 X-70.65 Y-22.096
N1058 X-57. Y29.63
N1060 Z-20.5 F10.
N1062 X-30. F120.
N1064 Y17.36
N1066 G3 X-59.558 Y-15.442
R40.
N1068 G1 X-70.65 Y-22.096
N1070 X-57. Y29.63
N1072 Z-21. F10.
N1074 X-30. F120.
N1076 Y17.36
N1078 G3 X-59.558 Y-15.442
R40.
N1080 G1 X-70.65 Y-22.096
N1082 X-57. Y29.63
N1084 Z-21.5 F10.
N1086 X-30. F120.
N1088 Y17.36
N1090 G3 X-59.558 Y-15.442
R40.
N1092 G1 X-70.65 Y-22.096
N1094 X-57. Y29.63
N1096 Z-22. F10.
N1098 X-30. F120.
N1100 Y17.36
N1102 G3 X-59.558 Y-15.442
R40.
N1104 G1 X-70.65 Y-22.096
N1106 X-57. Y29.63
N1108 Z-22.5 F10.
N1110 X-30. F120.

N1112 Y17.36
N1114 G3 X-59.558 Y-15.442
R40.
N1116 G1 X-70.65 Y-22.096
N1118 X-57. Y29.63
N1120 Z-23. F10.
N1122 X-30. F120.
N1124 Y17.36
N1126 G3 X-59.558 Y-15.442
R40.
N1128 G1 X-70.65 Y-22.096
N1130 X-57. Y29.63
N1132 Z-23.5 F10.
N1134 X-30. F120.
N1136 Y17.36
N1138 G3 X-59.558 Y-15.442
R40.
N1140 G1 X-70.65 Y-22.096
N1142 X-57. Y29.63
N1144 Z-24. F10.
N1146 X-30. F120.
N1148 Y17.36
N1150 G3 X-59.558 Y-15.442
R40.
N1152 G1 X-70.65 Y-22.096
N1154 X-57. Y29.63
N1156 Z-24.5 F10.
N1158 X-30. F120.
N1160 Y17.36
N1162 G3 X-59.558 Y-15.442
R40.
N1164 G1 X-70.65 Y-22.096
N1166 X-57. Y29.63
N1168 Z-25. F10.
N1170 X-30. F120.
N1172 Y17.36
N1174 G3 X-59.558 Y-15.442
R40.
N1176 G1 X-70.65 Y-22.096
N1178 X-57. Y29.63
N1180 Z-25.5 F10.
N1182 X-30. F120.
N1184 Y17.36
N1186 G3 X-59.558 Y-15.442
R40.
N1188 G1 X-70.65 Y-22.096
N1190 X-57. Y29.63
N1192 Z-26. F10.
N1194 X-30. F120.
N1196 Y17.36
N1198 G3 X-59.558 Y-15.442
R40.
N1200 G1 X-70.65 Y-22.096
N1202 G0 Z25.
N1204 X55. Y29.63
N1206 Z5.
N1208 G1 Z-.5 F10.
N1210 X30. F120.
N1212 Y17.36
N1214 G2 X59.733 Y-16.759
R40.
N1216 G1 X66.544 Y-23.077
N1218 X55. Y29.63
N1220 Z-1. F10.
N1222 X30. F120.
N1224 Y17.36
N1226 G2 X59.733 Y-16.759
R40.
N1228 G1 X66.544 Y-23.077
N1230 X55. Y29.63

N1232 Z-1.5 F10.
N1234 X30. F120.
N1236 Y17.36
N1238 G2 X59.733 Y-16.759
R40.
N1240 G1 X66.544 Y-23.077
N1242 X55. Y29.63
N1244 Z-2. F10.
N1246 X30. F120.
N1248 Y17.36
N1250 G2 X59.733 Y-16.759
R40.
N1252 G1 X66.544 Y-23.077
N1254 X55. Y29.63
N1256 Z-2.5 F10.
N1258 X30. F120.
N1260 Y17.36
N1262 G2 X59.733 Y-16.759
R40.
N1264 G1 X66.544 Y-23.077
N1266 X55. Y29.63
N1268 Z-3. F10.
N1270 X30. F120.
N1272 Y17.36
N1274 G2 X59.733 Y-16.759
R40.
N1276 G1 X66.544 Y-23.077
N1278 X55. Y29.63
N1280 Z-3.5 F10.
N1282 X30. F120.
N1284 Y17.36
N1286 G2 X59.733 Y-16.759
R40.
N1288 G1 X66.544 Y-23.077
N1290 X55. Y29.63
N1292 Z-4. F10.
N1294 X30. F120.
N1296 Y17.36
N1298 G2 X59.733 Y-16.759
R40.
N1300 G1 X66.544 Y-23.077
N1302 X55. Y29.63
N1304 Z-4.5 F10.
N1306 X30. F120.
N1308 Y17.36
N1310 G2 X59.733 Y-16.759
R40.
N1312 G1 X66.544 Y-23.077
N1314 X55. Y29.63
N1316 Z-5. F10.
N1318 X30. F120.
N1320 Y17.36
N1322 G2 X59.733 Y-16.759
R40.
N1324 G1 X66.544 Y-23.077
N1326 X55. Y29.63
N1328 Z-5.5 F10.
N1330 X30. F120.
N1332 Y17.36
N1334 G2 X59.733 Y-16.759
R40.
N1336 G1 X66.544 Y-23.077
N1338 X55. Y29.63
N1340 Z-6. F10.
N1342 X30. F120.
N1344 Y17.36
N1346 G2 X59.733 Y-16.759
R40.
N1348 G1 X66.544 Y-23.077
N1350 X55. Y29.63

N1352 Z-6.5 F10.
N1354 X30. F120.
N1356 Y17.36
N1358 G2 X59.733 Y-16.759
R40.
N1360 G1 X66.544 Y-23.077
N1362 X55. Y29.63
N1364 Z-7. F10.
N1366 X30. F120.
N1368 Y17.36
N1370 G2 X59.733 Y-16.759
R40.
N1372 G1 X66.544 Y-23.077
N1374 X55. Y29.63
N1376 Z-7.5 F10.
N1378 X30. F120.
N1380 Y17.36
N1382 G2 X59.733 Y-16.759
R40.
N1384 G1 X66.544 Y-23.077
N1386 X55. Y29.63
N1388 Z-8. F10.
N1390 X30. F120.
N1392 Y17.36
N1394 G2 X59.733 Y-16.759
R40.
N1396 G1 X66.544 Y-23.077
N1398 X55. Y29.63
N1400 Z-8.5 F10.
N1402 X30. F120.
N1404 Y17.36
N1406 G2 X59.733 Y-16.759
R40.
N1408 G1 X66.544 Y-23.077
N1410 X55. Y29.63
N1412 Z-9. F10.
N1414 X30. F120.
N1416 Y17.36
N1418 G2 X59.733 Y-16.759
R40.
N1420 G1 X66.544 Y-23.077
N1422 X55. Y29.63
N1424 Z-9.5 F10.
N1426 X30. F120.
N1428 Y17.36
N1430 G2 X59.733 Y-16.759
R40.
N1432 G1 X66.544 Y-23.077
N1434 X55. Y29.63
N1436 Z-10. F10.
N1438 X30. F120.
N1440 Y17.36
N1442 G2 X59.733 Y-16.759
R40.
N1444 G1 X66.544 Y-23.077
N1446 X55. Y29.63
N1448 Z-10.5 F10.
N1450 X30. F120.
N1452 Y17.36
N1454 G2 X59.733 Y-16.759
R40.
N1456 G1 X66.544 Y-23.077
N1458 X55. Y29.63
N1460 Z-11. F10.
N1462 X30. F120.
N1464 Y17.36
N1466 G2 X59.733 Y-16.759
R40.
N1468 G1 X66.544 Y-23.077
N1470 X55. Y29.63

N1472 Z-11.5 F10.
N1474 X30. F120.
N1476 Y17.36
N1478 G2 X59.733 Y-16.759
R40.
N1480 G1 X66.544 Y-23.077
N1482 X55. Y29.63
N1484 Z-12. F10.
N1486 X30. F120.
N1488 Y17.36
N1490 G2 X59.733 Y-16.759
R40.
N1492 G1 X66.544 Y-23.077
N1494 X55. Y29.63
N1496 Z-12.5 F10.
N1498 X30. F120.
N1500 Y17.36
N1502 G2 X59.733 Y-16.759
R40.
N1504 G1 X66.544 Y-23.077
N1506 X55. Y29.63
N1508 Z-13. F10.
N1510 X30. F120.
N1512 Y17.36
N1514 G2 X59.733 Y-16.759
R40.
N1516 G1 X66.544 Y-23.077
N1518 X55. Y29.63
N1520 Z-13.5 F10.
N1522 X30. F120.
N1524 Y17.36
N1526 G2 X59.733 Y-16.759
R40.
N1528 G1 X66.544 Y-23.077
N1530 X55. Y29.63
N1532 Z-14. F10.
N1534 X30. F120.
N1536 Y17.36
N1538 G2 X59.733 Y-16.759
R40.
N1540 G1 X66.544 Y-23.077
N1542 X55. Y29.63
N1544 Z-14.5 F10.
N1546 X30. F120.
N1548 Y17.36
N1550 G2 X59.733 Y-16.759
R40.
N1552 G1 X66.544 Y-23.077
N1554 X55. Y29.63
N1556 Z-15. F10.
N1558 X30. F120.
N1560 Y17.36
N1562 G2 X59.733 Y-16.759
R40.
N1564 G1 X66.544 Y-23.077
N1566 X55. Y29.63
N1568 Z-15.5 F10.
N1570 X30. F120.
N1572 Y17.36
N1574 G2 X59.733 Y-16.759
R40.
N1576 G1 X66.544 Y-23.077
N1578 X55. Y29.63
N1580 Z-16. F10.
N1582 X30. F120.
N1584 Y17.36
N1586 G2 X59.733 Y-16.759
R40.
N1588 G1 X66.544 Y-23.077
N1590 X55. Y29.63

N1592 Z-16.5 F10.
 N1594 X30. F120.
 N1596 Y17.36
 N1598 G2 X59.733 Y-16.759
 R40.
 N1600 G1 X66.544 Y-23.077
 N1602 X55. Y29.63
 N1604 Z-17. F10.
 N1606 X30. F120.
 N1608 Y17.36
 N1610 G2 X59.733 Y-16.759
 R40.
 N1612 G1 X66.544 Y-23.077
 N1614 X55. Y29.63
 N1616 Z-17.5 F10.
 N1618 X30. F120.
 N1620 Y17.36
 N1622 G2 X59.733 Y-16.759
 R40.
 N1624 G1 X66.544 Y-23.077
 N1626 X55. Y29.63
 N1628 Z-18. F10.
 N1630 X30. F120.
 N1632 Y17.36
 N1634 G2 X59.733 Y-16.759
 R40.
 N1636 G1 X66.544 Y-23.077
 N1638 X55. Y29.63
 N1640 Z-18.5 F10.
 N1642 X30. F120.
 N1644 Y17.36
 N1646 G2 X59.733 Y-16.759
 R40.
 N1648 G1 X66.544 Y-23.077
 N1650 X55. Y29.63
 N1652 Z-19. F10.
 N1654 X30. F120.
 N1656 Y17.36
 N1658 G2 X59.733 Y-16.759
 R40.
 N1660 G1 X66.544 Y-23.077
 N1662 X55. Y29.63
 N1664 Z-19.5 F10.
 N1666 X30. F120.
 N1668 Y17.36
 N1670 G2 X59.733 Y-16.759
 R40.
 N1672 G1 X66.544 Y-23.077
 N1674 X55. Y29.63
 N1676 Z-20. F10.
 N1678 X30. F120.
 N1680 Y17.36
 N1682 G2 X59.733 Y-16.759
 R40.
 N1684 G1 X66.544 Y-23.077
 N1686 X55. Y29.63
 N1688 Z-20.5 F10.
 N1690 X30. F120.
 N1692 Y17.36
 N1694 G2 X59.733 Y-16.759
 R40.
 N1696 G1 X66.544 Y-23.077
 N1698 X55. Y29.63
 N1700 Z-21. F10.
 N1702 X30. F120.
 N1704 Y17.36
 N1706 G2 X59.733 Y-16.759
 R40.
 N1708 G1 X66.544 Y-23.077
 N1710 X55. Y29.63

N1712 Z-21.5 F10.
 N1714 X30. F120.
 N1716 Y17.36
 N1718 G2 X59.733 Y-16.759
 R40.
 N1720 G1 X66.544 Y-23.077
 N1722 X55. Y29.63
 N1724 Z-22. F10.
 N1726 X30. F120.
 N1728 Y17.36
 N1730 G2 X59.733 Y-16.759
 R40.
 N1732 G1 X66.544 Y-23.077
 N1734 X55. Y29.63
 N1736 Z-22.5 F10.
 N1738 X30. F120.
 N1740 Y17.36
 N1742 G2 X59.733 Y-16.759
 R40.
 N1744 G1 X66.544 Y-23.077
 N1746 X55. Y29.63
 N1748 Z-23. F10.
 N1750 X30. F120.
 N1752 Y17.36
 N1754 G2 X59.733 Y-16.759
 R40.
 N1756 G1 X66.544 Y-23.077
 N1758 X55. Y29.63
 N1760 Z-23.5 F10.
 N1762 X30. F120.
 N1764 Y17.36
 N1766 G2 X59.733 Y-16.759
 R40.
 N1768 G1 X66.544 Y-23.077
 N1770 X55. Y29.63
 N1772 Z-24. F10.
 N1774 X30. F120.
 N1776 Y17.36
 N1778 G2 X59.733 Y-16.759
 R40.
 N1780 G1 X66.544 Y-23.077
 N1782 X55. Y29.63
 N1784 Z-24.5 F10.
 N1786 X30. F120.
 N1788 Y17.36
 N1790 G2 X59.733 Y-16.759
 R40.
 N1792 G1 X66.544 Y-23.077
 N1794 X55. Y29.63
 N1796 Z-25. F10.
 N1798 X30. F120.
 N1800 Y17.36
 N1802 G2 X59.733 Y-16.759
 R40.
 N1804 G1 X66.544 Y-23.077
 N1806 X55. Y29.63
 N1808 Z-25.5 F10.
 N1810 X30. F120.
 N1812 Y17.36
 N1814 G2 X59.733 Y-16.759
 R40.
 N1816 G1 X66.544 Y-23.077
 N1818 X55. Y29.63
 N1820 Z-26. F10.
 N1822 X30. F120.
 N1824 Y17.36
 N1826 G2 X59.733 Y-16.759
 R40.
 N1828 G1 X66.544 Y-23.077
 N1830 G0 Z25.

N1832 M5
 N1834 G91 G28 Z0.
 N1836 G28 X0. Y0. A0.
 N1838 M30
 %

```

%
O0007
(PROGRAM NAME - DRILL 8MM
FOUNDATION )
( DATE=DD-MM-YY - 05-01-12
TIME=HH:MM - 14:12 )
N100 G21
N102 G0 G17 G40 G49 G80 G90
( 8. FLAT ENDMILL TOOL
- 1 DIA. OFF. - 217 LEN. -
1 DIA. - 8. )
N104 T2 M6
N106 G0 G90 G54 X-42.75
Y12.6 A0. S1200 M3
N108 G43 H2 Z25.
N110 Z5.
N112 G1 Z-3.75 F10.
N114 X-34.75 F50.
N116 X-42.75
N118 Z-7.5 F10.
N120 X-34.75 F50.
N122 X-42.75
N124 Z-11.25 F10.
N126 X-34.75 F50.
N128 X-42.75
N130 Z-15. F10.
N132 X-34.75 F50.
N134 G0 Z10.
N136 Z25.
N138 X34.75
N140 Z5.
N142 G1 Z-3.75 F10.
N144 X42.75 F50.
N146 X34.75
N148 Z-7.5 F10.
N150 X42.75 F50.
N152 X34.75
N154 Z-11.25 F10.
N156 X42.75 F50.
N158 X34.75
N160 Z-15. F10.
N162 X42.75 F50.
N164 G0 Z10.
N166 Z25.
N168 X34.75 Y-12.64
N170 Z5.
N172 G1 Z-3.75 F10.
N174 X42.75 F50.
N176 X34.75
N178 Z-7.5 F10.
N180 X42.75 F50.
N182 X34.75
N184 Z-11.25 F10.
N186 X42.75 F50.
N188 X34.75
N190 Z-15. F10.
N192 X42.75 F50.
N194 G0 Z10.
N196 Z25.
N198 X-42.75
N200 Z5.
N202 G1 Z-3.75 F10.
N204 X-34.75 F50.
N206 X-42.75
N208 Z-7.5 F10.
N210 X-34.75 F50.
N212 X-42.75
N214 Z-11.25 F10.
N216 X-34.75 F50.
N218 X-42.75

```

```

N220 Z-15. F10.
N222 X-34.75 F50.
N224 G0 Z25.
N226 M5
N228 G91 G28 Z0.
N230 G28 X0. Y0. A0.
N232 M30
%

```